Max-Planck-Institut für Polymerforschung
Max Planck Institute for Polymer Research

Influence of different factors on the interaction between polymeric nanomaterials and blood plasma proteins

Dissertation

Zur Erlangung des Grades

„Doktor der Naturwissenschaften“

im Promotionsfach Chemie

am Fachbereich Chemie, Pharmazie und Geowissenschaften

der Johannes-Gutenberg Universität in Mainz

D77 - Mainzer Dissertation

Svenja Winzen

geb. in Gießen

Mainz, 2015

Dekan:

1. Gutachter:
2. Gutachter:

Tag der mündlichen Prüfung:

Abstract

In recent years, nanomaterials received increasing attention for their application as drug delivery devices to prolong their blood circulation times and improve their targeting efficiency. Since most drug delivery devices are applied intravenously, a new biological interface is created after the nanocarriers interact with blood components: the protein corona. Proteins from the blood plasma adsorb to the nanocarrier surfaces and thereby change its chemical and physical characteristics like size, surface charge and exposed functional groups. The adsorption process itself depends on many factors of which four different ones have been examined in this work.

First the effect of shear force during sample preparation of nanoparticle-protein complexes was examined and different analysis techniques were applied to compare the results. Via a complementary analysis it was possible to distinguish between hard and soft corona proteins and the information can be used for further experiments. Second, the role of surfactants stabilizing the nanocarriers was investigated. It was found that both the type and the concentration of surfactant significantly influence the adsorption properties of the proteins. Accordingly, first tests to develop a method for surfactant quantification in the presence of nanoparticles were successfully conducted. The third factor considered was the modification of proteins with fluorescent dyes which is often used for biochemical analysis techniques. It was observed that the attached label can interfere with the adsorption process depending on the type of interaction with the nanomaterial. These insights are useful for further measurements including modified proteins. At last, the protein adsorption was studied at different temperatures. It could be demonstrated that the comparison of the thermodynamic adsorption parameters can be used to determine the reversibility of the adsorption process.

In summary, the detailed investigation of the factors shear force, surfactants, protein labels and temperature helps to understand the involved processes of protein adsorption and provides useful tools for future investigations.

Zusammenfassung

In den letzten Jahren haben Nanomaterialen für den Wirkstofftransport zunehmend mehr Beachtung erfahren, unter anderem, um die Blutzirkulationszeit der Wirkstoffe zu erhöhen und eine gezielte Wirkstofffreisetzung zu erreichen. Da die meisten Wirkstofftransporter intravenös appliziert werden, entsteht nach Interaktion der Nanocarrier mit Blutbestandteilen eine neue biologische Grenzfläche: die Protein-Corona. Proteine des Blutplasmas adsorbieren auf der Oberfläche der Nanocarrier und verändern dadurch deren chemischen und physikalischen Eigenschaften sowie an der Oberfläche exponierte funktionelle Gruppen. Der Adsorptionsprozess ist von verschiedenen Faktoren abhängig, von denen vier in dieser Arbeit untersucht wurden.

Zunächst wurde der Effekt von mechanischer Einwirkung während der Probenpräparation von Nanopartikel-Protein-Komplexen untersucht und dabei verschiedene Analysemethoden zum Vergleich der Resultate genutzt. Es konnte gezeigt werden, dass es durch die Kombination der Techniken möglich ist, zwischen Proteinen der sogenannten harten und weichen Protein-Corona zu unterscheiden, was für weitere Experimente von essentieller Bedeutung ist. Als zweites wurde die Rolle von Partikel-stabilisierenden Tensiden untersucht. Es wurde herausgefunden, dass sowohl die Art als auch die Konzentration der Tenside erheblichen Einfluss auf die Adsorption hat. Infolgedessen wurden vorläufige Tests zur Entwicklung einer Methode, Tenside in der Anwesenheit von Nanopartikeln zu quantifizieren, erfolgreich durchgeführt. Den dritten untersuchten Faktor stellt die Modifizierung von Proteinen mit Fluoreszenzfarbstoffen dar. Es wurde beobachtet, dass eine Markierung je nach Interaktionsart mit dem Nanomaterial mit dem Adsorptionsprozess interferieren kann, was für weitere Experimente mit modifizierten Proteinen sehr wichtig ist. Als letztes wurde die Proteinadsorption bei verschiedenen Temperaturen verglichen. Es wurde gezeigt, dass der Vergleich der thermodynamischen Adsorptionsparameter genutzt werden kann, um die Reversibilität von Adsorptionsprozessen zu beurteilen.

Zusammenfassend lässt sich sagen, dass die Untersuchung der Faktoren Scherkraft, Tenside, Proteinmodifikation und Temperatur hilft, die Prozesse, welche in die Proteinadsorption involviert sind, besser zu verstehen und wichtige Hilfsmittel für weitere Studien darstellt.

Table of Contents

1. Introduction

Recently, nanoparticles have received increasing attention in different fields like material science and technology or nanomedicine. While for material science mostly physical parameters are important, for nanoparticles designed as diagnostic or therapeutic agents a greater focus is put on parameters like release and pharmacokinetics. However, it is crucial to determine a defined structure – effect relationship and the biological responses when a nanomaterial enters an organism. Currently, a large number of systems are being investigated for drug delivery purposes.[1, 2] Many of them are characterized with regards to their physico-chemical properties and then tested in *in vitro* or *in vivo* experiments. However, the effect caused in an organism is often very different from the one in cell experiments and also still in many cases based on trial and error. Therefore, the necessity to understand the processes taking place when nanoparticles enter bodily fluids developed. As most drug delivery devices are applied intravenously, the first interaction medium for the nanoparticles is blood. Blood plasma proteins adsorb to the particle surfaces and form a protein 'corona'.[3-5] The protein corona is subject to investigation in several current studies with the main aim to understand different factors influencing the adsorption process.

In recent investigations it was found that one of the main factors driving the adsorption process is the hydrophobicity of the nanomaterial surface.[6-8] Hydrophobic interactions seem to be very strong in the aqueous blood plasma medium, as some proteins also possess hydrophobic structure elements. Therefore, hydrophilic materials decrease protein interaction while more hydrophobic materials enhance it. Accordingly, it was found that the influence of functional groups is not as significant as expected.[9] However, when very strong positive or negative charges are introduced at the particle surface, many times aggregation effects were observed, while for slightly charged surfaces this effect is reduced.[10-12] Two different factors, the size of the nanomaterial[7, 13, 14] as well as the time dependency of the corona composition[5, 15, 16] were also subject to investigation. While for smaller nanoparticles, surface curvature plays a role in terms of protein structural changes;[17] it is legitimate to expect that this effect might become less important for larger nanomaterials, where the surface appears flat to the proteins. Studying the time dependence, it was shown, that protein adsorption is a very fast process

initially and that the corona composition undergoes some changes after longer incubation times. However, it was indicated that the corona composition only changed quantitatively and not qualitatively for the investigated materials.[16] Additionally, in a recent study it was shown, that surface functionalization used for targeting could potentially be covered by proteins, so that they are not recognized by cells anymore and a new biological 'identity' of the particles is created.[18] Also, the enrichment of certain proteins in the protein corona can lead to different cell uptake behaviors compared to the bare nanoparticles due to this new identity.[19] To avoid protein adsorption and prolong the circulation time of particles in the blood, the attachment of polyethylene glycol (PEG) chains has become a standard method creating 'stealth' nanoparticles invisible for the immune system.[20, 21] However, the grafting density and chain length of the attached PEG was shown to be of importance for the effectiveness of the phenomenon.[22, 23]

In this work, four important influence factors have been investigated in detail. First, it was shown that the sample preparation with different kinds of techniques and therefore different ways of applying shear force to the protein corona has a significant effect in the type of analyzed corona: the 'hard' or the 'soft' corona. Here, a combination of methods was proven to be most useful to obtain a thorough analysis of the adsorbed proteins with and without mechanical stress applied. In addition, the role of surfactants adsorbed to the nanoparticle surface for stabilization was investigated. It is often believed that the remaining amount of surfactant (needed for synthesis) after purification of the particles is minor and not effecting the biological responses. Here, it was demonstrated that very small concentration changes and also the type of surfactant can influence the protein adsorption properties dramatically. Resulting from this, a method to detect sodium dodecyl sulfate (SDS) in the presence of nanoparticles was developed. Next, the modification of proteins via fluorescence labels was examined in detail. It was observed that the label significantly changed the adsorption behavior of the protein depending on the nature of interactions involved. When the label blocked the primary way of interaction, the adsorption could even be completely suppressed. At last, the influence of temperature on the thermodynamics of the adsorption processes was analyzed. Evidence was obtained that adsorption can be either enhanced or decreased depending on the driving force of the process (enthalpy or entropy).

2. Theoretical Background

Here, certain aspects of the biochemistry concerning blood and blood proteins as well as nanocarriers and the interaction forces between both will be discussed. More detailed information about the biochemistry of the involved materials can be found in common literature.[24] Additionally, the information regarding colloid chemistry can also be found in standard works.[25]

2.1 Blood

Blood as the body fluid transporting oxygen, carbon dioxide, nutrients and metabolic products throughout the body consists of blood cells suspended in blood plasma. The fluid part (blood plasma) takes up about 55% of the whole blood while the cellular fraction (45%) is composed of leukocytes, erythrocytes and thrombocytes (Figure 2.1.1). By volume, the red blood cells dominate the cellular part by far to be able to provide the amounts of hemoglobin needed for the oxygen transport. The constituents of the plasma are around 90% of water with 10% of soluble substances like proteins, electrolytes, sugars, hormones and other small molecules.

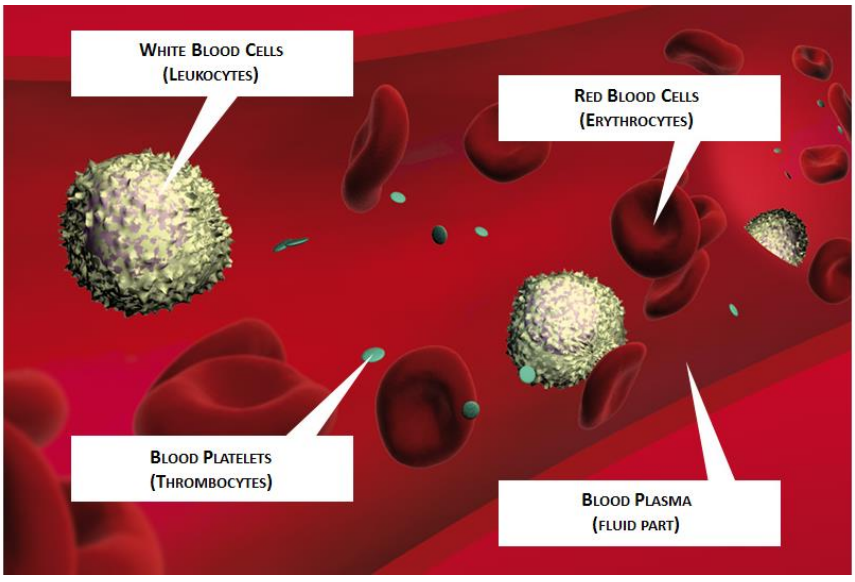

Figure 2.1.1 Schematic representation of the cellular and fluid fractions of blood[26]

2.1.1 Definition of blood plasma and serum

To be able to store and analyze the fluid component of blood, the blood has to be treated in certain ways to prevent the clotting of coagulation factors and proteins. This can be done by adding stabilizing agents like sodium citrate or heparin to the blood. After that, the blood is centrifuged and all solid components (cellular fraction) will sediment (see Figure 2.1.2). The remaining liquid is the blood plasma with all coagulation factors left. Another method to stabilize the liquid component of blood is to actively induce blood clotting. After clotting the blood is also being centrifuged and the remaining liquid yields the blood serum. The serum is now free of coagulation factors and proteins like fibrinogen and fibrin.[27]

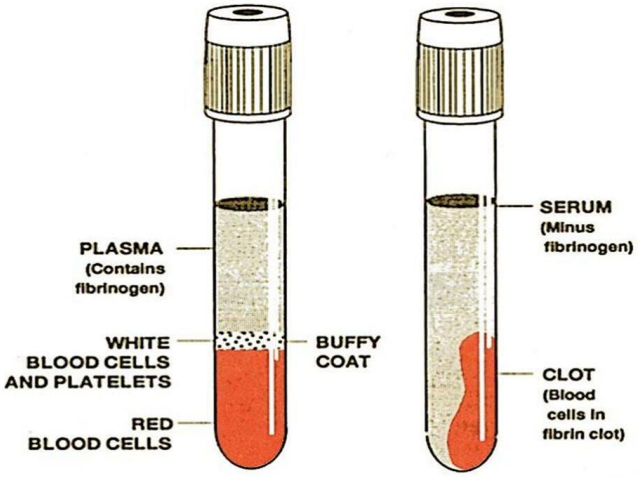

Figure 2.1.2 Schematic representation of plasma vs. serum[28]

To analyze the interaction of certain substances with components of the blood fluid, the coagulation factors and proteins also have to be considered as e.g. fibrinogen is one of the high abundance proteins in blood (~ 2.7 $g \cdot L^{-1}$).[29] Therefore, in this work human plasma is used for all analyses instead of serum.

2.1.2 Blood proteome

The sum of all proteins dissolved in the blood plasma is called plasma proteome. Usually the human blood plasma exhibits a protein concentration of around 60 – 80 $g \cdot L^{-1}$. The proteins can be classified according to their electrophoretic mobility (albumins and globulins) or their function. The concentration of blood proteins is shown in Figure 2.1.3.

While the high abundance proteins like albumin (~ 44 g·L^{-1}),[30] immunoglobulin G (IgG) (~ 10 g·L^{-1}),[31] transferrin (~ 2.7 g·L^{-1})[32] and fibrinogen (~ 2.7 g·L^{-1})[29] are easy to access, many interesting proteins only have a very low plasma abundance and cannot or only with great effort be isolated. While 90% of the protein mass is made up of only 10 plasma proteins (albumin, immunoglobulins, coagulation proteins), 9 wt% consist of another 12 proteins (mainly complement factors and apolipoproteins). The remaining 1 wt% contains all other proteins, many of which are not identified yet.

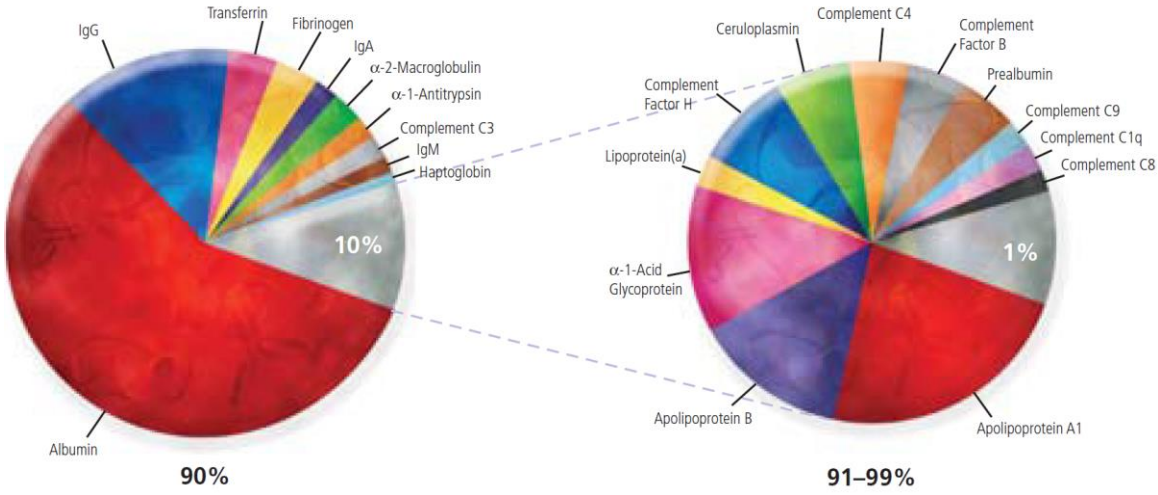

Figure 2.1.3 Protein fractions of the blood proteome[33]

2.2 Important blood proteins

2.2.1 Human serum albumin

Human serum albumin (HSA) is a globular protein and is with around 44 g·L^{-1} the highest concentrated protein in blood plasma (see above). It has a molecular mass of 67 kDa and a secondary structure that is mainly α-helical (see Figure 2.2.1). The roles of albumin are quite diverse, but one of the most important ones is to maintain the oncotic (colloid osmotic) pressure of the blood. Additionally, it helps building up the buffer capacity of blood because of its ampholytic character. Since albumin also has a hydrophobic pocket in the center of the molecule, it has the ability to bind hydrophobic molecules and transport them in the blood stream. Many water insoluble molecules like

bilirubin or fatty acids cannot be transported without albumin. This carrier function is also often used for the binding and transport of drugs.

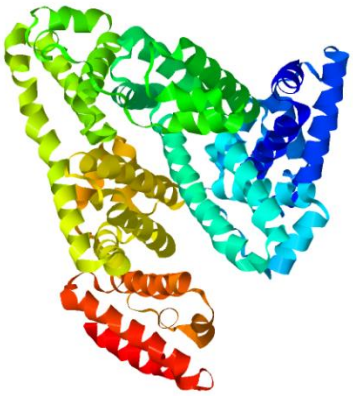

Figure 2.2.1 Crystal structure of human serum albumin obtained from the protein database (PDB) ID: 1E7H.

2.2.2 Apolipoproteins

Apolipoproteins are a group of mostly small proteins, which usually cannot be found in plasma in a free soluble form. They are part of bigger structures called lipoproteins (see Figure 2.2.2). Lipoproteins consist of phospholipids, cholesterol, cholesterol esters and triglycerides in addition to apolipoproteins in order to transport their non-water-soluble fats to various locations in the human body. The composition of the lipoproteins differs in the amounts of the various constituents and is therefore classified according to their density: chylomicrons, very low density lipoproteins (VLDL), intermediate density lipoproteins (IDL), lipoprotein a (Lp(a)), low density lipoproteins (LDL) and high density lipoproteins (HDL). While the apolipoproteins in the shell of the lipoproteins also give them some stability, their main function is to guide the lipoprotein to its destination and facilitate the uptake or release of hydrophobic molecules. Therefore, various receptors exist to bind the different classes of apolipoproteins as ligands. All apolipoproteins are thus specific for certain lipoprotein classes.

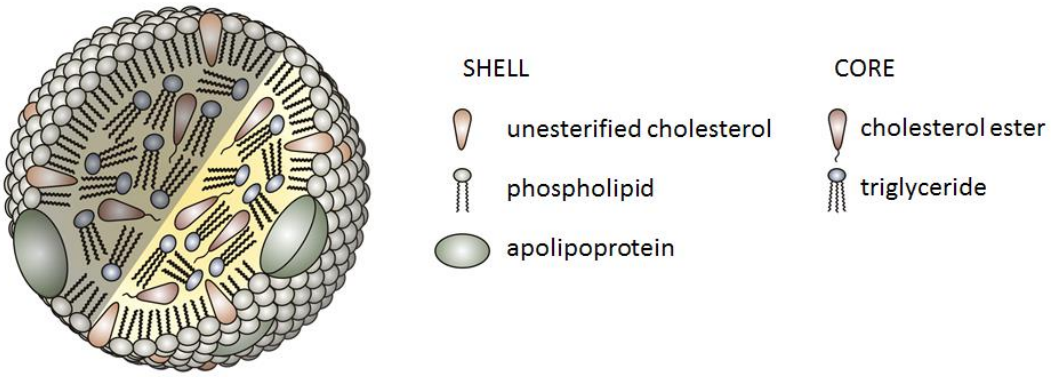

Figure 2.2.2 Schematic illustration of a lipoprotein modified from Wikimedia Commons[34]. © AntiSense / CC BY-SA 3.0

In the following, two apolipoproteins will be discussed in more detail. Apolipoprotein A-I (ApoA-I) is a 28 kDa protein and can be found on chylomicrons and HDL. In Figure 2.2.3 the crystal structure of lipid bound ApoA-I is shown. According to this model the α-helical chains of ApoA-I wrap around the phospholipids and cholesterol. ApoA-I is an important activator and cofactor for the enzyme lecithin-cholesterol acyltransferase (LCAT), which binds to HDL particles and facilitates the uptake of cholesterol from extrahepatic tissue into HDL by esterification of cholesterol. HDLs are transported to the liver where cholesterol can then be degraded and eliminated. This means ApoA-I is part of the reverse cholesterol transport (RCT) way.

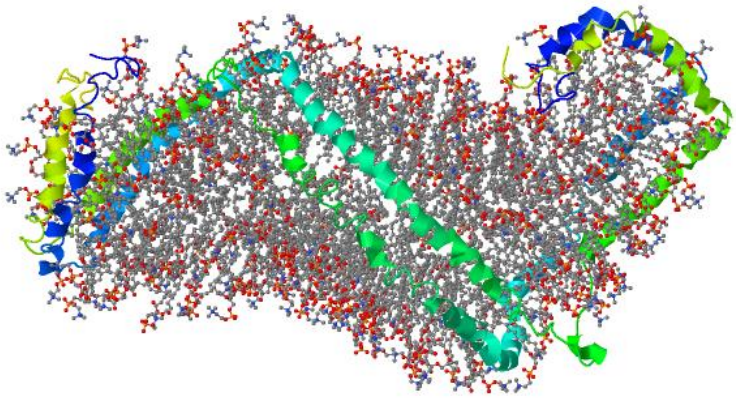

Figure 2.2.3 Crystal structure of apolipoprotein A-I obtained from PDB ID: 3K2S.

A different protein, apolipoprotein E (ApoE), is a 37 kDa protein which is mainly found on chylomicrons and IDLs. ApoA-I is mostly α-helical (see Figure 2.2.4) and is a ligand for ApoE specific receptors. Therefore ApoE allows the binding of chylomicron-remnants (chylomicrons after triglycerids are released) and IDLs (VLDLs after release of

triglycerids) to those receptors and accordingly their uptake into hepatic cells as those receptors are mostly located in the liver. This means that ApoE is mostly located on lipoproteins being involved in the transport of lipids and cholesterol from the intestine and the liver into peripheric tissues.

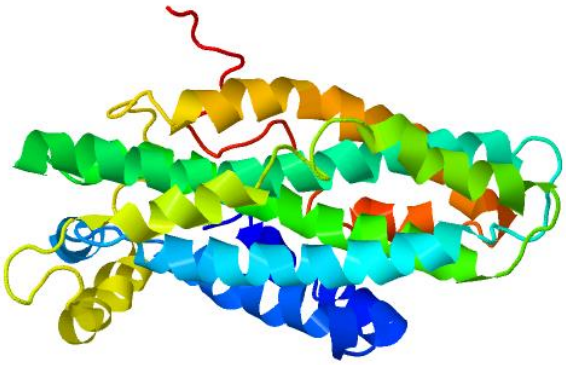

Figure 2.2.4 Crystal structure of apolipoprotein E obtained from PDB ID: 2L7B.

2.2.3 Immunoglobulin G

In general, immunoglobulins are proteins of the immune system and are also known as antibodies. They possess structural elements, which recognize foreign molecules (antigens) in the body and bind to them. This way, the antigens are marked for phagocytes that take up the complexes. Also, the binding of antibodies to antigens can inactivate the antigen itself or activate the complement system. Immunoglobulin G (IgG) is one of the five antibody classes and has the highest concentration in blood plasma. It has a molecular mass of 150 kDa and appears in its monomeric form. Depending on the binding affinity to phagocytes and the complement activation IgG can be divided into four subclasses, where IgG1 is the most common. IgG is produced by plasma cells and is composed of two light (25 kDa) and two heavy chains (50 kDa) connected via disulfide bonds. The crystal structure (see Figure 2.2.5) reveals three distinct fragments of IgG, which can be divided in the two ‘arms’ – the F_{ab} fragments – and the ‘stem’ – the F_c fragment. The F_{ab} fragments of the antibodies contain the antigen recognizing structures called epitopes. IgG is generally produced in a late stage of immune response and then circulates in the blood for a long time. Therefore, it has a memory effect and recognizes reoccurring antigens fast, which is used for vaccination treatments.

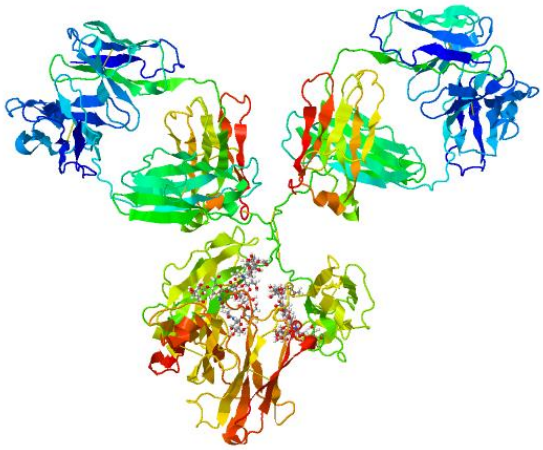

Figure 2.2.5 Crystal structure of IgG1 obtained from PDB ID: 1IGY.

2.2.4 Fibrinogen

Fibrinogen is a protein that is involved in the coagulation process in blood. It is a heterohexamer of each two α-, β- and γ-chains with an α-helical structure that are connected with disulfide bonds. The helices are forming coils, which point in opposite directions from the center of the molecule (see Figure 2.2.6). Fibrinogen has a molecular weight of 340 kDa, which is being cut by thrombin upon activation. The products are fibrin monomers that spontaneously start to polymerize to fibrin fibers that are insoluble and form a complex with thrombocytes in the blood. Also, fibrinogen can form heteropolymers with fibronectin.

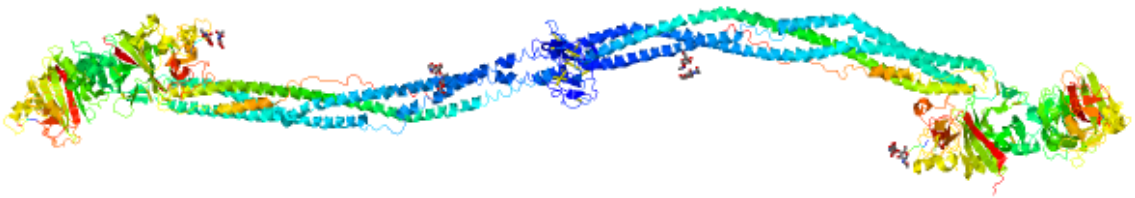

Figure 2.2.6 Crystal structure of fibrinogen obtained from PDB ID: 1M1J.

2.2.5 Fibronectin

As mentioned above, plasma fibronectin is also part of the coagulation process. It incorporates into fibrin complexes and induces a response of the immune system with its binding sites for immune cells. Additionally it possesses binding sites for fibroblasts and

keratinocytes, which help regenerating the injured tissue. Fibronectin itself also has a rod-like structure built up of two chains connected with a disulfide bond at the C-terminus. Each chain (see Figure 2.2.7) has a molecular weight of 230 kDa and is composed of domains containing antiparallel β-sheet structures. The domains are divided according to their homology (type I, II and III) and their functions.

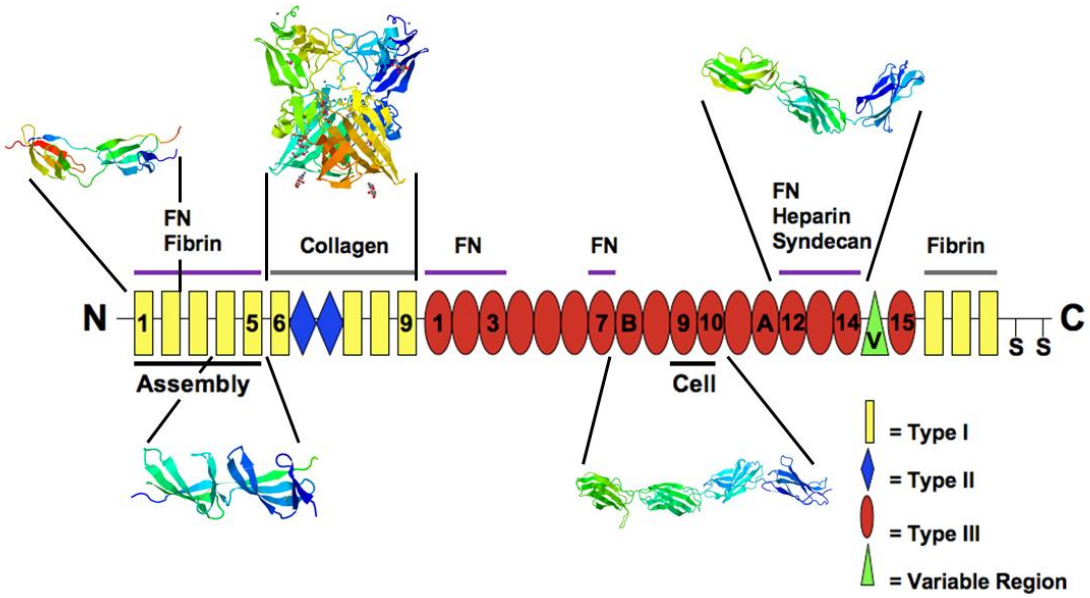

Figure 2.2.7 Fibronectin structural units modified from Wikimedia[35] (© AllWorthLettingGo / CC BY-SA 3.0) with PDBs: 1O9A, 2RKY, 3M7P, 1FNF, 3R8Q.

2.2.6 Plasminogen

Later in the blood coagulation process, plasminogen comes into play. It circulates in the blood stream in its inactive form until it passes a blood clot. It then binds to the clots and is being converted into plasmin, the active form. Plasmin is an enzyme (serine protease), which dissolves the formed blood clot after it fulfilled its purpose. It cleaves fibrin, fibronectin and some other involved proteins, a process that is called fibrinolysis. Plasminogen has a molecular weight of 88 kDa and has a mainly unordered structure with some β-sheet elements (see Figure 2.2.8).

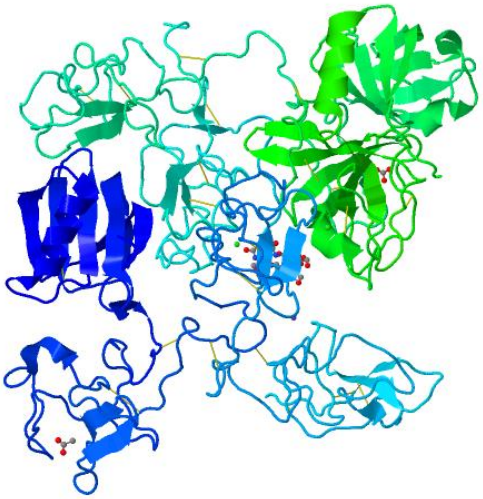

Figure 2.2.8 Crystal structure of Plasminogen obtained from PDB ID: 4DUR.

2.2.7 Transferrin

In the blood, iron ions are delivered by the protein transferrin, because iron ions cannot pass cell membranes on their own due to their high charge. Each transferrin molecule can carry two iron ions with each ion coupled with a carbonate ion. Once it finds its iron atoms, transferrin flows through the blood until it binds to a transferrin receptor on the surface of a cell. Transferrin is then internalized by cell into lysosomes, which cause the release of iron in an acidic environment. Usually 30% of the transferrin in blood is loaded with iron ions. Transferrin has a molecular weight of 75 kDa and its structure is composed of mixed elements of α-helices and β-sheets (see Figure 2.2.9).

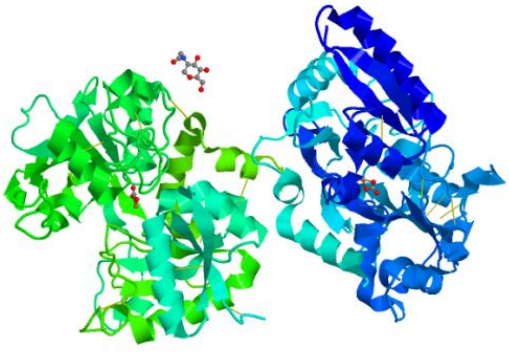

Figure 2.2.9 Crystal structure of Transferrin obtained from PDB ID: 1H76.

2.3 Nanocarriers for medical applications

The idea of nanocarriers as drug delivery systems was investigated already in the 70ies and later on modified and advanced to more complex systems.[2, 36] While first, single macromolecules were used to couple drugs and other functionalities covalently, now larger colloidal systems of assembled polymers or crosslinked materials are being developed. The main idea of using carrier systems for drug delivery is to be able to avoid systemic drug effects and guide the pharmaceutically active component to the desired location in the body. Also by 'packaging' the drug it can be protected from degradation before it reaches the target location. Like this also the circulation time in the blood stream can be prolonged.[37] This is especially important for sensitive molecules like DNA or RNA. Additionally, the packaging can be used to transport hydrophobic cargo or more than one drug or active molecule to a certain location, which is very difficult if both components are diffusing separately but are required to interact together at the target. For guiding the nanocarriers to a specific location, passive or active targeting strategies can be used. Passive targeting usually means accumulation of the carrier at a certain spot due to the characteristics of the tissue around (e.g. the 'enhanced-retention-and-permeation' effect in tumor tissues[38]). On the contrary, active targeting requires a certain functional structure attached to the carrier which 'addresses' a recognizing structure in the body. The targeting can involve the tailoring of size, charge, hydrophilicity and attached functional groups or larger molecules like antibodies, which can be bound by receptors.

In addition, nanomaterials are generally also used for diagnostic purposes.[39, 40] Depending on the particle material, they can be used for different types of imaging techniques, which also often take advantage of the nanoparticle accumulation at a certain location. Here, an example is the coupling of radiolabels to nanoparticles, which can then be detected using positron emission tomography (PET) or single photon emission computed tomography (SPECT). Also, the packaging of a contrast agent can be used to increase the sensitivity of existing imaging methods, e.g. magnetic resonance imaging (MRI). A general aim is to combine diagnostic and therapeutic characteristics of nanomaterials to obtain so-called 'theranostic' agents.[41, 42] This involves the delivery of a pharmacologically active substance to the desired site of action, while the targeted structure can also be imaged and thus the therapy can be controlled.

2.3.1 Types of nanocarriers

Typical forms of nanocarriers are shown in Figure 2.3.1. They all exhibit different characteristics, advantages and disadvantages. For example, hydrophobic cargos can be transported with micellar systems, while polymersomes and liposomes carry water soluble drugs. For the use of some transport systems like polymer conjugates the drug needs to be covalently attached. In contrast, nanocapsules have a liquid core with the cargo dissolved. Again other systems use complexation of oppositely charges macromolecules like poly-lysine and DNA. Even virus particles that do not contain any viral DNA can be used as biocompatible transport systems for proteins etc. In this work only the surface modifications and the carrier surface material are of interest. Also, the carrier systems discussed are limited to polymeric nanoparticles (E) and nanocapsules (F).

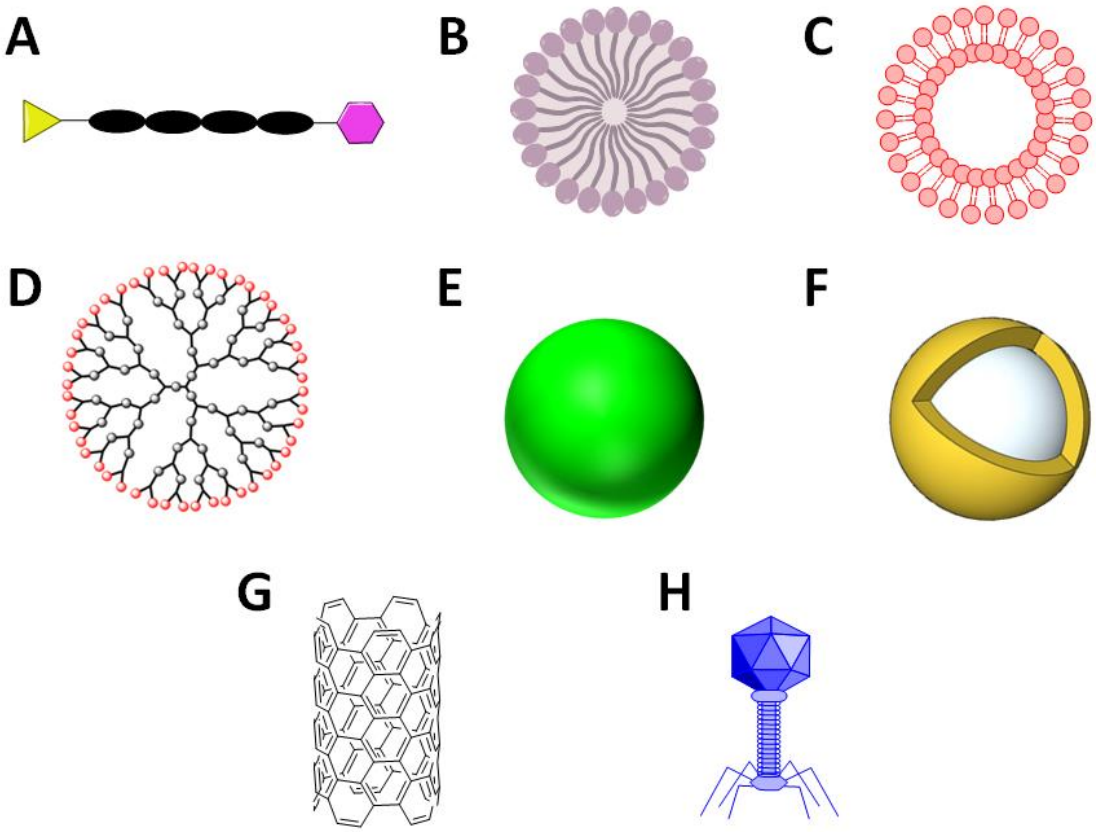

Figure 2.3.1 Types of nanocarriers. A) Polymer conjugates, B) polymeric micelles, C) liposomes/polymersomes, D) dendrimers, E) organic or inorganic nanoparticles, F) polymeric nanocapsules, G) carbon nanotubes, H) virus particles.

2.3.2 Interaction between nanomaterials and biological components

Nanomaterials are predominantly administered intravenously where they first come into contact with human blood.[2] They are being transported to the heart and from there distributed over the body after passing the lung. Along their way, they can be taken up into organs or tissues and even by cells of the immune system, e.g. macrophages. The *in vivo* fate of the nanocarriers is therefore being determined by their size and surface characteristics influencing their behavior in blood.

Blood plasma is the non-cellular component of blood and consists of over 3,000 different proteins that are capable of interacting with the nanomaterial surface and form a so called 'protein corona' (see Figure 2.3.2).[9, 43] This process describes a physical adsorption of the proteins onto the surface, which means that they can be desorbed again and are not covalently bound. The adsorption in principle can be either enthalpy or entropy driven. The formed corona creates a new interface, which influences the nanomaterial's biological identity as recognized by cells.[44]

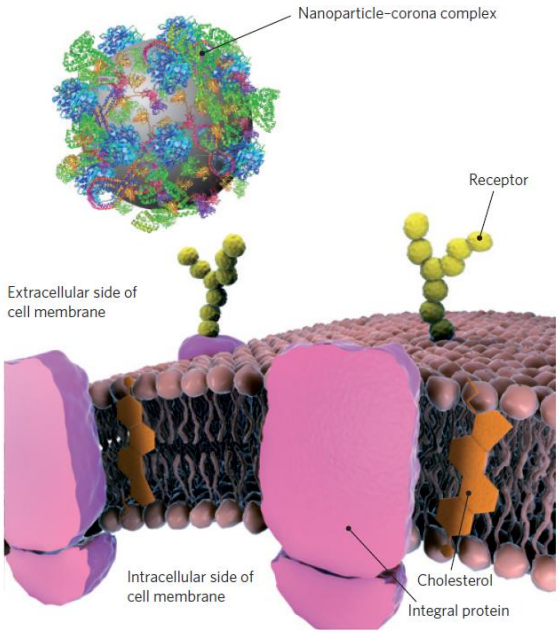

Figure 2.3.2 Nanoparticle with protein corona in a biological environment.[43] Reprinted by permission from Macmillan Publishers Ltd.

This biological identity can be rather different from the original chemical identity, as for example targeting structures can eventually lose their functionality

after coverage with plasma proteins.[18] The enrichment of certain protein types in the corona can even promote or decrease the uptake into certain cells.[19] Also the variation of charge and size can strongly influence the body distribution of the nanomaterials. In addition, the release profiles of biomolecules transported by the nanomaterials could potentially change in the presence of a protein corona, so that the desired effect might not be achieved. It becomes even more difficult when the adsorption leads to changes in the structure of the proteins. Denaturation of those proteins on the nanomaterial surfaces can trigger responses of the immune system and therefore induce inflammatory reactions.[45] Thus it is crucial to characterize the protein corona of those nanomaterials before they can be applied *in vivo*.

2.3.3 Forces and influence factors of protein adsorption

As mentioned above, the process of physical adsorption of a protein can be either enthalpy or entropy driven according to the Gibbs free energy ΔG. Usually, the forces involved can include hydrophobic interactions, electrostatic interactions, hydrogen bonding and charge transfer. For protein adsorption in aqueous solutions it has been shown that hydrophobic interactions dominate the other forces by far. This can be explained by the hydrophilic medium surrounding the proteins and particles, which tend to bind together with hydrophobic patches to decrease the area exposed to water. Also, electrostatic interactions are mostly weak because of the physiological salt concentrations in blood plasma. The salts can screen charges exposed to the solution depending on their concentration. When protein adsorption is entropy driven, this is a result of water molecules being released from the hydration shells of both the nanocarrier and the protein. Those molecules are released from the contact area of both. The larger the contact area, the more entropy gain is achieved. Consequently, proteins with labile tertiary or secondary structures can undergo structural changes to increase their contact area with the nanomaterial and stretch out flat over the surface.

As so many different driving forces can be involved, the adsorption process itself is complex and can be influenced by a sum of different factors. The factors can be grouped into two main types. The first group involves the surrounding medium like proteins, ions and external factors and the second group the characteristics of the particle (see Figure 2.3.3). Concerning the first group, the

three factors, protein concentration, protein mobility and time, are basically described by the so-called Vroman effect.[46, 47] The Vroman effect says that initially proteins with a high concentration in plasma and a high mobility (related to a small size) will adsorb to a particle. After a while, they will be replaced by proteins with a lower concentration and mobility but a higher affinity. This is not true for all adsorption processes since some of them are not reversible, but a change of the protein corona composition over time has been shown.[16] Additionally the ionic strength and pH of the aqueous medium influence the adsorption. Although they are constant in the whole blood plasma, this can change in other cellular compartments or body fluids. As already described, the salt concentration determines the strength of electrostatic interactions, while the pH can change the charge patterns of both the particle material and the proteins. As external factors also the temperature and the shear force during protein adsorption are important. Those two factors will be discussed in detail in the Results and Discussion section.

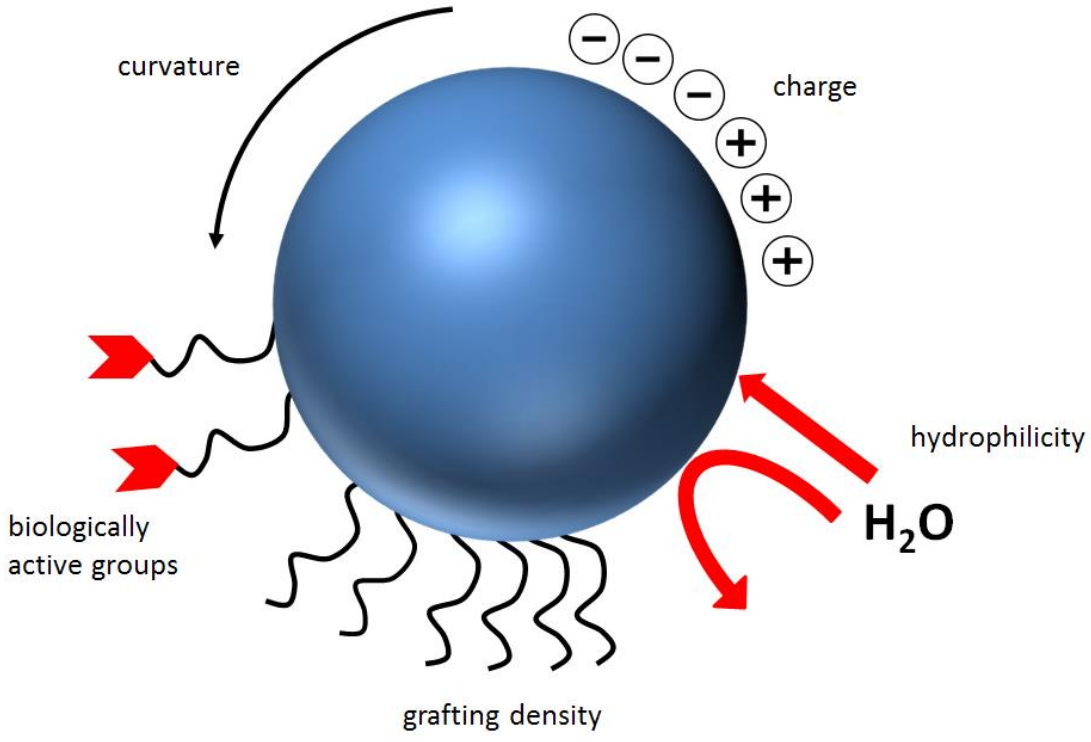

Figure 2.3.3 Nanomaterial characteristics influencing the interaction process with proteins.

The factors relating to the particle characteristics can be tuned during the synthesis. Basically, two main characteristics can be named: the size of the particle

and the surface conditions. The nanoparticle size however is probably only relevant in the size range smaller than approximately 100 nm, where the proteins might bend their structure to cover the surface. Larger particles exhibit very low surface curvatures, so that they appear flat to the proteins. Very small particles (smaller than the proteins themselves) might actually not form a protein corona. Rather it can be assumed that the particles might form a 'particle corona' around them. The surface state of the particles can be very different. Mostly, the hydrophobicity of the initial particle material and the attachment of different functional groups like e.g. PEG (polyethylene glycol) chains are important. When surface functionalities are introduced, the density of those groups is crucial, since they can also completely cover the initial material. This can be especially challenging to control for example in the case of stabilizing molecules (surfactants) at the particle-water interface, which are not covalently attached.

2.4 Surfactants for nanomaterial stabilization

Surfactants are a group of amphiphilic molecules that are surface active - meaning they are reducing the surface tension at an interface between a hydrophilic and a hydrophobic phase. In colloid chemistry they are used for the synthesis and stabilization of nanomaterials, because nanometer sized particles are not solely soluble in water. Usually, after the synthesis most of the surfactants are being removed to avoid them affecting the particle characteristics too much, but they cannot be removed completely due to stability reasons. Two main groups of surfactants can be defined: ionic and nonionic surfactants. They provide different stabilization methods that are explained below.

2.4.1 Ionic surfactants – electrostatic stabilization

Ionic surfactants are composed of hydrophobic tails and hydrophilic charged head groups. The head groups can be either anionic, cationic or even zwitterionic in nature. The surfactants assemble at the surface of the colloids with the hydrophilic group pointing towards the aqueous solution. Like this, the charge of the head group is presented to other molecules or colloids in the surrounding. The stabilizing effect of electrostatic repulsion can be explained by the DLVO (Derjaguin-Landau-Verwey-

Overbeek) theory[48] and can in the same way be achieved by covalently attached charged surface groups. In short, the colloids or more exactly the molecules on the colloid surface will attract each other when they are very close (van-der-Waals attraction, see Figure 2.4.1). This means that the interaction free energy ΔG is negative and the colloids will stick together. When charges are introduced at the colloid surface, the electrostatic repulsion between the colloids counteracts the attractive forces and a positive ΔG can be obtained. The electrostatic repulsion strongly depends on the thickness of the electrochemical double layer of counter ions around the surface. This can be influenced dramatically by the ionic strength of the solution. Additionally, when the colloids come too close, attractive forces will dominate and the particles form aggregates. This happens when a certain particle concentration is exceeded.

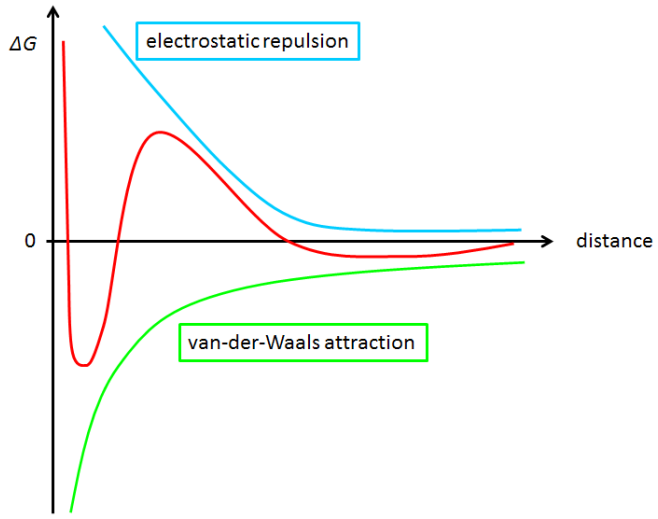

Figure 2.4.1 Total interaction free energy resulting from a combination of attractive and repulsive forces between colloids.

2.4.2 Nonionic surfactants – steric stabilization

Nonionic surfactants usually exhibit a different structure. The hydrophilic part of the molecule is composed of a long hydrophilic chain (like polyethylene glycol) that sticks out from the surface into the solution. In the same way, the hydrophilic chains can also be attached covalently to the particles without possessing a hydrophobic block. When the hydrophilic chains reach out into solution, two colloids approaching each other will be repelled due to two reasons. Firstly, in a space where the chains of both colloids

are very close, the local concentration of them is higher than in the rest of the solution. Therefore as an osmotic effect, solvent molecules will flow into the space, pushing the chains apart from each other. Secondly, the entanglement of different chains from two colloids is entropically unfavorable because the degrees of freedom for chains are reduced.

2.5 Fluorescence labels for proteins

In biochemistry, fluorescent labeling of molecules and cells allows visualization for certain applications. Usually the biomolecules labeled are proteins, nucleic acids or other molecules like lipids. When labeled with fluorescent dyes, they become fluorescent probes for techniques like laser scanning microscopy, fluorescence correlation spectroscopy, flow cytometry, assays etc.[49] While in classic biochemical analysis mostly cells and organelles and their interactions with molecules are examined, fluorescent labeling of proteins is also used for physicochemical characterization methods. The fluorescent labeling of proteins can be performed in different ways: Either the dye molecule is only complexed with the protein (electrostatically or with hydrophobic interactions) or covalently attached. Usually the type of labeling applied depends on the application and can have advantages and disadvantages. When covalent attachment of dye molecules is chosen, there are different methods available to perform the labeling reaction. Dyes with different functionalities are available to conjugate them to functional groups of the protein. The most common method involves the binding of the fluorophore to amine reactive side groups or the N-terminus of the protein via e.g. active esters or isocyanates. Sometimes also thiol groups in amino acids are used for coupling, especially when amino groups need to be preserved or the fluorescent label needs to be located at a specific position. However, not all proteins possess amino acids with thiol side groups (cysteins) so that this method is not easily applicable. When amino groups are labeled often several labels are attached to one protein due to the fact that several amino groups are present on the surface.

3. Characterization methods

3.1 Isothermal titration calorimetry (ITC)

Isothermal titration calorimetry (ITC) is a tool to characterize the interactions between two components. Usually the two components are single molecules like an enzyme and a ligand, which is why the method is mainly used for biochemical questions. With ITC, the thermodynamic properties of a reaction can be characterized without any preparation of the samples with the only requirement that the reactants must be in solution. This also includes turbid samples like dispersions, which are hard to analyze with other techniques.

3.1.1 Measurement principle

The instrument consists of an isolating mantle with two different cells inside (see Figure 3.1.1). With the mantle, the temperature of the instrument is kept constant and can only be regulated by the instrument itself. One of the two cells is called the measurement cell, which is where component 1 of the two reactants is placed. The cell is completely filled with solution, so that the thermal conduction around the cell walls is the same everywhere. In the second cell, a reference solution with the same thermal conduction properties is filled. Usually, this is the solvent of component 1 – meaning that water is used for all biochemical reactions.

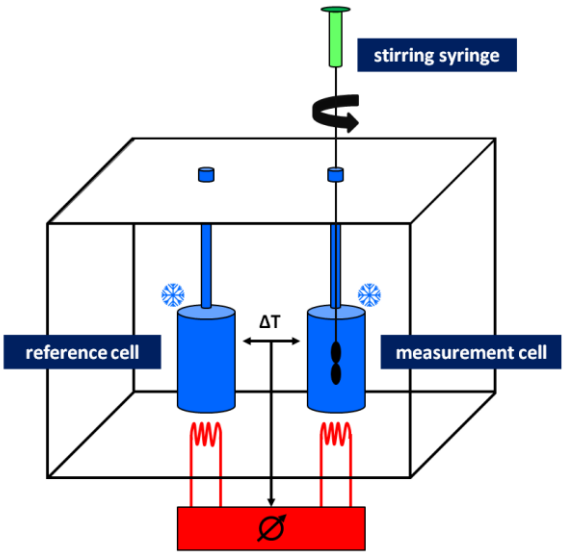

Figure 3.1.1 Schematic setup of an ITC instrument.

Additionally, a stirring syringe is placed on top of the measurement cell with the stirrer going down into the cell. In the syringe, component 2 is placed also as a solution. With this syringe, component 2 can be titrated into the cell with component 1 in very small steps. At all times, the temperature difference between the measurement cell and the reference cell is being monitored and kept constant. This is being done by heating and cooling both cells at the same time. Like that, a very fast response to temperature changes can be achieved. Once a small amount of component 2 is being titrated into the measurement cell, a temperature change will occur due to the heat release or absorption during the reaction. Then the temperature is being adjusted by regulating the heating power. This heat rate is being recorded as the raw signal of the measurement (see Figure 3.1.2). When the temperature in the cell is constant again after the injection, the signal goes back to the baseline. Depending on whether an endothermic or exothermic reaction is taking place, a positive or a negative signal will be obtained.

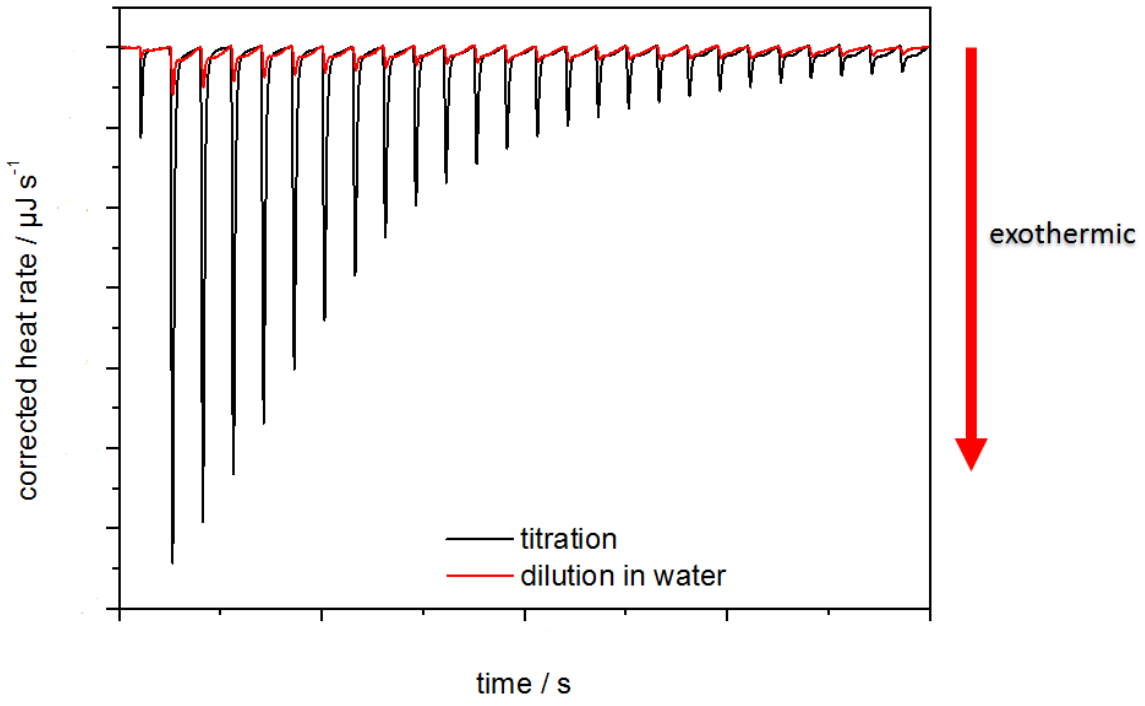

Figure 3.1.2 Raw data of an ITC measurement. The black solid line represents the titration of component 1 into component 2, while the red solid line represents the dilution of component 2.

For each titration also reference measurements have to be performed. This is done by titrating component 2 into the solvent of component 1. The heat of dilution is being recorded and after integration of the raw data subtracted from the initial measurement. The heat of dilution of component 1 usually is much smaller because a large volume is

diluted with a very small volume. Therefore, in the most cases this heat is being neglected.

3.1.2 Data analysis

After integration of the raw data and subtraction of the dilution heat, the reaction isotherm is obtained and can be analyzed with different fit models. In this dissertation, all obtained heat changes were analyzed with a fit according to an independent binding model[50, 51] (equation 3.1). This model is based on the assumption that a ligand L (or protein) independently binds to one site of a macromolecule M (or particle) without any cooperativity effects.

$$\Delta q = \left(\frac{(N[M]K_a+[L]K_a+1)-\sqrt{(N[M]K_a+[L]K_a+1)^2-4NK_a{}^2[M][L]}}{2K_a} \right) - [ML]_{n-1}\Delta H \Delta V_{cell} \quad (3.1)$$

From the fit the parameters N, K_a and ΔH are obtained, whereas $[M]$ is the concentration of the macromolecule, $[L]$ the concentration of the ligand, $[ML]$ the concentration of the formed complex and ΔV_{cell} the change of the total cell volume during the titration. To calculate the entropy change ΔS of the reaction, the reaction isotherm equation (equation 3.2) was combined with the Gibbs-Helmholtz equation (equation 3.3) and solved for ΔS (equation 3.4).

$$\Delta G = -RT \cdot \ln K_a \quad (3.2)$$

$$\Delta G = \Delta H - T \cdot \Delta S \quad (3.3)$$

$$\Delta S = R \cdot \ln K_a + \frac{\Delta H}{T} \quad (3.4)$$

Here, ΔG is the Gibbs free energy, R is the universal gas constant and T the temperature, so that for known K_a and ΔH the entropy change can be calculated. For interactions between particles and proteins this model is over simplified and has some limitations that have to be kept in mind. First, this model assumes that the reaction taking place (adsorption of a protein to a surface) is an equilibrium and therefore reversible. This will only be true, if no irreversible structure changes of the protein occur. Also,

cooperativity effects are completely neglected in this model. When a first layer of proteins is adsorbed and then more proteins interact with the built up layer, they will have a different binding affinity. However, the output of the fit only gives an overall value. Last and most important might be the problem, that the fit is only well applicable when an isotherm with a sigmoidal curve shape is obtained. Otherwise the fit parameters can only give an estimation of the real values. Often, the monitored reactions between particles and proteins do not exhibit those binding characteristics, so that absolute values of the thermodynamic parameters have to be taken with care.

3.2 Light Scattering

The theory of light scattering is described in detail in the literature and can be found in standard works.[52,53,54,55] In this chapter only the parts relevant for this dissertation will be discussed.

When a light wave hits a molecule, an oscillating dipole results, because the effect follows the periodic oscillation of the light wave. The dipole emits an electromagnetic wave of the same wavelength like the incoming wave (primary light), which is why the effect is called elastic light scattering. The resulting wave is emitted isotropically in all directions perpendicular to the oscillator. The intensity of the effect is determined by the polarizability of the molecule. For particles $d < \lambda/20$ it can be assumed that there is only one scattering center per molecule or that the distance between several scattering centers is insignificantly small. For scattering particles $d > \lambda/20$ several scattering centers occur in one molecule, so that several resulting waves are generated. Those resulting waves interfere with each other and phase shifts are occurring (see Figure 3.2.1). Therefore, the intensity of the scattered wave is not isotropic any more but has an angular dependency. The interference pattern is typical for the shape and size of a molecule and is characterized by the form factor.

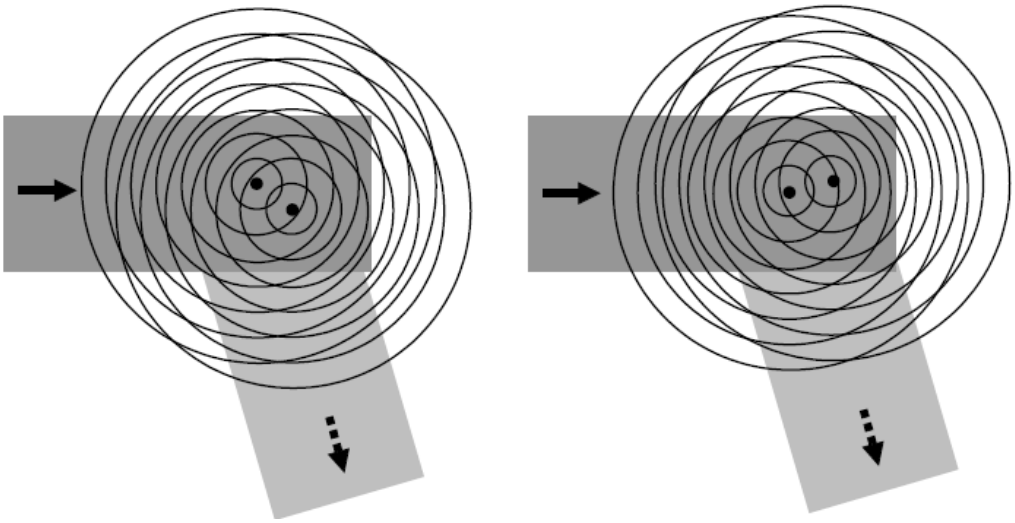

Figure 3.2.1 Intramolecular interference of resulting waves. [56] With permission of Springer Science + Business Media.

To describe the angular dependency of the scattering intensity, the scattering vector $\vec{q}$ is introduced. $\vec{q}$ exactly corresponds to the difference between the wave vectors of the incoming and scattered light waves:

$$|\vec{q}| = q = \frac{4\pi n_D \sin(\theta/2)}{\lambda} \tag{3.5}$$

n_D is the refractive index of the solvent, which also has to be taken into account. The dimension of q in a light scattering experiment relates to the magnification of the particle that is being observed. In Figure 3.2.2 this is demonstrated by means of a random polymer coil.

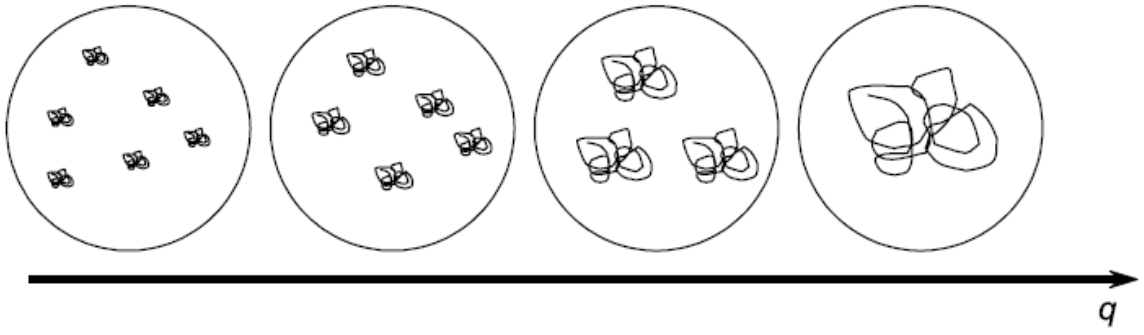

Figure 3.2.2 Magnification in a light scattering experiment depending on the scattering vector q.[56] With permission of Springer Science + Business Media.

Additionally, if a solution with scattering particles is examined, diffusion, which takes place because of the Brownian motion, has to be considered. For this reason, the interference pattern is changing over time for a given scattering angle. This is the basis for dynamic light scattering.

3.2.1 Dynamic light scattering (DLS)

Dynamic light scattering (DLS) uses the diffusion of molecules inside solutions, which takes place because of thermal fluctuations of the solvent. For a given scattering angle θ the scattering intensity varies over time, because particles diffuse in and out of the scattering volume. While in static light scattering the average scattering intensity is used, the fluctuation of the scattering intensity over time is gives the raw signal for dynamic light scattering. This fluctuation is converted into a so called autocorrelation function by a correlator. Therefore, the time dependent scattering intensity $I(q,t)$ is multiplied with a value $I(q,t+\tau)$ that is shifted by a distinct time τ. This multiplication is performed for the whole measurement time. The autocorrelation function is calculated for different values of τ, which typically are in in the order of 100 ns to several seconds. Like this, the intensity autocorrelation function $g_2(q,t)$ is obtained:

$$g_2(q,t) = \frac{\langle I(q,t)I(q,t+\tau)\rangle}{\langle I(q,t)^2\rangle} \tag{3.6}$$

The Siegert equation[57] describes the relation between $g_2(q,t)$ and the experimentally measurable field autocorrelation function $g_1(q,t)$:

$$g_2(q,t) = B \cdot (1 + f^* |g_1(q,t)|^2) \tag{3.7}$$

f^* is a coherence factor, which works as a variable parameter in data analysis, while B describes the baseline. The field autocorrelation function originates from the fact that the correlation of the single values decreases for increasing time intervals τ. The decrease is described by a characteristic relaxation rate $\Gamma = 1/\tau$. For monodisperse particles, $g_2(q,t)$ corresponds to a simple exponential decay, which contains the translational diffusion coefficient D:

$$g_2(q,t) = B \cdot \exp(-q^2 D t) \tag{3.8}$$

with:

$$q^2 D = \Gamma \tag{3.9}$$

For systems containing several different relaxation rates originating from different diffusing species, $g_2(q,t)$ can be described by the CONTIN algorithm:[58,59,60]

$$g_2(q,t) = \int_{-\infty}^{\infty} H_\tau(\ln\tau) \exp\left[-\frac{t}{\tau}\right] d(\ln\tau) \tag{3.10}$$

$H_\tau(\ln\tau)$ denotes the distribution of relaxation times und gives a peak with a maximum at a distinct relaxation time τ. From the characteristic relaxation time, the relaxation rate Γ can be calculated for each peak. Γ can then be converted into the diffusion coefficient according to equation (3.21). However, the diffusion coefficient for polydisperse samples and non-spherical structures is dependent on the scattering angle. Therefore, the true diffusion coefficient has to be calculated by extrapolating $q \to 0$. The extrapolated diffusion coefficient D_z can be converted into the z-averaged hydrodynamic radius R_h via the Stokes-Einstein equation:

$$\langle 1/R_\mathrm{h} \rangle_z^{-1} = \frac{kT}{6\pi\eta D_\mathrm{z}} \tag{3.11}$$

Therefore the sample temperature T and viscosity η of the solvent have to be known. The hydrodynamic radius R_h and the radius of gyration R_G are related as follows:

$$\rho = \frac{R_\mathrm{G}}{R_\mathrm{h}} \tag{3.12}$$

ρ is defined as the structural parameter and gives information about the density of the diffusing structure. This parameter is characteristic for a given particle shape and is higher for polydisperse systems than for monodisperse ones.

3.2.2 Analysis of multicomponent systems

In this dissertation the analysis of multicomponent systems was performed with the software HDRC programmed by Oliver Nirschl.[a] The software uses a simplex algorithm (downhill-simplex) to fit experimental data iteratively with non-linear functions depending on several parameters. The advantage of the algorithm is the remarkable robustness of the fit. Using the software, dynamic light scattering data of mixtures of two

[a] Diploma student in the workgroup of Prof. Manfred Schmidt at the Johannes Gutenberg University Mainz, 2007

components can be characterized. The components of the mixtures can be polydisperse themselves and are first analyzed individually. From the measurements of the single components, the fit functions of the field autocorrelation functions and therefore the parameters of the present decay times and intensity fractions are obtained. When both single components are coexisting unchanged in the mixture, the mixture can be described by the sum of both individual fit functions. If this is not the case and interaction between the components occurs, the fit of the mixture will be modified by an additional fit function describing the aggregate. The sum of two fit functions of the coexisting species in the mixture is called the force fit. Of the force fit the intensity contributions for component A f_{A} and component B f_{B} are the only fit parameters (equation 3.13).

$$g_{1,m}(t) = f_A g_{1,A}(t) + f_B g_{1,B}(t) \tag{3.13}$$

When the mixture cannot be described by this force fit, the modified equation 3.14 is used.

$$g_{1,m}(t) = f_A g_{1,A}(t) + f_B g_{1,B}(t) + f_{agg} g_{1,agg}(t) \tag{3.14}$$

with f_{agg} the intensity contribution of the formed aggregates and the unknown relaxation time $\tau_{1,agg}$ of the aggregates (equation 3.15):

$$g_{1,agg}(t) = a_{1,agg}\, exp\left(-\frac{t}{\tau_{1,agg}}\right) \tag{3.15}$$

Free fitting parameters are the intensity contributions as well as the function of the additional aggregate. From the obtained relaxation time of the aggregate the hydrodynamic radius can be calculated and the intensity contributions can be put in relation for all three components.

3.3 SDS polyacrylamide gel electrophoresis (SDS-PAGE)

The SDS polyacrylamide gel electrophoresis (SDS-PAGE) is a method used for the separation of proteins. Before the electrophoresis procedure, the proteins are being incubated with SDS and heated to denature them. Afterwards, almost linear protein chains are obtained that are complexed with SDS molecules (proportional to the number of amino acids). These protein complexes are loaded onto a polyacrylamide gel and an

electrical field is applied. The pores in the gel act as a filter, so that the protein complexes migrate towards the cathode according to their size. Small proteins easily diffuse through the pores, while larger ones are slower. Additionally a marker with proteins of known size is loaded next to the samples to be able to compare them. After finished electrophoresis the gel can be stained with different methods to visualize the proteins. The staining can be done with dyes like Coomassie Blue and Stains All, fluorescent dyes or silver ions.

3.4 Zeta potential

When charged colloids / particles are placed in solution, the net charge of the particle surface affects the distribution of the ions around it. A layer of oppositely charged ions from the solution is being adsorbed on the surface, which is called 'Stern' layer (see Figure 3.4.1). Around that a diffuse layer with less strongly associated ions exists. When the colloid is subjected to an electrical field, it will move in the direction of the oppositely charged electrode. As a result some ions within the diffuse layer will move with the particle, while the outer ions will stay where they are. At this 'slipping plane' a potential builds up, which is called zeta potential.

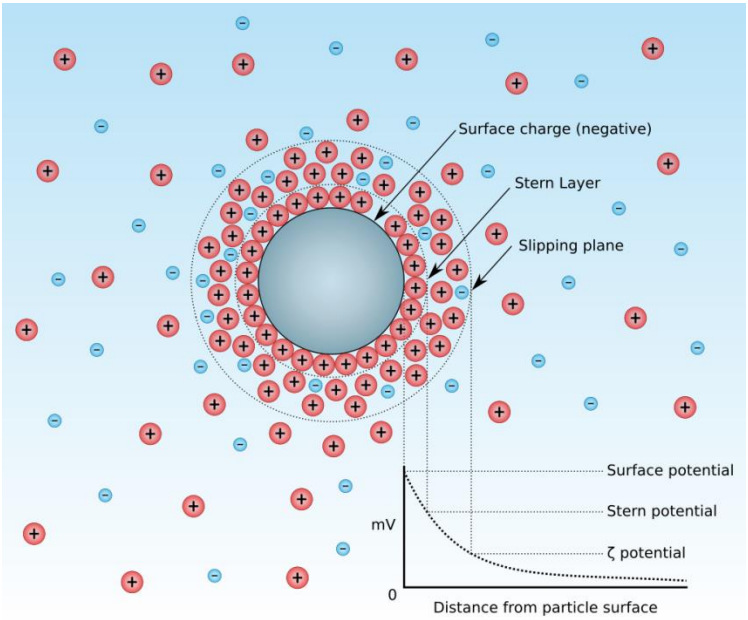

Figure 3.4.1 Schematic representation of the electrical layers around a particle in solution with the different developing potentials.[61] © Larryisgood / Mjones1984 / CC BY-SA 3.0

The zeta potential can be measured by monitoring the particle movement during electrophoresis. The velocity of a particle in an electric field is called electrophoretic mobility and can be used to calculate the zeta potential ζ through the Smoluchowski equation[62] for particles larger than 200 nm dispersed in electrolytes with > 10^{-3} M salt:

$$\zeta = \frac{\eta \cdot U}{\varepsilon} \tag{3.17}$$

η is the viscosity, U the electrophoretic mobility and ε the dielectric constant. The electrophoretic mobility can be measured using laser Doppler electrophoresis, which is based on the scattered light from a laser beam passing the sample. Particles in the measurement volume will cause fluctuations of the scattered light with a frequency proportional to their velocity, which has already been discussed in the chapter on light scattering. The calculated zeta potential is not equal but proportional to the charge of the particle, since the potential is not determined directly at the surface. Therefore, it is generally used as a value to describe the surface charge of a particle.

3.5 Nuclear magnetic resonance (NMR) spectroscopy

Nuclear magnetic resonance (NMR) spectroscopy is a technique to analyze the electronic surrounding of atoms and their interactions with neighboring atoms. This allows the structure determination of organic molecules and their dynamics. The technique is based on the magnetic resonance of atomic nuclei in a strong alternating magnetic field. All isotopes with a nuclear spin different from 0 are suitable for NMR, of which the easiest and most common one is ^{1}H. In modern NMR spectrometers, the pulse technique is applied, which means that a single radio frequency pulse is applied to the sample in the magnetic field. After the pulse, the decay of the magnetization of the sample is measured (free induction decay, FID) until the system has returned to equilibrium. The FID is modulated by the frequency shift caused by chemical shift and coupling effects. Using Fourier transformation, the distribution of frequencies can be calculated from the FID, which then gives the typical NMR spectrum.

An important field of NMR is the diffusion analysis of molecules via field gradient NMR. In contrast to conventional NMR, an inhomogeneous magnetic field is used. This means that also the nuclear resonance frequencies are dependent on the position of the

molecule in the sample. This means that for each molecule a diffusion coefficient can be measured (diffusion ordered spectroscopy, DOSY). In a DOSY spectrum, one dimension shows the ^{1}H-NMR spectrum of the sample, while in the second dimension a diffusion coefficient is assigned to each ^{1}H signal. Like this, different diffusing molecules can be distinguished in a mixture.

3.6 Fluorescence correlation spectroscopy (FCS)

The basis for FCS measurements is a confocal microscope.[63] A laser which is being focused inside the sample solution is used as the light source. The illuminated region inside the sample is called confocal volume. With the laser, fluorescent dyes can be excited and their intensity fluctuations in the confocal volume can be measured over time. The fluctuations occur because of fluorescent species diffusing in and out of the confocal volume. Because of the small dimensions of the volume, single particles can be detected. Similar to dynamic light scattering the intensity fluctuations $\delta I(t)$ can be converted into an autocorrelation function $\mathrm{G}(t) = 1 + \langle \delta I(t) \cdot \delta I(t+\tau) \rangle / \langle \delta I(t) \rangle^2$. As has been shown theoretically, for an ensemble of identical freely diffusing fluorescence species, $\mathrm{G}(t)$ has the following analytical form:

$$\mathrm{G}(t) = 1 + \left[1 + \frac{f_T}{1-f_T} e^{-t/\tau_T}\right] \frac{1}{N} \frac{1}{\left[1+\frac{\tau}{\tau_D}\right]\sqrt{1+\frac{\tau}{S^2\tau_D}}} \tag{3.16}$$

Here, N is the average number of diffusing fluorescence species in the observation volume, f_T and τ_T are the fraction and the decay time of the triplet state, τ_D is the diffusion time of the species and S is the so-called structure parameter $S = z_0/r_0$, where z_0 and r_0 represent the axial and radial dimensions of the confocal volume, respectively. Furthermore the diffusion time τ_D is related to the respective diffusion coefficient D, through $D = {r_0}^2/4\tau_D$.[64] The experimentally obtained $\mathrm{G}(t)$ can be fitted with equation 3.16 yielding the corresponding diffusion times and subsequently the diffusion coefficients of the fluorescent species. Next, the hydrodynamic radii R_h can be calculated according to dynamic light scattering using the Stokes-Einstein relation. The fluorescent brightness of the studied species can also be determined by dividing the average fluorescent intensity to the average number of fluorescent species in the probing volume i.e. $\langle I(t) \rangle / N$.

4. Results and Discussion

4.1 Complementary analysis of the hard and soft protein corona - the effect of sample preparation

The work presented in this chapter is already published in the journal *Nanoscale*, vol. **7** (7), pages 2992 - 3001.

The protein corona of a nanomaterial can be divided into the 'hard' and 'soft' protein corona. They differ in the binding strength and exchange rates of the proteins associated with the nanomaterial surface. A 'hard' protein corona consists of proteins with high binding affinities that are tightly bound and show exchange times greater than the time needed for internalization of a particle.[65] This adsorption behavior is also often referred to as irreversible protein binding. However, proteins which are loosely bound to the nanomaterial surface, or are connected with the hard protein corona via week protein-protein interactions, form the so called 'soft' protein corona.[6, 9, 65-68] These proteins are believed to have high exchange rates and can be replaced easily in a biological environment.[65] In practice, the hard corona can be defined as those proteins which are not removed from the nanomaterial's surface during preparation procedures such as washing and centrifugation. These procedures can interrupt the relatively weak protein-protein interactions which would remove the soft protein corona (Figure 4.1.1).

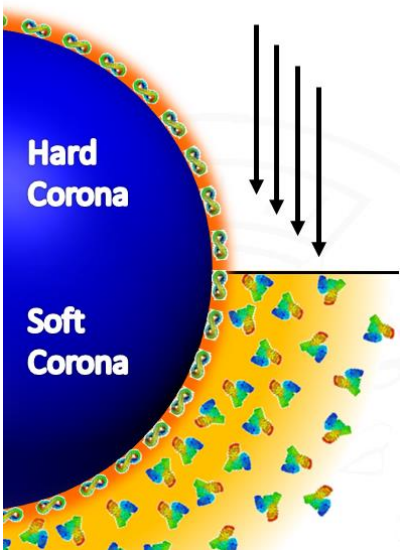

Figure 4.1.1 Schematic representation of the hard and soft corona around nanomaterials and the effect of shear force (black arrows indicate the direction in which proteins are being removed).

However it is still not clear, which form of protein corona exists under physiological conditions that also involve some shear forces in the blood stream. Accordingly it is difficult to determine the biologically relevant entity that for example is read by cellular processing. It has been shown that in some cases the hard protein corona is responsible for the interaction pathways,[69] but usually there is no information gained about the role of the soft corona proteins.

The majority of published studies that investigate the protein corona involve isolation of the nanomaterial from the biological media after employing washing steps.[4, 14, 66, 70, 71] As defined above, these investigations tend to explore the hard protein corona. The composition, impact and relevance of the soft protein corona are matters that still require attention.[65, 72] There are only a few analytical methods available to investigate nanomaterials inside the relevant biological media. Using dynamic light scattering (DLS) one can sensitively detect size changes of particles in undiluted blood plasma.[11, 73, 74] Additionally, it is possible to monitor the change in heat that results from protein adsorption onto nanomaterials with isothermal titration calorimetry (ITC). As an analytical tool, ITC can provide protein binding affinities and stoichiometry.[3, 75] An alternative method to investigate nanomaterial-protein interactions in contact media with a high sensitivity is fluorescence correlation spectroscopy (FCS).[76-78] The drawback of this technique is that FCS requires either fluorescently labeled nanoparticles or labeled proteins.

Nanomaterials which should be applied as drug delivery devices are often functionalized with poly(ethylene glycol) (PEG) chains to prevent unspecific cell uptake and to suppress protein adsorption to some extent.[20, 79, 80] Suppressing protein adsorption can increase the circulation time of nanocarriers in the bloodstream, leading to a better bioavailability of transported drugs.[79] Since sugar-based polymers like dextranes also exhibit a low protein adsorption,[81, 82] hydroxyethyl starch (HES) is being discussed as a natural nontoxic alternative for PEG with similar protein repellent characteristics.[83-85] The investigated nanocarriers in our study were synthesized from HES to obtain capsules with a shell that decreases protein adsorption.

Here, we have investigated the hard and soft protein corona of HES capsules in human plasma, human serum albumin (HSA) and apolipoprotein A-I (ApoA-I) solution using a combination of sodium dodecyl sulfate polyacrylamide gel electrophoresis (SDS-PAGE), a protein quantitation assay, ITC and DLS. In addition to non-functionalized capsules, we also analyzed carboxy-functionalized (HES-COOH) and amino-

functionalized (HES-NH_2) capsules in order to investigate the effect of different charges at neutral pH value.

This approach enables a comparison between the behavior of the capsules with plasma proteins and with isolated proteins. HSA was chosen for the analysis because it is highly abundant in blood plasma ($\sim 44\ g \cdot L^{-1}$ average)[30] and well characterized. Furthermore, HSA was found to be depleted in the hard protein corona of the previously investigated particles with comparison to its concentration in plasma.[14] In contrast, ApoA-I was shown to be enriched in the protein corona of the same nanomaterials as well as liposomes,[6, 14, 16, 80] and should be considered an interesting protein for adsorption measurements. Our work effectively shows that different analytical investigations are required to provide a full picture of a nanocapsule's hard and soft protein corona.

4.1.1 Characterization of prepared hydroxyethyl starch (HES) nanocapsules

For the interaction of proteins with nanocarriers, HES capsules in an aqueous dispersion were synthesized and characterized by Dr. Grit Baier (MPIP Mainz, Germany). The obtained nanocapsules were stable colloids and no precipitation or aggregation was observed during six months of storage under constant stirring at room temperature. Scanning electron microscopy (SEM) studies of HES nanocapsules confirmed the formation of a core-shell structure (see Figure 4.1.2). The collapse of the nanocapsule walls is due to drying effects and the electron beam during the SEM measurement.

All nanocapsules exhibited a negative zeta potential due to a redispersion in water with SDS. The capsules are purified by extensive dialysis after redispersion to remove most of the SDS. However a small amount is needed on the surface to keep the capsules stable in solution. A functionalization with NH_2-groups on the capsule surface leads to a slight increase in zeta potential because of their positive charge at neutral pH values. The amount of functional groups per nanocapsule was determined using particle charge detection (PCD, see Experimental Section).

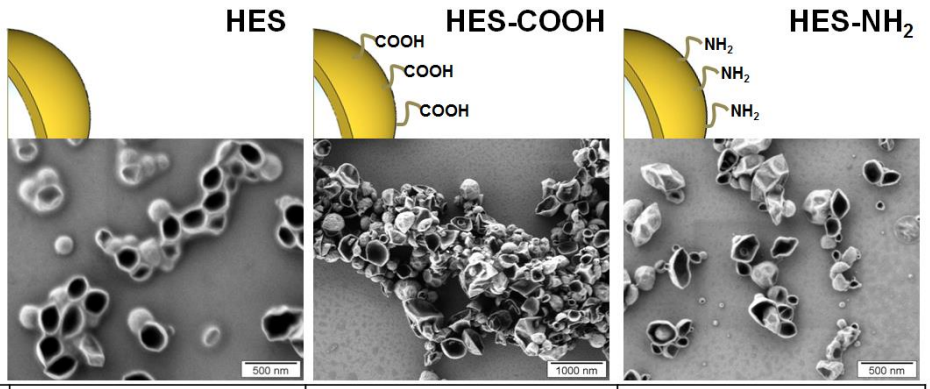

R_h, nm	275 ± 28	200 ± 20	256 ± 26
ζ – Potential, mV	-34 ± 3	-34 ± 3	-27 ± 3
Groups / NC	-	45300 ± 4500	21100 ± 2100

Figure 4.1.2 SEM images and characteristics of HES nanocapsules with different surface functionalizations.[86] Published by The Royal Society of Chemistry.

4.1.2 Protein corona characterization with gel electrophoresis and protein assay

To analyze the proteins strongly associated with the different capsule surfaces, the interaction of the HES capsules with human plasma was investigated by Dr. Susanne Schöttler (MPIP Mainz, Germany) with SDS-PAGE and a protein quantitation assay. After incubation with plasma, the capsules were thoroughly washed (three centrifugation steps followed by resuspension in buffer) and the remaining proteins removed from their surface using a mixture of urea, thiourea and buffer (see Experimental Part). Thus the hard protein corona of the HES capsules with varying surface functionalizations was analyzed. The protein patterns of the three types of capsules and the pure plasma are shown in the SDS-PAGE gel in Figure 4.1.3. In the pure plasma the most dominant protein bands can be assigned to those proteins that are known to have high plasma concentrations: Albumin (~ 44 g·L^{-1}, 67 kDa)[30], immunoglobulin G (~ 10 g·L^{-1}, heavy chain 50 kDa, light chain 25 kDa)[31] and transferrin (~ 2.6 g·L^{-1}, 75 kDa).[32] The protein patterns recovered from the nanocapsules differ significantly from the pure plasma. It is important to note that the general adsorption pattern is independent of the functionalization of the capsules. The protein bands are very similar in all cases. Interestingly, the most abundant protein in the plasma (albumin) cannot be identified in the hard corona of the capsules.

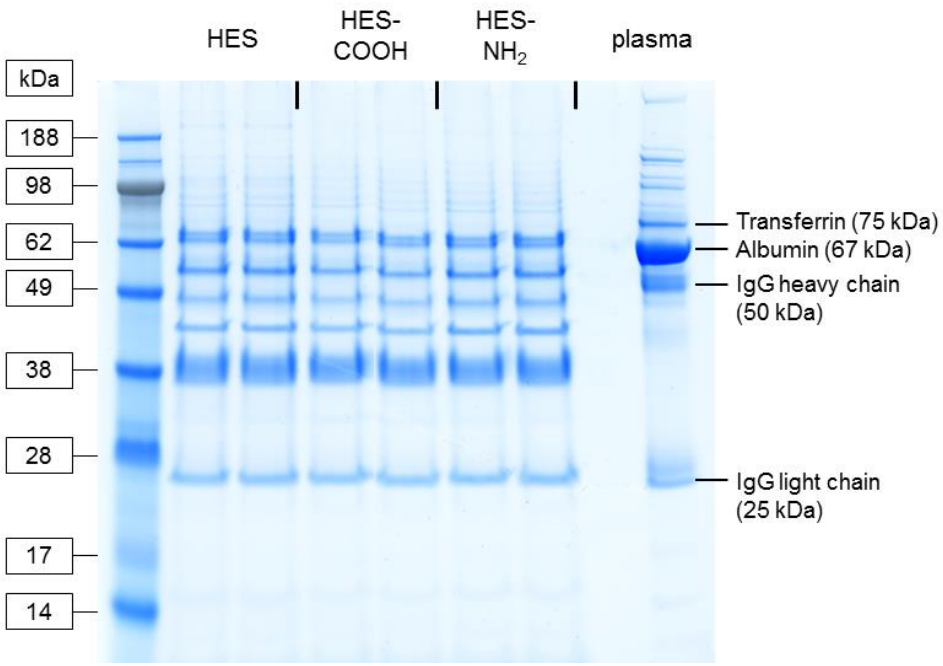

Figure 4.1.3 Coomassie-stained gel after SDS-PAGE of plasma proteins recovered from the surface of differently functionalized HES nanocapsules. Pure plasma (right lane) served as a reference.[86] Published by The Royal Society of Chemistry.

A quantitative analysis of the adsorbed proteins was performed via a Pierce 660 nm protein assay. Samples were prepared following the SDS-PAGE procedure and analyzed photometrically. The obtained protein amounts were normalized with regards to the nanocapsules' surface area and are shown in Figure 4.1.4.

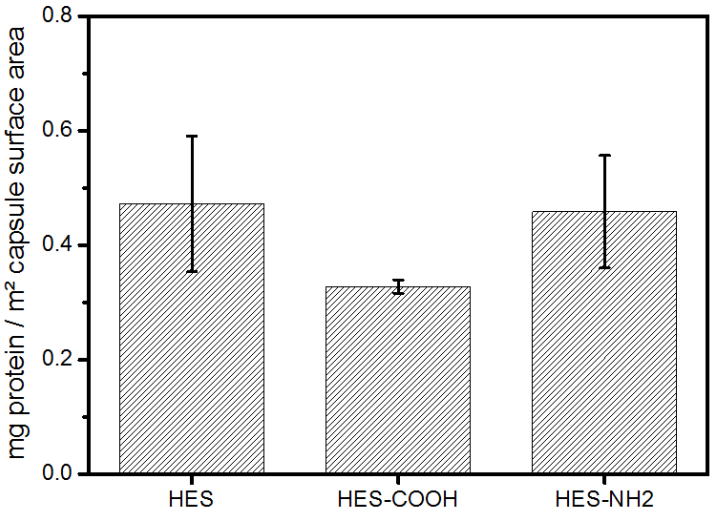

Figure 4.1.4 Adsorbed protein masses on HES nanocapsules with different functionalities. Quantification was performed via a Pierce 660 nm Assay (Thermo Scientific, Rockford, USA), mean values (n = 3).[86] Published by The Royal Society of Chemistry.

For the non- and amino-functionalized capsules, values of 0.47 ± 0.11 mg·m^{-2} and 0.46 ± 0.09 mg·m^{-2} respectively were obtained, whereas for the carboxy-functionalized capsule the value decreased to 0.32 ± 0.01 mg·m^{-2}. This quantitation suggests that the carboxy-functionalized capsules bind fewer proteins than the other two types of capsules. The described methods require extraction from the interaction medium before analysis. Consequently, proteins that possess a binding affinity below a certain threshold, currently undefined, are likely to be removed during sample preparation. Therefore, we further applied ITC and DLS to investigate the protein–nanocapsule interaction directly in the application medium.

4.1.3 Calorimetric analysis of the adsorption processes

To analyze the soft corona of the HES nanocapsules, the adsorption processes of plasma and single proteins were analyzed by ITC measurements. This technique allows the characterization of the capsules directly in physiological media while minimizing alteration of the developed protein corona by additional preparation procedures. Plasma, HSA and ApoA-I solutions were titrated into suspensions of the three types of HES nanocapsules. All titrations were performed at neutral pH, which is above the isoelectric points of both HSA and ApoA-I. The change in heat during every titration was measured, integrated and corrected for the respective heats of dilution of the titrants (proteins). The heat of dilution from the titration of pure water into the capsule dispersion was negligible. The measured heat changes of the analyzed capsule surfaces and proteins as well as the corresponding adsorption isotherms are shown in Figure 4.1.5. In all monitored adsorption processes, interactions between HES capsules and proteins were observed. In all cases, heat different from the heat of dilution is being released or absorbed. From the integrated heat, the adsorption enthalpy (ΔH), stoichiometry (N) and association constant (K_a) were calculated using a fit according to an independent binding model[50, 51] (see equation 3.1, Methods section). The entropy change (ΔS) for each reaction was calculated using the reaction isotherm equation and the Gibbs-Helmholtz equation (see equations 3.2 and 3.3). The obtained parameters are summarized in Table 4.1.1.

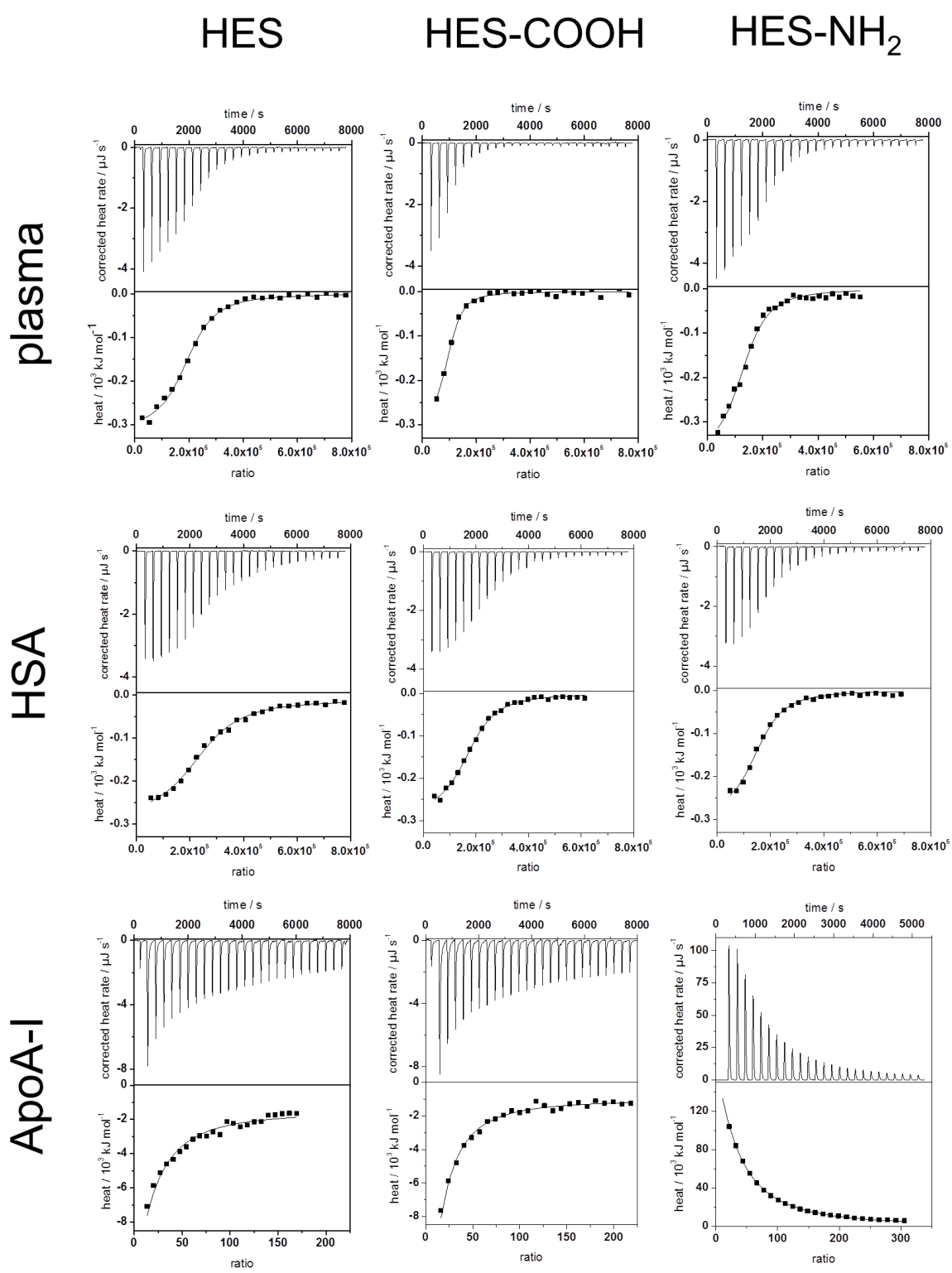

Figure 4.1.5 ITC data for the adsorption of plasma, HSA and ApoA-I onto HES nanocapsules. Upper graphs represent the raw data obtained from the titrations (baseline corrected heat rates) and lower graphs the integrated heats of each peak (black squares ■) with a corresponding independent binding fit (straight line –). For plasma measurements the molarity refers to the average HSA concentration of plasma.[86] Published by The Royal Society of Chemistry.

Table 4.1.1 Parameters obtained from ITC measurements and fitting according to an independent binding model.[86] Published by The Royal Society of Chemistry.

Capsule	Protein	ΔH / kJ mol^{-1}	K_a / 10^6 L mol^{-1}	ΔS / J K^{-1} mol^{-1}	N	Number of proteins per 10 nm²
HES	Plasma	-285 ± 97	1.0 ± 0.4	-845 ± 329	182000 ± 39000	2.00
	HSA	-277 ± 43	0.8 ± 0.3	-818 ± 147	114000 ± 16000	1.25
	ApoA-I	-6010 ± 185	333 ± 124	-20000 ± 613	10 ± 4	$1.05 \cdot 10^{-4}$
HES-COOH	Plasma	-306 ± 192	1.0 ± 0.8	-1217 ± 318	70000 ± 13500	1.40
	HSA	-308 ± 30	0.4 ± 0.2	-928 ± 103	156000 ± 36000	3.00
	ApoA-I	-5150 ± 787	188 ± 79	-17100 ± 2640	6 ± 3	$1.19 \cdot 10^{-4}$
HES-NH_2	Plasma	-281 ± 139	1.2 ± 0.6	-827 ± 468	121000 ± 29000	1.40
	HSA	-277 ± 45	0.5 ± 0.1	-820 ± 152	184000 ± 33000	2.00
	ApoA-I	883000 ± 24000	5.4 ± 0.1	$2.4 \pm 0.9 \cdot 10^6$	8 ± 6	$0.97 \cdot 10^{-4}$

These experiments determined that the interactions between human plasma and each type of HES capsule are exothermic and therefore enthalpically favored. For the analysis of the plasma measurements, the molarity refers to the average concentration of HSA in the plasma. Increasing the concentration consequently leads to a slightly higher stoichiometry *N*, while the other parameters do not change significantly. The results obtained from the fitting (see Table 4.1.1) are in agreement with the analysis of the hard protein corona. The enthalpy change is similar for each different surface functionalization. Furthermore, K_a and ΔS are the same. Given the high number of proteins interacting with one capsule in combination with the small reaction enthalpy, it can be concluded that the proteins are loosely associated with the capsule surface. Additionally, the number of proteins per 10 nm^2 of surface area was calculated based on the stoichiometry and the hydrodynamic radius of the capsules. For all functionalities a similar number of around 1-2 proteins was obtained. Thus, the lower protein amount on the carboxy-functionalized particles measured with the protein assay is due to preparation effects. It is important to note that 1-2 proteins per 10 nm² is not enough space for one protein to obtain a monolayer spread out flat on the surface. Groups of proteins are likely adsorbing at the same time, e.g. protein-protein aggregates formed previously in solution.

The adsorption of pure HSA onto the HES capsules was investigated. In general, the titration isotherms and fit parameters obtained from plasma and HSA are quite similar. This can be explained by the high HSA content in human plasma. Still, slight deviations of K_a, *N* and the protein per surface area values can be

observed. For all capsule types, K_a of HSA was reduced compared to the K_a of plasma, which is the result of additional proteins in the plasma that have a higher binding affinity than HSA. The number of proteins per surface area changes only slightly in comparison to plasma. Those changes can be attributed to different protein compositions of the soft coronas formed in plasma. Moreover, the affinity of HSA towards the HES capsules is roughly 4 times smaller than the protein's affinity towards polystyrene particles, which has been previously investigated.[87] This finding can be explained by taking into account the more hydrophilic nature of HES compared to polystyrene, which results in less hydrophobic interactions between the capsule surface and the proteins. However, the number of proteins per 10 nm² is approximately 10-20 times higher than the values reported for the polystyrene particles.[87] From the protein amounts adsorbed it can be concluded that the soft corona formed for HES nanocapsules contains much more proteins than the soft corona of polystyrene particles. Therefore, the difference between the hard and soft corona is more significant for the HES capsules.

The low affinity of HSA to the HES capsules, given by the parameter K_a, in combination with the stoichiometry and the depletion of HSA in the hard protein corona (observed in SDS-PAGE experiments) leads to the identification of HSA as a soft corona protein. These results match the findings reported in literature.[15, 88]
In contrast to the HSA adsorption, a significant amount of heat is generated when ApoA-I is titrated into pure HES capsules (see Figure 4.1.5). Also, K_a differs by about an order of magnitude, which implies that the capsules have a greater affinity towards ApoA-I than to HSA. Meanwhile, N and the protein number per surface area are several orders of magnitude smaller than the values for the HSA molecules. These findings identify ApoA-I as a hard corona protein for the investigated system. This is in good agreement with a previous study of Cedervall *et al.*, who found a high binding affinity of ApoA-I to *N*-isopropylacrylamide (NIPAM) particles.[13] Our results also support the theory that the high binding affinity of ApoA-I is due to the surface characteristics of the nanomaterial rather than the adsorption of fats from the plasma before interaction with the protein.

While the non-functionalized and the carboxy-functionalized capsules display similar behavior, the amino-functionalized capsules maintain an endothermic interaction with ApoA-I. The large amount of heat absorbed during the titration suggests an entropy-driven interaction process. The independent binding fit (Table

4.1.1) confirms these findings, revealing an entropy gain contrasting the entropy loss in the other interactions studied. This entropy gain could partially be attributed to protein structural changes and unfolding during adsorption. An unfolded protein occupies a higher surface area on the capsule and, therefore, more water molecules of the hydration shell are released. However, the amount of heat generally needed for an unfolding of proteins[89, 90] is lower than the heat absorbed in this reaction. This suggests that there is another interaction process going on, which could involve the surfactant SDS. At least the surfactant does not seem to screen the functional groups of the capsule surfaces, since the endothermic reaction was only observed for the NH_2-functionalised capsule.

4.1.4 Dynamic light scattering (DLS) and zeta-potential analysis of capsules after protein adsorption

The adsorption of certain proteins can significantly influence the aggregation behavior of the nanocapsules. The functionalized HES capsules were further studied with regards to their aggregation behavior in human plasma, HSA and ApoA-I solutions via DLS. The analysis was performed according to the procedure described in chapter 3.2.2.[73] Data obtained from light scattering analysis of human plasma is shown in Figure 4.1.6.

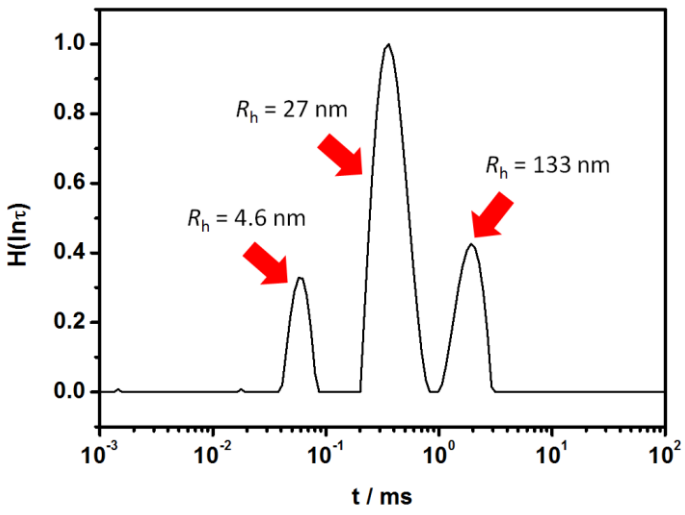

Figure 4.1.6 Distribution of relaxation times $H(\ln \tau)$ for plasma at a scattering angle of $\theta = 90°$ obtained by a CONTIN[58, 60] data analysis. The sample shows three independently diffusing species corresponding to the hydrodynamic radii indicated by the red arrows.[86] Published by The Royal Society of Chemistry.

As it can be seen, the CONTIN analysis shows three different diffusion processes, so that accordingly the autocorrelation function (ACF) of human plasma could be perfectly described by a sum of three exponentials (equation 4.1).

$$g_{1,P}(t) = a_{1,P}\, exp\left(-\frac{t}{\tau_{1,P}}\right) + a_{2,P}\, exp\left(-\frac{t}{\tau_{2,P}}\right) + a_{3,P}\, exp\left(-\frac{t}{\tau_{3,P}}\right) \qquad (4.1)$$

with the amplitudes a_i and the decay times τ_i.

The ACFs for the HES capsules alone can successfully be fitted by a sum of two exponentials (equation 4.2).

$$g_{1,C}(t) = a_{1,C}\, exp\left(-\frac{t}{\tau_{1,C}}\right) + a_{2,P}\, exp\left(-\frac{t}{\tau_{2,C}}\right) \qquad (4.2)$$

Knowing the ACF of human plasma and the respective HES capsule, the correlation function of the plasma capsule mixtures could be analyzed. If no aggregation were to occur, the resulting ACF of the plasma capsule mixture would correlate to the force fit (see equation 3.13, methods section). However, interactions of HES capsules with plasma components resulted in larger sizes than the plasma components and HES capsules themselves; consequently, the ACFs could not be described by the force fit. The fit needed to be modified by an additional, longer ACF relaxation time related to the size of the formed structures (equation 3.14, methods section).

The multicomponent analyses of the HSA and ApoA-I capsule mixtures were performed accordingly. The exemplary analysis of the ACF $g_1(t)$ of the mixture of non-functionalized HES capsules with human plasma is shown in Figure 4.1.7 A, while the ACFs for functionalized capsules can be seen in Figure 4.1.8 and 4.1.9. The force fit (sum of individual components) did not describe the data correctly. In contrast, the fit including an additional aggregate component was suitable for the capsule/plasma mixture. The fitting procedure for each angle produced the corresponding hydrodynamic radius R_h shown in Figure 4.1.7 B. From the extrapolated diffusion coefficients the z-averaged hydrodynamic radius $\langle 1/R_h \rangle_z^{-1}$ was calculated by the application of Stokes law and can be found in Table 4.1.2.

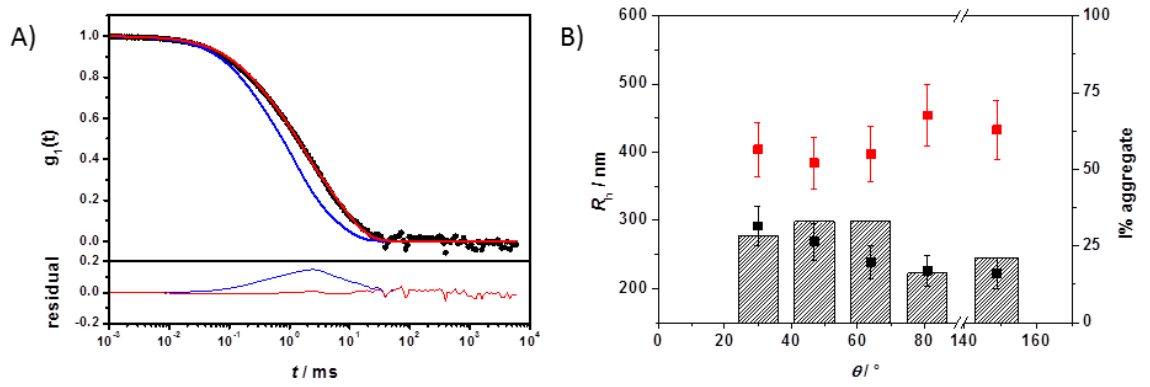

Figure 4.1.7 A) Upper graph: Autocorrelation function $g_1(t)$ (black circles ●) of non-functionalized HES capsules mixed with plasma at θ = 64°. The blue line (–) represents the forced fit composed of the sum of the individual components whereas the red line (–) represents the fit with an additional aggregation function. Lower graph: Corresponding residuals resulting from the difference between the data and the two fits. B) Hydrodynamic radii of pure non-functionalized HES capsules (black squares ■) and of the aggregate formed in plasma (red squares ■). Striped columns represent the intensity fraction of aggregates in the mixture.[86] Published by The Royal Society of Chemistry.

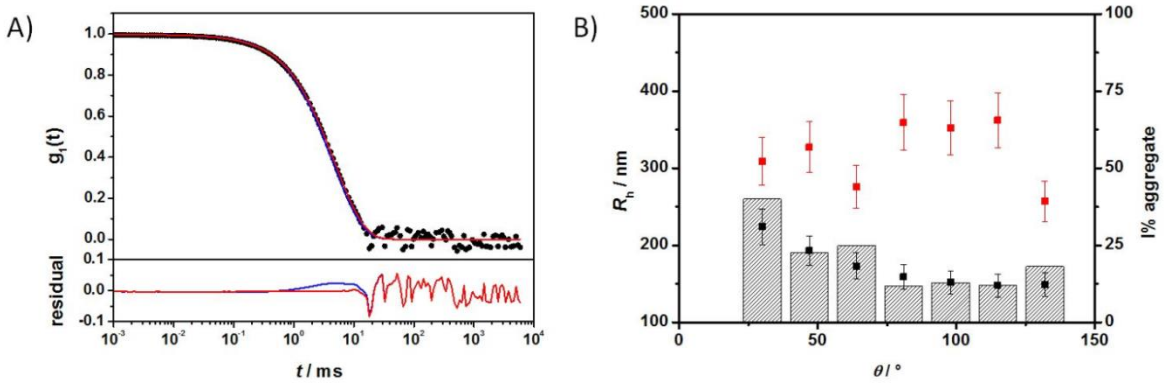

Figure 4.1.8 A) Upper graph: Autocorrelation function $g_1(t)$ (black circles ●) of COOH-functionalized HES capsules mixed with plasma at θ = 64°. Lower graph: Corresponding residuals resulting from the difference between the data and the two fits. B) Hydrodynamic radii of pure COOH-functionalized HES capsules (black squares ■) and of the aggregate formed in plasma (red squares ■). Striped columns represent the intensity fraction of aggregates in the mixture.[86] Published by The Royal Society of Chemistry.

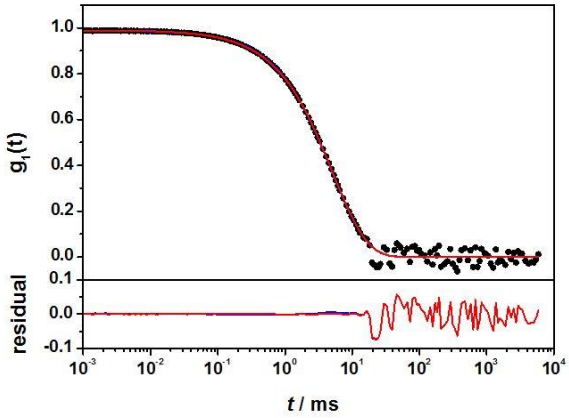

Figure 4.1.9 Upper graph: Autocorrelation function $g_1(t)$ (black circles ●) of NH_2-functionalized HES capsules mixed with plasma at θ = 64°. Lower graph: Corresponding residuals resulting from the difference between the data and the two fits.[86] Published by The Royal Society of Chemistry.

Table 4.1.2 Sizes, aggregate intensity fractions and zeta-potential of HES capsules after interaction with plasma.[86] Published by The Royal Society of Chemistry.

capsule	No protein		Plasma		
	R_h / nm	ζ-potential [1] / mV	$R_{h,Agg}$ / nm	$I\%_{Agg}$ [2]	ζ-potential[1] / mV
HES	275 ± 26	-34 ± 3	390 ± 39	33	-22 ± 9
HES-COOH	200 ± 20	-34 ± 3	319 ± 32	25	-13 ± 5
HES-NH_2	256 ± 26	-27 ± 3	-	-	-11 ± 4

[1] ζ-potential at pH 7 in 0.001 M KCl solution

[2] Intensity fractions of the aggregates ($I\%_{Agg}$) are exemplarily given for a scattering angle of 64°.

Figure 4.1.7 demonstrates the increase of R_h, which occurs after interaction with plasma. The size increase of around 100 nm for non-functionalized capsules is too small to be caused by aggregation between several capsules, so it is attributed to coating with plasma proteins. Additionally, the intensity contribution of the aggregates (see Table 4.1.2) was calculated and is also shown in Figure 4.1.7 B. The fraction of the new species (protein-coated capsules) being formed is significant in comparison to the fraction of pure capsules. The remaining fraction of the capsules in the mixture can be attributed to the natural distribution of the thickness of the protein corona and the polydispersity of capsules and aggregates. As the applied method is highly sensitive for the detection of aggregates with sizes

larger than the largest size present in the pure components solutions, changes within the size distribution of plasma and capsules are only detectable if the amplitudes (i.e. the intensity fractions) of the newly formed sizes are sufficiently large (and thus detectable by DLS). Typically, intensity fractions between 3% (for sizes larger than the largest component in the mixture) and 20% (for sizes in the same size range of the mixture components) of newly formed particles are necessary in order to become detectable by the described fitting procedure.[91] Consequently, small capsules with a thin protein corona are not recognized as aggregates.

The DLS experiments were repeated after 24 h of incubation time to check for any changes related to the protein adsorption kinetics. However there was no significant difference found in the aggregation behavior. According to reports in the literature, the composition of the protein corona changes quantitatively but not qualitatively.[16] Therefore, it is likely that slight changes in the protein corona compositions of the mixtures with plasma cannot be detected with this type of analysis.

Additionally, the zeta-potential was measured for all samples before and after the mixture with proteins (see Table 4.1.2) to monitor the change of the capsules' surface charge after protein adsorption.

The average size increase of around 120 nm for the non- and carboxy-functionalized capsules coated with plasma (Figure 4.1.8) and the significant intensity fraction of the resulting larger structures can be attributed to the formation of a protein corona. For the amino-functionalized capsules no component larger than the components of the mixture was found via DLS (Figure 4.1.9), even though the ITC measurements suggested adsorption processes similar to the other capsules. The DLS results are in agreement with previous studies of amino-functionalized nanoparticles that did not show any aggregate formation.[11] It has to be noted that the aggregation behavior cannot be attributed to a positive overall particle charge due to the amino functionalization as the amino-functionalized particles observed a negative zeta potential because of their redispersion in water with SDS. Concerning the difference between the findings from ITC and DLS, it is important to note that the samples taken from ITC measurements were diluted for the DLS experiments (see Experimental section). While a high concentration is needed to obtain a sufficient signal in ITC, it has to be decreased for light

scattering due to the high turbidity of the capsules above a certain concentration. Light scattering measurements would then be complicated by multiple and back scattering artifacts.[92, 93] Therefore, it is possible that a formed protein corona changes upon dilution due to concentration dependencies. The soft protein corona is especially affected because of the high protein exchange rates reported in literature.[65] Nevertheless, the zeta-potential for all three surface functionalizations was increased after protein adsorption. This suggests coverage with proteins, as the negative charges from SDS are shielded, or even replaced, by proteins with a lower negative charge compared to their volume or positive charge.

The same analysis was performed with HSA and yielded results similar to the plasma measurements (see Figures 4.1.10 - 4.1.12, Table 4.1.3).

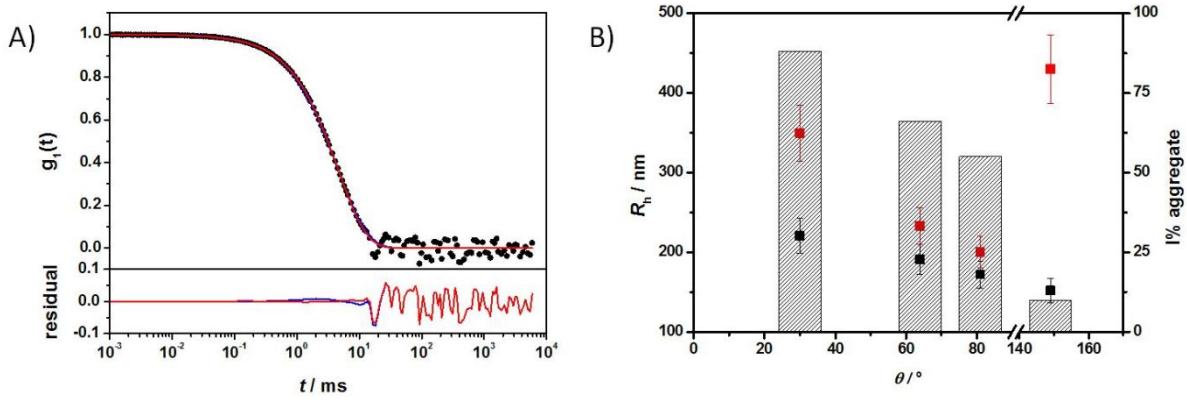

Figure 4.1.10 A) Upper graph: Autocorrelation function $g_1(t)$ (black circles ●) of non-functionalized HES capsules mixed with HSA solution at θ = 64°. Lower graph: Corresponding residuals resulting from the difference between the data and the two fits. B) Hydrodynamic radii of pure non-functionalized HES capsules (black squares ■) and of the aggregate formed in plasma (red squares ■). Striped columns represent the intensity fraction of aggregates in the mixture.[86] Published by The Royal Society of Chemistry.

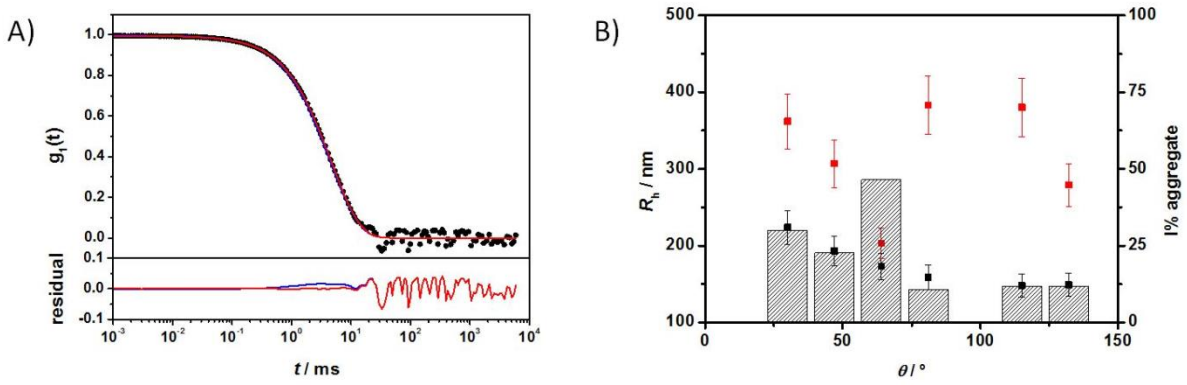

Figure 4.1.11 A) Upper graph: Autocorrelation function $g_1(t)$ (black circles ●) of COOH-functionalized HES capsules mixed with HSA solution at θ = 64°. Lower graph: Corresponding residuals resulting from the difference between the data and the two fits. B) Hydrodynamic radii of pure COOH-functionalized HES capsules (black squares ■) and of the aggregate formed in plasma (red squares ■). Striped columns represent the intensity fraction of aggregates in the mixture.[86] Published by The Royal Society of Chemistry.

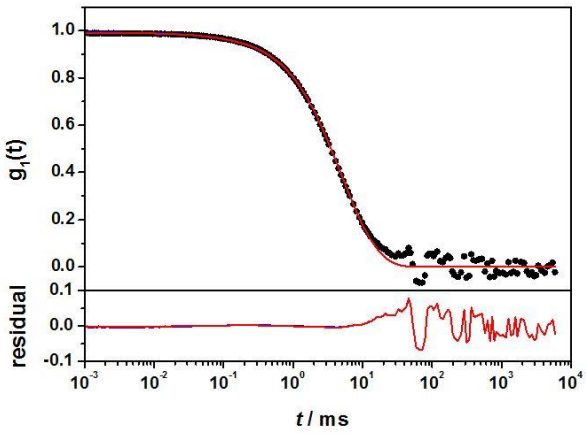

Figure 4.1.12 Upper graph: Autocorrelation function $g_1(t)$ (black circles ●) of NH_2-functionalized HES capsules mixed with HSA solution at θ = 64°. Lower graph: Corresponding residuals resulting from the difference between the data and the two fits.[86] Published by The Royal Society of Chemistry.

Table 4.1.3 Sizes, aggregate intensity fractions and zeta-potential of HES capsules after interaction with HSA.[86] Published by The Royal Society of Chemistry.

capsule	No protein		HSA		
	R_h / nm	ζ-potential [1] / mV	$R_{h,Agg}$ / nm	$I\%_{Agg}$ [2]	ζ-potential / mV [1]
HES	275 ± 26	-34 ± 3	347 ± 35	28	-18 ± 1
HES-COOH	200 ± 20	-34 ± 3	352 ± 35	47	-15 ± 4
HES-NH_2	256 ± 26	-27 ± 3	-	-	-10 ± 1

[1] ζ-potential at pH 7 in 0.001 M KCl solution

[2] Intensity fractions of the aggregates ($I\%_{Agg}$) are exemplarily given for a scattering angle of 64°.

This reaffirms the conclusion drawn from the ITC experiments that HSA is adsorbed to the capsule surface with a high stoichiometry and thus leads to the formation of a thick soft protein corona. The combination of these results with the depletion of HSA in the SDS-PAGE identifies HSA as a soft corona protein. Again, no additional aggregates were found in the sample containing amino-functionalized capsules (Figure 4.1.12). Also, the zeta-potential increase suggests the coverage with proteins. In contrast to plasma and HSA, no additional aggregates were formed from the interaction of all capsule types with ApoA-I (see Figures 4.1.13 – 15, Table 4.1.4).

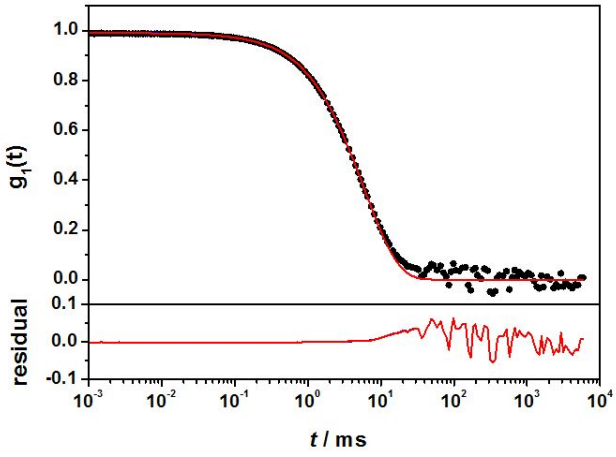

Figure 4.1.13 Upper graph: Autocorrelation function $g_1(t)$ (black circles ●) of non-functionalized HES capsules mixed with ApoA-I solution at θ = 64°. Lower graph: Corresponding residuals resulting from the difference between the data and the two fits.[86] Published by The Royal Society of Chemistry.

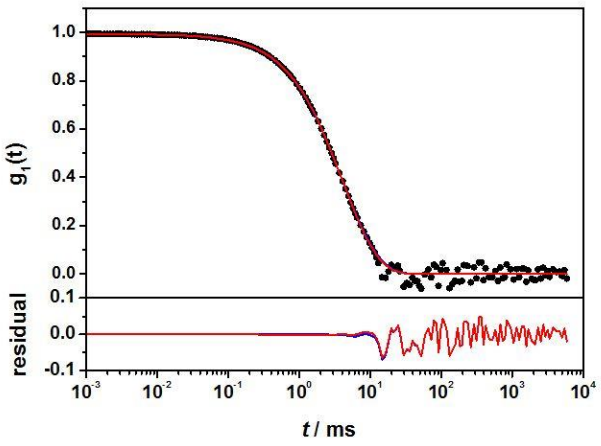

Figure 4.1.14 Upper graph: Autocorrelation function $g_1(t)$ (black circles ●) of COOH-functionalized HES capsules mixed with ApoA-I solution at θ = 64°. Lower graph: Corresponding residuals resulting from the difference between the data and the two fits.[86] Published by The Royal Society of Chemistry.

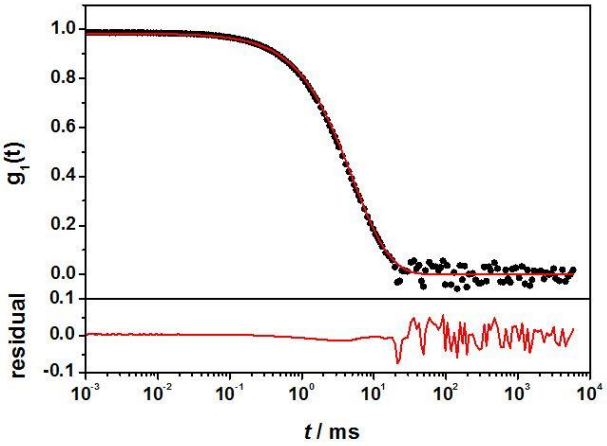

Figure 4.1.15 Upper graph: Autocorrelation function $g_1(t)$ (black circles ●) of NH_2-functionalized HES capsules mixed with ApoA-I solution at θ = 64°. Lower graph: Corresponding residuals resulting from the difference between the data and the two fits.[86] Published by The Royal Society of Chemistry.

Table 4.1.4 Sizes, aggregate intensity fractions and zeta-potential of HES capsules after interaction with ApoA-I.[86] Published by The Royal Society of Chemistry.

capsule	No protein		ApoA-I	
	R_h / nm	ζ-potential [1] / mV	$R_{h,Agg}$ / nm	ζ-potential[1] / mV
HES	275 ± 26	-34 ± 3	-	-7 ± 6
HES-COOH	200 ± 20	-34 ± 3	-	-8 ± 7
HES-NH_2	256 ± 26	-27 ± 3	-	-18 ± 8

[1] ζ-potential at pH 7 in 0.001 M KCl solution

[2] Intensity fractions of the aggregates ($I\%_{Agg}$) are exemplarily given for a scattering angle of 64°.

This agrees with the ITC results, given that few molecules (around 10 ApoA-I molecules per capsule) adsorbed to the capsule surface. The formation of aggregates was not expected because the size increase due to formation of an ApoA-I monolayer would not be greater than 8 nm in radius. The size of the protein ($R_h \approx 3.8$ nm)[94] is only around 1.5% of the capsule size, so the size change is in the experimental error of the light scattering experiment. These results in combination with the high binding affinity for ApoA-I (Table 4.1.1) classify ApoA-I as a hard corona protein.

4.1.5 Conclusion

There is currently a major gap in knowledge with regards to a defined physicochemical characterization of the protein corona that forms on a nanomaterial's surface once it enters the blood stream. Effects of the preparation procedure required for different techniques are unknown and with that the understanding of the true biological identity is still challenging. In this chapter, different techniques to obtain complementary information about the protein corona of HES nanocapsules were applied. For the first time data concerning the hard protein corona derived from SDS-PAGE and protein quantification with information from ITC and DLS about the soft corona was compared. It was demonstrated that ITC and DLS are valuable methods to investigate the soft protein corona as they allow characterizing particles in the incubation medium. This is in stark contrast to SDS-PAGE and protein assays, which require particle extraction prior to characterization. With a combination of these techniques we have been able to compare the characteristics of the hard and soft corona and at the same time detect differences in the adsorption behaviors of single proteins. For future investigations it still remains crucial to obtain a better understanding of the soft corona. The true biologically relevant corona composition is still not clear and most probably not only involves the hard protein corona in the case of low-affinity nanocapsules.

4.2 Influence of surfactant type and concentration on albumin adsorption on model nanoparticles

The work described in this chapter (4.2.1 – 4.2.3 partially) is submitted as a communication manuscript.

It has been illustrated in literature that the surface chemistry of nanomaterials strongly influences the adsorption processes, but the different factors remain poorly understood.[95] In previous studies, nanoparticles with different covalently linked functional groups were synthesized to evaluate the various structural effects.[8, 10, 16] This is especially important for all kinds of nanoparticles since certain functional groups are needed to stabilize them in aqueous solution. Aggregation of the nanoparticles can be prevented by either electrostatic or steric stabilization (see Theory). Depending on the synthesis procedure, the stabilizing groups do not necessarily have to be covalently bound but can also be physisorbed, e.g. by the use of surfactants.

Surfactants have to be taken into account in the particle-protein interactions, since they are both commonly utilized and actively influence the surface chemistry of nanoparticles. Isolated surfactants interact with proteins, as demonstrated in analytical techniques such as SDS-PAGE.[96] Those interactions are mostly unspecific, meaning that all proteins form complexes with a given surfactant; but in some cases they are limited to certain single proteins e.g. as reported for CHAPS[b] with ApoA-I.[97] The influence of different stabilization methods has been evaluated previously,[98, 99] but currently there is no quantitative description of the effect on protein adsorption available.

4.2.1 Preparation of suitable model nanoparticles with different surfactant amounts

In this chapter, two types of model polystyrene (PS) nanoparticles with different stabilizing agents were synthesized via miniemulsion polymerization,[100, 101] to study their interaction with proteins (Figure 4.2.1). One ionic (SDS) and one nonionic PEG-based (Lutensol AT50) surfactant were chosen as representative surfactants. SDS features a negatively charged headgroup and therefore provides an electrostatic repulsion between particles (see Figure 4.2.2). Lutensol AT50 (Lut) is a polymeric surfactant composed of a C16-C18 hydrophobic saturated fatty alcohol and a hydrophilic poly(ethylene glycol) (PEG) block (see Figure 4.2.2). Therefore Lut works as a steric stabilization agent. Additionally both surfactants differ in their hydrophilic - lipophilic balance (HLB) value.

[b] 3-((3-Cholamidopropyl)dimethylammonio)-1-propanesulfonate

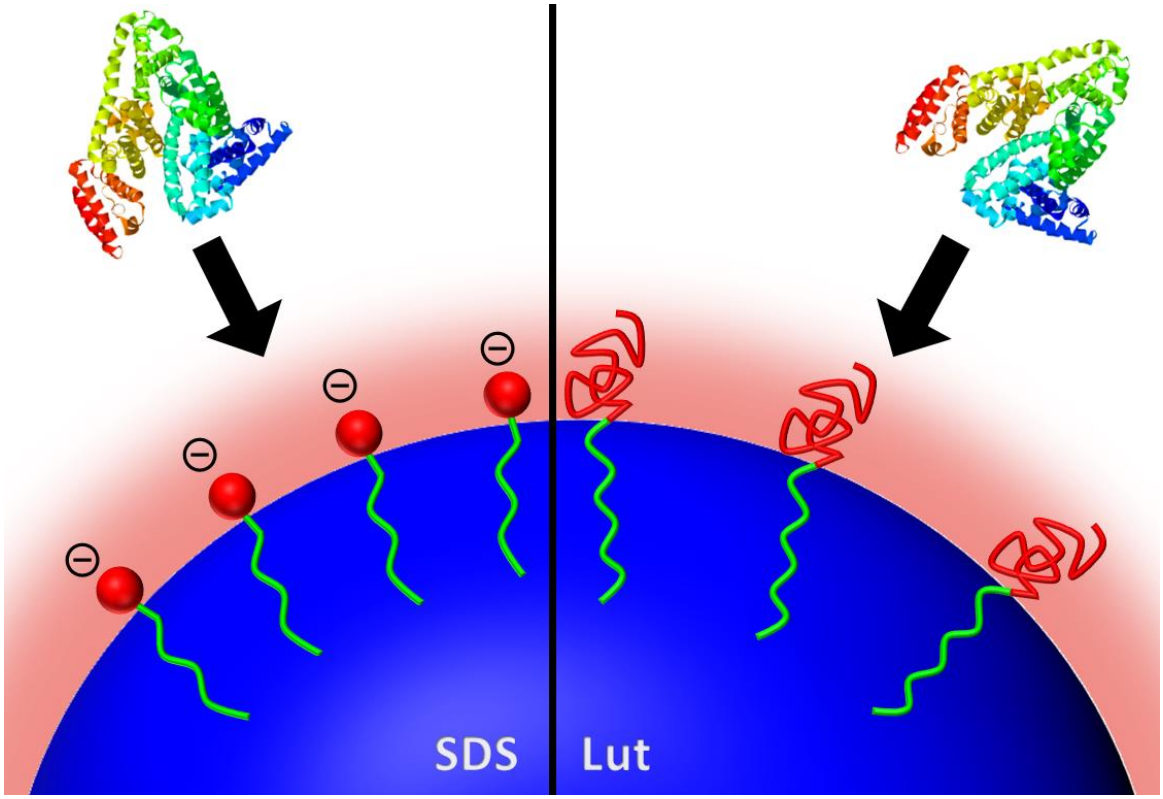

Figure 4.2.1 Schematic representation of the model nanoparticles stabilized by different surfactants, to study interaction with HSA.

surfactant	structure	Hydrophilic-Lipophilic Balance (HLB)
SDS	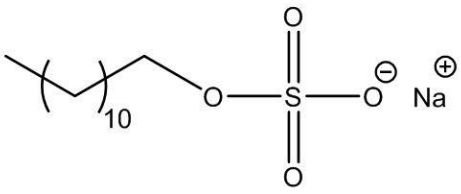	40
Lutensol AT50	 x = 15 - 17	18

Figure 4.2.2 Chemical structures and corresponding HLB values of SDS and Lut calculated after Davies[102] and Griffin[103].

The nanoparticles were prepared according to previously published procedures.[100] To be able to compare different amounts of surfactant present at the particle surfaces, an aliquot of each sample was thoroughly purified. Standard procedures for each surfactant type were used (dialysis for SDS and centrifugation for Lut - details see Experimental). However, the usual purification time was extended to ensure that the minimal surfactant amount needed for stable particles was obtained. As a control, the surface tension of the air-water interface of each sample was measured and compared to the value for pure water (72.75 $mN \cdot m^{-1}$) (surface tension measurements performed by Elke Muth).[104] For the nanoparticles stabilized with SDS it was possible to obtain a surface tension of 72.79 ± 0.10 $mN \cdot m^{-1}$ (1.3% surface coverage). In the case of Lut stabilized particles, the highest surface tension reached was 67.83 $mN \cdot m^{-1}$. Further removal of the surfactant results in aggregate formation, indicating that the concentration of Lutensol was too low to stabilize all particles. Those highly purified samples (see Figure 4.2.3) were taken as reference samples with minimal surfactant left, so for the following experiments they were considered 'surfactant-free'. After purification defined amounts of each surfactant were added again to the corresponding samples (see Figure 4.2.4) (sample purification and preparation by James Schwabacher, MPIP Mainz, Germany).

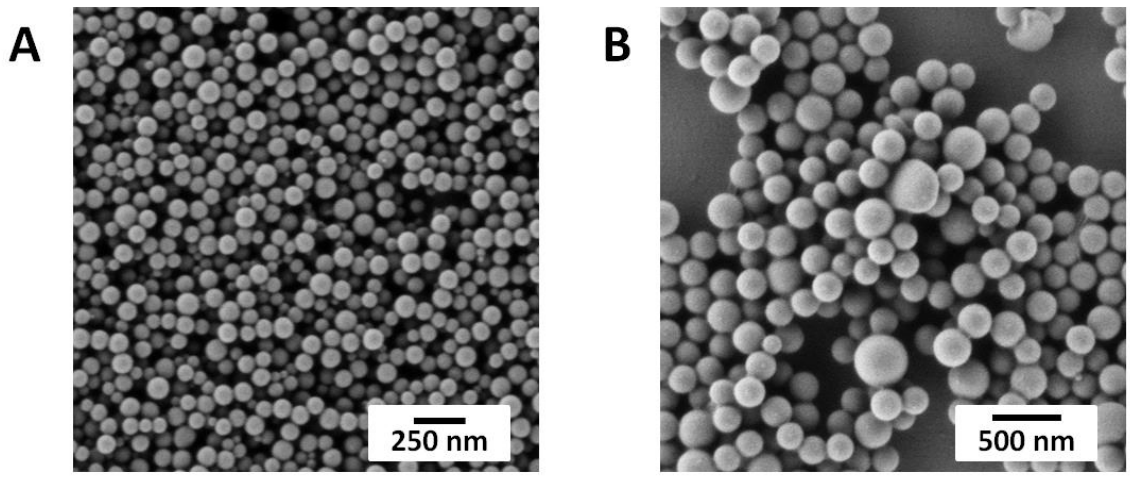

Figure 4.2.3 Scanning electron microscopy (SEM) images of A) SDS and B) Lut stabilized samples after purification taken by Gunnar Glaßer, MPIP Mainz, Germany.

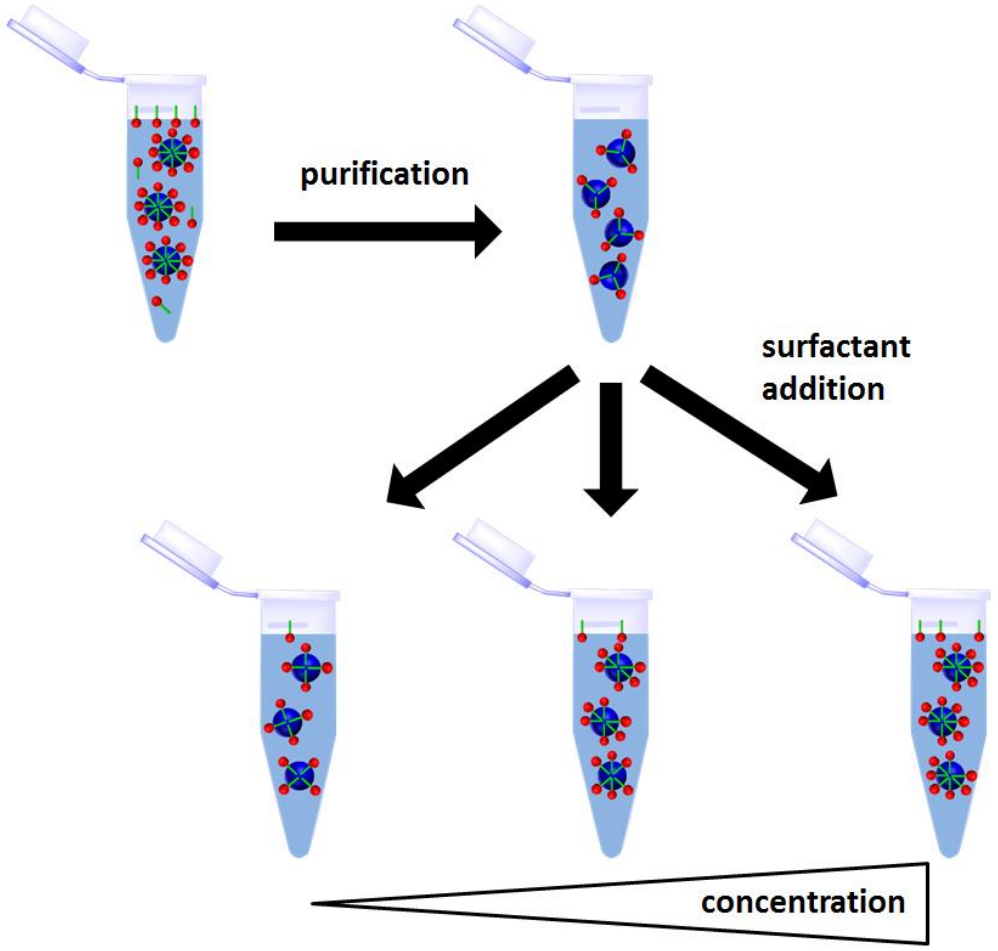

Figure 4.2.4 Sample preparation scheme for nanoparticles with different surfactant concentrations.

Using this procedure, five samples with different surfactant concentrations were obtained for both nanoparticle batches. All samples were characterized with DLS to ensure that the change in surfactant concentration did not influence the size or size distribution of the particles significantly (see Figures 4.2.5 and 4.2.6).

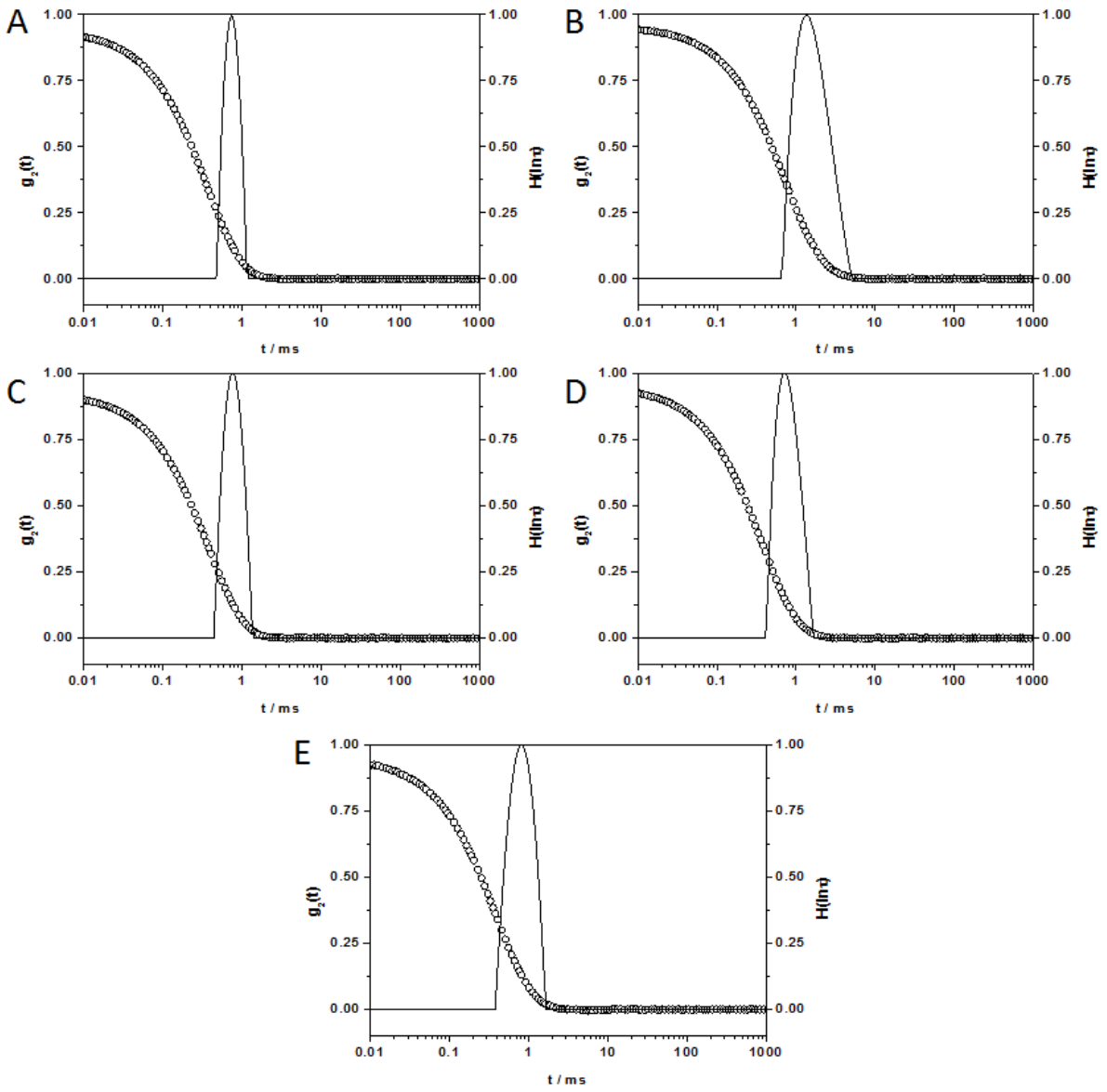

Figure 4.2.5 Intensity Autocorrelation functions $g_2(t)$ (open circles ○) and distribution of relaxation times H(ln τ) resulting from a CONTIN[60] fit (straight lines−) for SDS-stabilized nanoparticles at a scattering angle of 90° (q = 0.014 nm^{-1}): A) purified PS-NP, B) 0.20 mM SDS added, C) 0.41 mM SDS added, D) 0.67 mM SDS added, E) unpurified PS-NP.

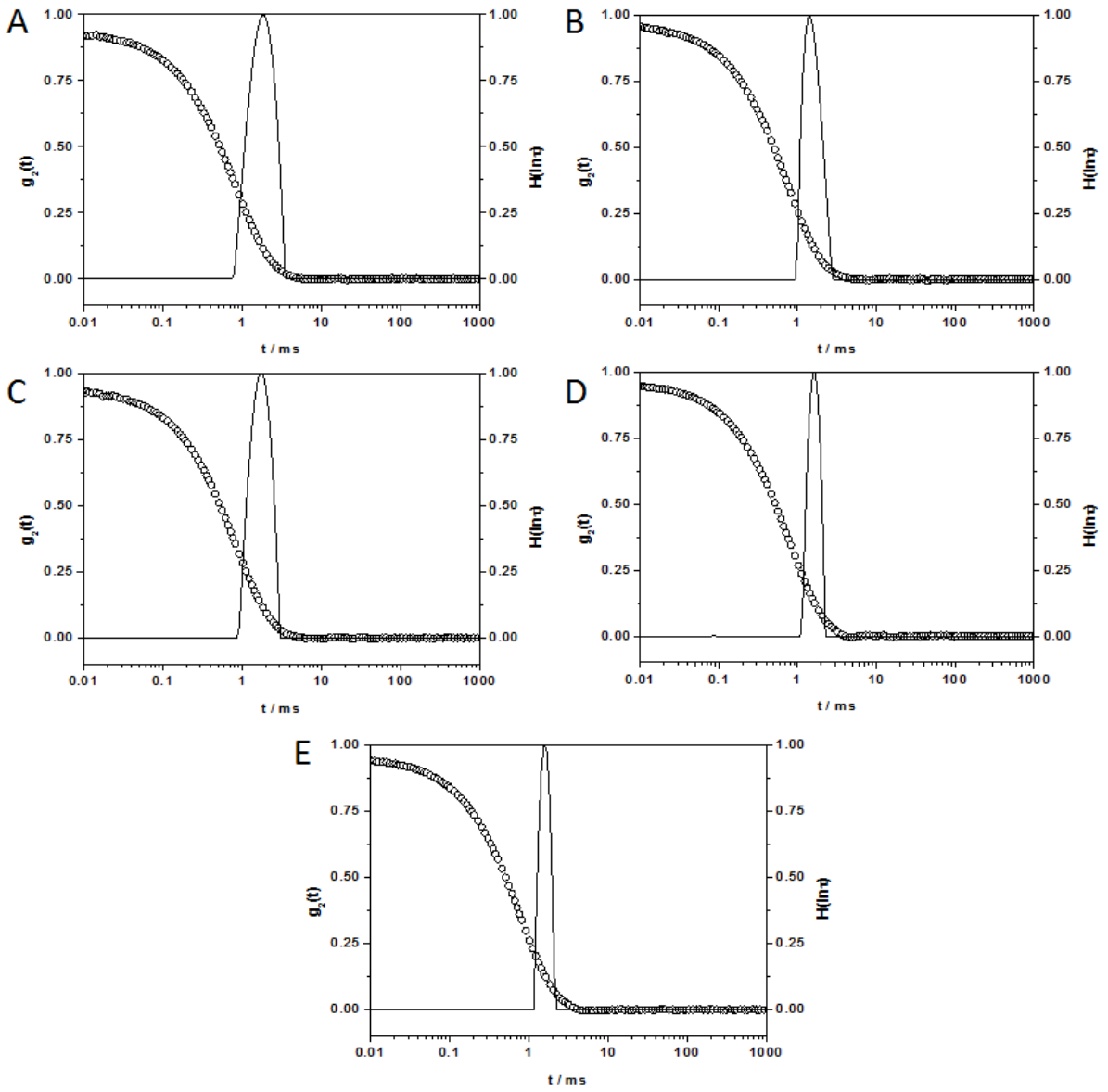

Figure 4.2.6 Intensity Autocorrelation functions $g_2(t)$ (open circles ○) and distribution of relaxation times H(ln τ) resulting from a CONTIN[60] fit (straight lines−) for Lut-stabilized nanoparticles at a scattering angle of 90° (q = 0.014 nm^{-1}): A) purified PS-NP, B) unpurified PS-NP, C) 0.10 mM Lutensol added, D) 0.20 mM Lutensol added, E) 0.34 mM Lutensol added.

Additionally, the samples were characterized with regards to surface tension and zeta potential to ensure that different surface coverages of surfactant were obtained. When SDS is added to pure water in the used concentrations it significantly reduces the surface tension, while there is only a small change detectable when particles are present in solution (see Figure 4.2.7). It can be concluded that SDS adsorption to the

nanoparticles' surface is proportional to the accumulation at the air-water interface. However the equilibrium between both interfaces is shifted towards the nanoparticle surface. When Lut is added to water in small concentrations it immediately reduces the surface tension at the air-water interface, even when nanoparticles are present. In summary, additionally added SDS covers the particle surfaces and air-water interface at the same time and the number of SDS molecules per particle can be calculated from the surface tension, as previously reported.[100] In the case of Lutensol, this is not possible due to the reduction of the surface tension with particles present. It could be the case that small impurities are present in the commercially available Lut, which then preferentially accumulate at the air-water interface.

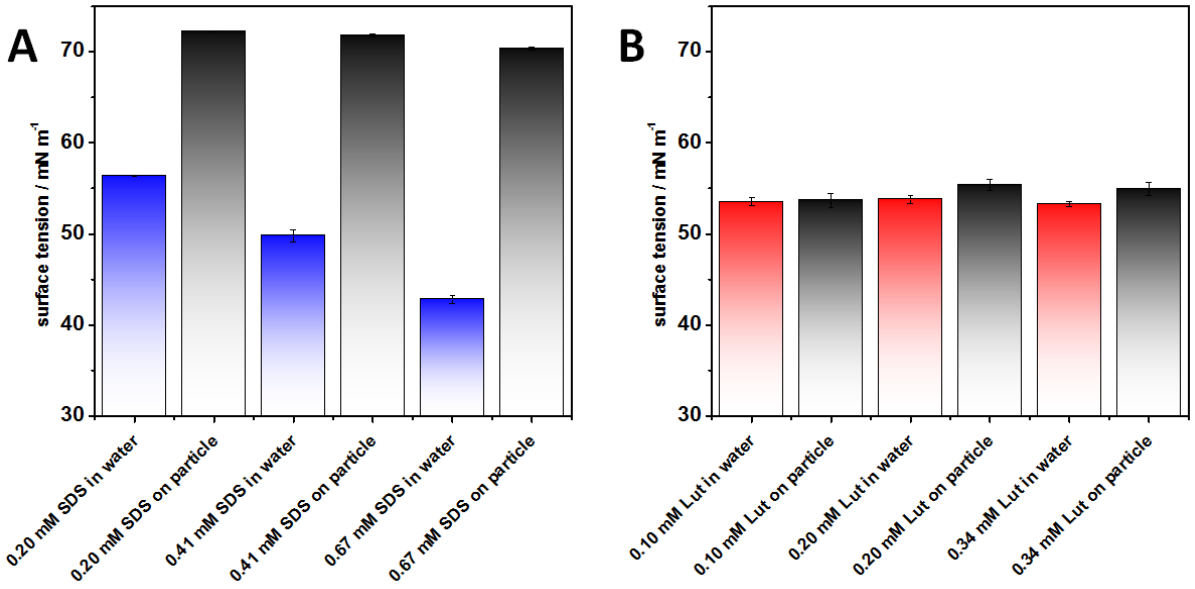

Figure 4.2.7 Comparison between surface tension measured for samples with subsequently added surfactant and aqueous solutions containing the same surfactant concentrations: A) SDS samples B) Lut samples.

To verify that the nanoparticles present different amounts of surfactant on their surface, the zeta potentials of all particles was determined. The measured zeta potentials for each nanoparticle sample are displayed in Figure 4.2.8 and show that indeed all particles exhibit different coverages of surfactant. All determined particle characteristics are finally summed up in Table 4.2.1.

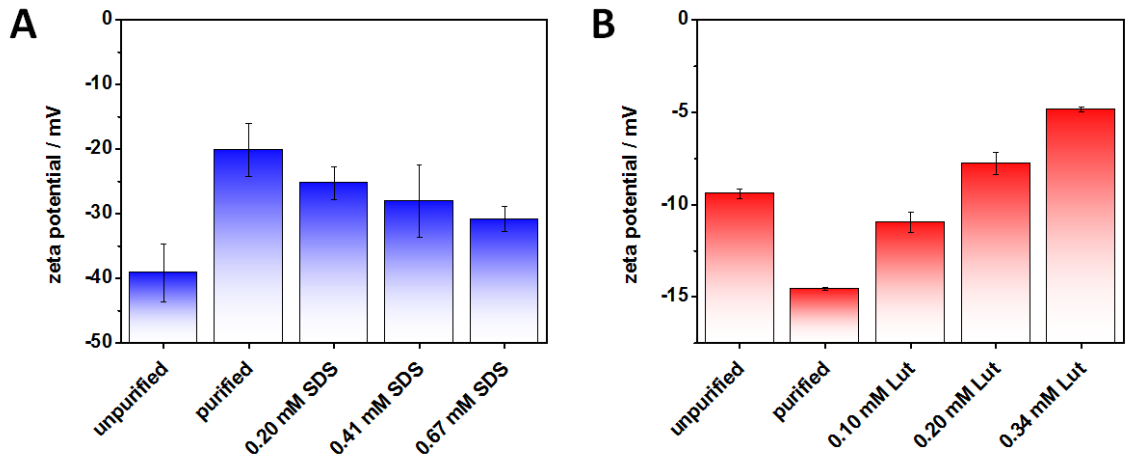

Figure 4.2.8 Zeta potential results of A) SDS stabilized and B) Lut stabilized PS-NPs.

Table 4.2.1 Characterization of nanoparticle samples.

sample		surface tension / $mN \cdot m^{-1}$	ζ-potential / mV	R_h / nm	surfactant molecules per particle[a]	surface coverage with surfactant / %
PS (SDS)	purified	72.79 ± 0.10	-20 ± 4	59 ± 6	min (≈ 0)[b]	
	0.20 mM	72.25 ± 0.05	-25 ± 2	55 ± 6	770	1.3
	0.40 mM	71.78 ± 0.18	-28 ± 5	55 ± 6	1250	2.1
	0.67 mM	70.37 ± 0.18	-31 ± 2	60 ± 6	3450	5.8
	unpurified	67.70 ± 0.03	-39 ± 4	61 ± 6	7900	13.3
PS (Lut)	purified	67.83 ± 0.15	-14.6 ± 0.1	127 ± 13	-	
	unpurified	52.38 ± 0.02	-9.4 ± 0.3	112 ± 11	-	
	0.10 mM	53.70 ± 0.76	-11.0 ± 0.6	126 ± 13	-	
	0.20 mM	55.41 ± 0.61	-7.8 ± 0.6	122 ± 12	-	
	0.34 mM	54.94 ± 0.77	-4.8 ± 0.1	118 ± 12	-	

[a] calculated from surface tension, assuming an SDS area per molecule of 0.62 nm^2 for a dense SDS layer.[105]
[b] below detection limit.

4.2.2 Calorimetric analysis of the surfactant influence on binding parameters

To evaluate the influence of both surfactant type and concentration on the interaction with blood plasma proteins, HSA was chosen as a representative protein for binding studies. Here, ITC was used to determine parameters like binding affinity, stoichiometry and binding enthalpy of HSA-nanoparticle interactions. Each nanoparticle sample was titrated with an aqueous solution of HSA (raw data see Figures 4.2.9 and 4.2.10) and the resulting heats were analyzed with an independent binding model. For reference the pure surfactants were each titrated with HSA (Figure 4.2.11). The obtained

binding parameters for the different surfactant types and concentrations are summarized in Table 4.2.2.

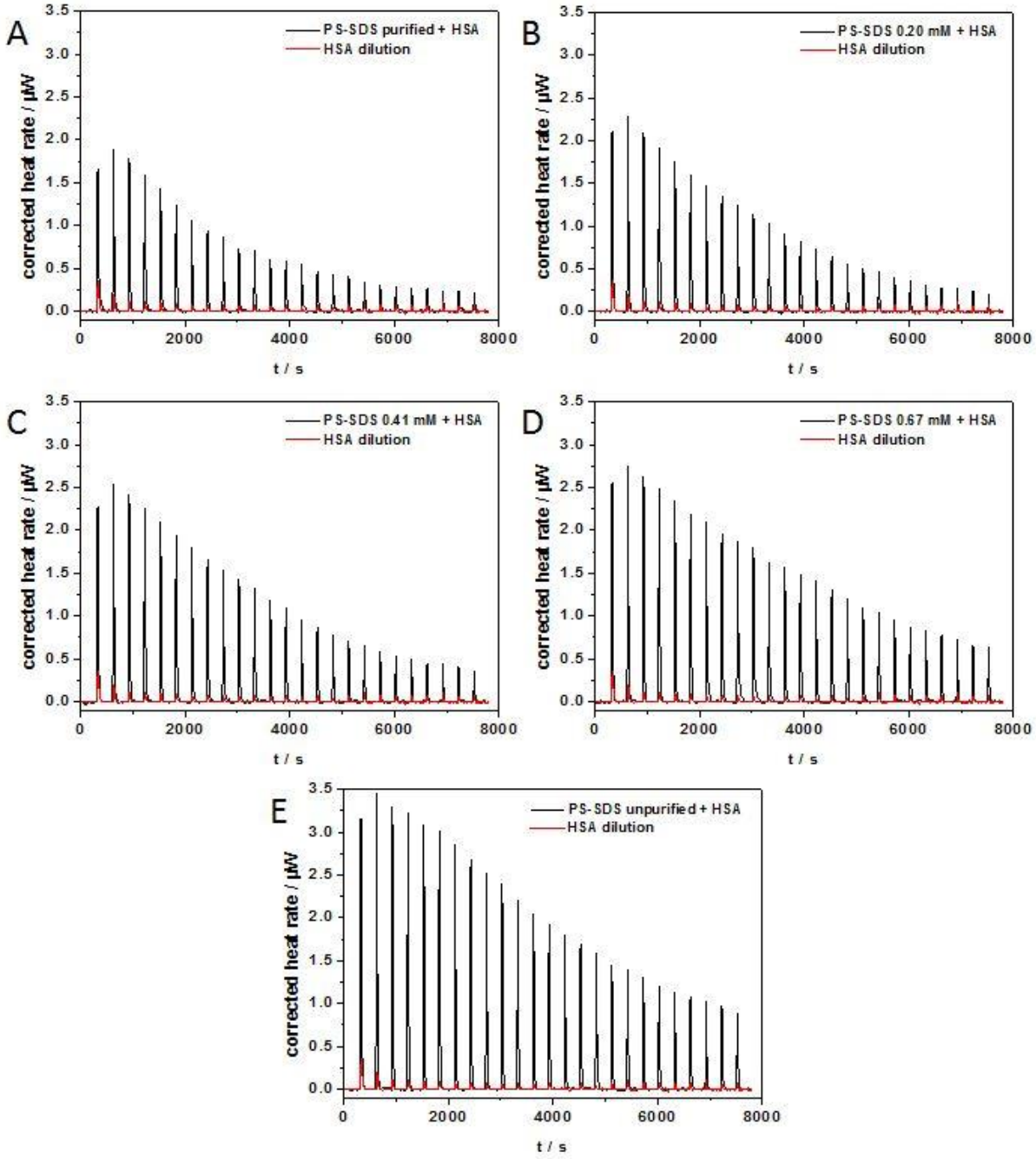

Figure 4.2.9 ITC raw data of SDS-stabilized PS-NP titrated with HSA: baseline corrected heat rates of A) purified PS-NP, B) 0.20 mM SDS added, C) 0.41 mM SDS added, D) 0.67 mM SDS added, E) unpurified PS-NP samples (black lines −) and the corresponding heat rate of the HSA dilution for reference (red lines −). The particle concentration ($8.9 \cdot 10^{-6}$ mM) as well as the HSA concentration (0.15 mM) were kept constant for all titrations.

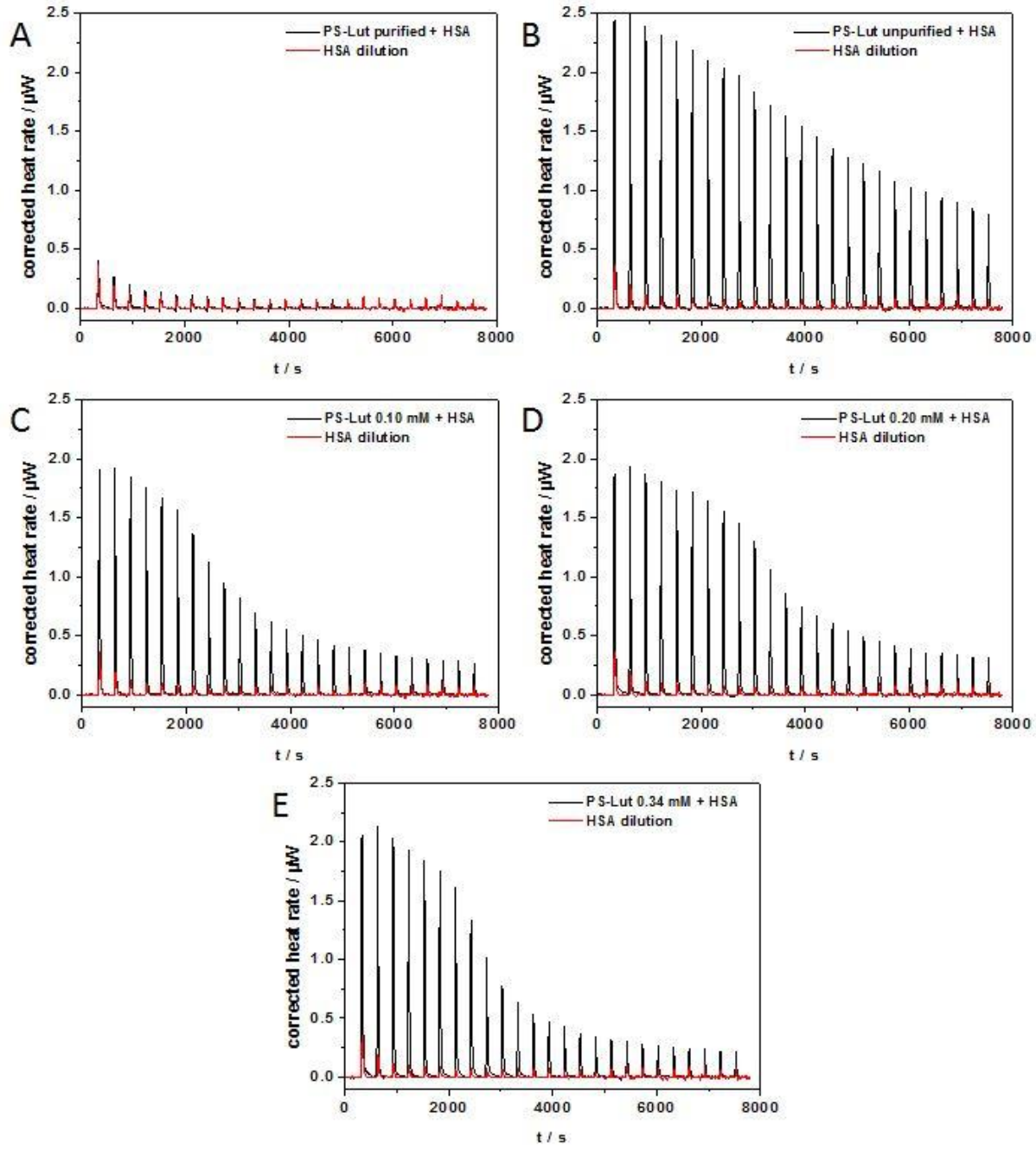

Figure 4.2.10 ITC raw data of Lutensol-stabilized PS-NP titrated with HSA: baseline corrected heat rates of A) purified PS-NP, B) unpurified PS-NP, C) 0.10 mM Lutensol added, D) 0.20 mM Lutensol added, E) 0.34 mM Lutensol added samples (black lines −) and the corresponding heat rate of the HSA dilution for reference (red lines −). The particle concentration was adjusted for each sample (see Experimental section), while the HSA concentration (0.15 mM) was kept constant for all titrations.

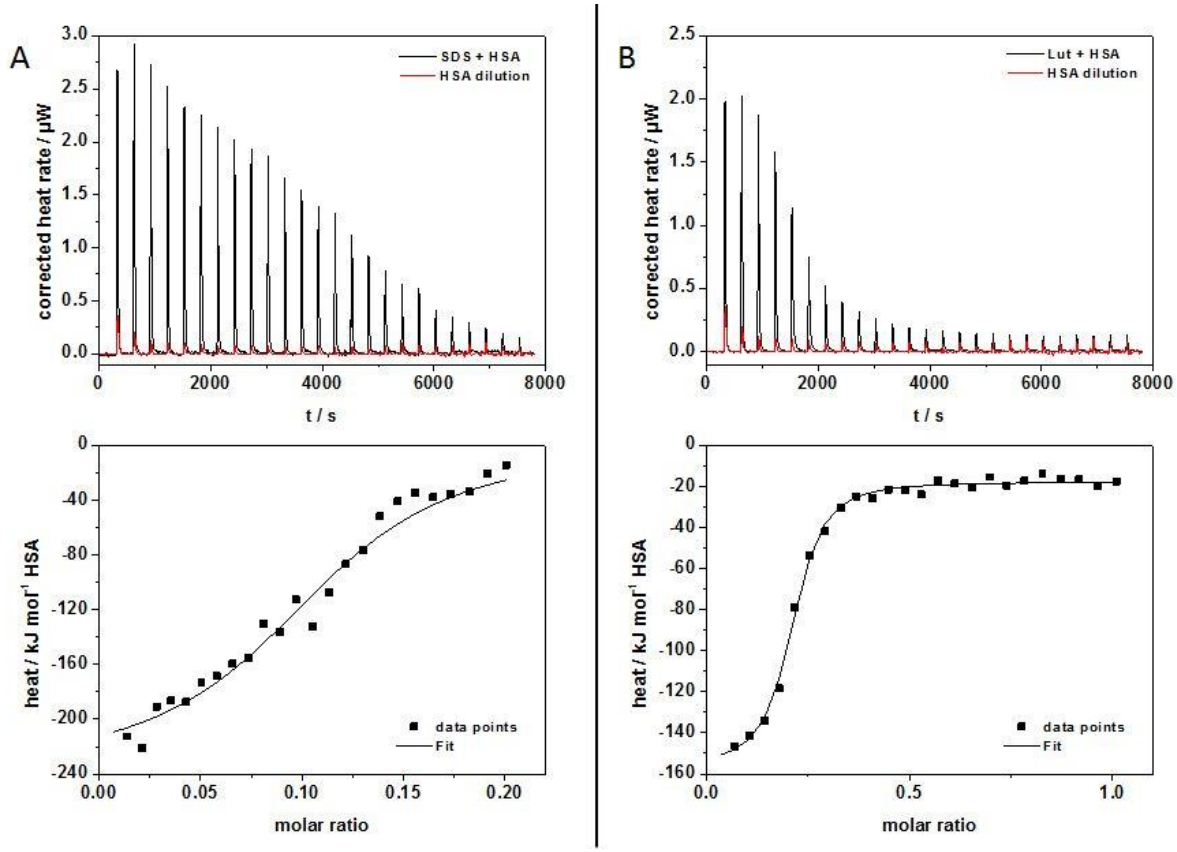

Figure 4.2.11 ITC raw data (upper graphs) and integrated normalized heats (lower graphs) of pure surfactants titrated with HSA: A) SDS, B) Lutensol.

For both surfactant types it can be observed that the surfactant concentration significantly influences the binding parameters (see Figure 4.2.12). Interestingly, the trends are quite different whether SDS or Lut is used. The SDS samples with subsequently increased surfactant concentration exhibit binding parameters between the 'surfactant-free' and the unpurified samples. This is expected since the unpurified sample contains the highest SDS concentration as obtained from the synthesis (13.3% surface coverage of the particles). The binding enthalpy and the number of interacting proteins per particle increase with increasing SDS content. In contrast, the calculated binding affinity decreases and approaches the value for pure SDS binding to HSA. This finding indicates that even though the particle surface is not completely covered by SDS it dominates the interaction with HSA over the initial surface material (PS). Prior research reports that, in an initial step, about 10 SDS molecules bind to positively charged amino groups of the HSA lysine residues.[106, 107] This corresponds to the reaction of SDS and HSA monitored in ITC, where a stoichiometry of 8-9 SDS molecules per protein is obtained. At much higher surfactant concentrations (around 96 molecules per HSA) a

second binding step was observed for different alkyl sulfate homologs (C8-C12) and attributed to hydrophobic interactions between the alkyl chain of the surfactant and exposed hydrophobic amino acid residues.[106] Most likely, the SDS – HSA interaction at the nanoparticle surface consists of electrostatic interactions corresponding to the first binding process described. Our most important finding, though, is that a miniscule change in the number of SDS molecules per particle leads to significantly different protein binding parameters (compare Table 4.2.2).

The Lut stabilized PS nanoparticles present a different protein binding behavior. Notably, it was not possible to measure a significant amount of heat released during protein interaction with the purified sample (see Figure 4.2.13) for the applied concentrations. The heats obtained are too small to apply a reliable independent binding model fit. It was not possible to increase the nanoparticle sample concentrations due to stability issues.

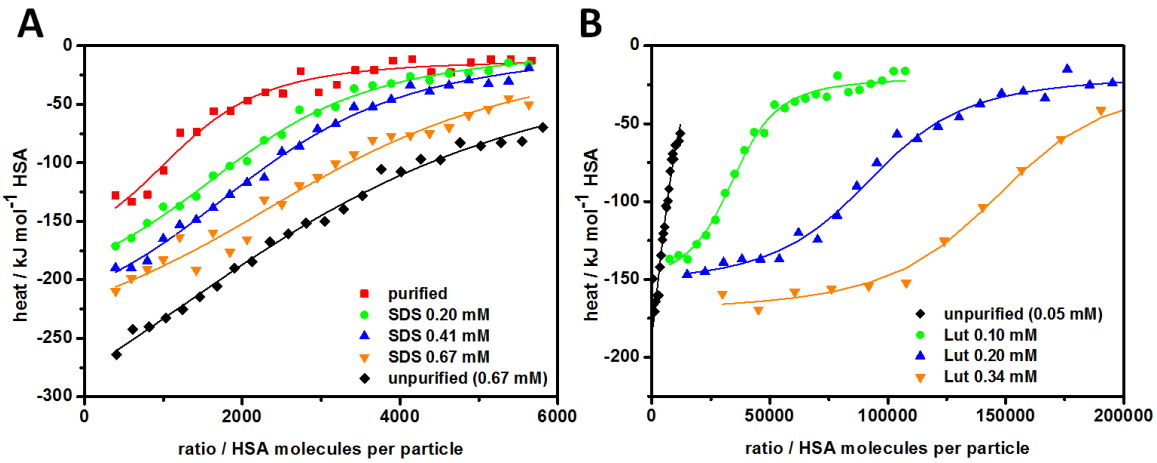

Figure 4.2.12 Isothermal titration calorimetry (ITC) binding isotherms obtained from the titration of all nanoparticle samples with HSA: A) SDS stabilized, B) Lut stabilized. The graphs display the integrated heats of each titration step minus the heat of dilution (symbols) with the corresponding independent binding model fit (straight lines).

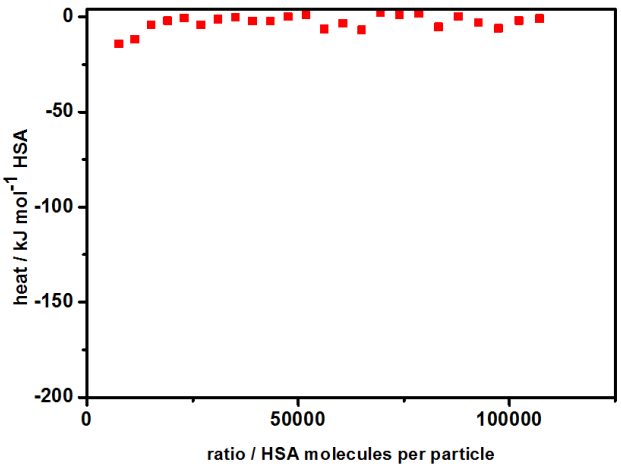

Figure 4.2.13 Integrated normalized heats of the purified PS-Lut NP titrated with HSA.

Table 4.2.2 Parameters obtained from fits of ITC measurements of PS-NP / surfactants and HSA according to an independent binding model.

sample		K_a / 10^5 L mol^{-1}	N	ΔH / kJ mol^{-1}	ΔS / J K^{-1} mol^{-1}
PS (SDS)	purified	2.4 ± 0.8	1,358 ± 135	-192 ± 45	-540 ± 151
	0.20 mM	2.1 ± 0.03	2,180 ± 49	-225 ± 6	-648 ± 26
	0.41 mM	1.8 ± 0.2	2,367 ± 301	-273 ± 45	-814 ± 153
	0.67 mM	1.2 ± 0.2	3,431 ± 286	-283 ± 25	-851 ± 85
	unpurified	0.7 ± 0.04	3,556 ± 312	-406 ± 5	-1,269 ± 15
SDS		1.8 ± 1.2	0.12 ± 0.01	-291 ± 60	-880 ± 207
PS (Lut)	purified	-	-	-	-
	unpurified	1.4 ± 0.1	7,629 ± 1,258	-184 ± 8	-519 ± 29
	0.10 mM	7.3 ± 1.0	36,206 ± 1,076	-139 ± 9	-334 ± 0
	0.20 mM	10.7 ± 4.6	94,966 ± 6,870	-137 ± 12	-344 ± 44
	0.34 mM	22.5 ± 3.8	141,382 ± 2,786	-139 ± 17	-345 ± 59
Lut		20.6 ± 9.0	0.21 ± 0.01	-150 ± 16	-386 ± 59

Errors represent the mean standard deviation of values obtained from 3 or more individual experiments

With higher Lut concentrations the interaction process becomes visible and both K_a and N increase simultaneously. At the highest concentration measured, the binding parameters match those obtained for pure Lut interacting with HSA. As previously reported, the affinity of HSA towards Lut (low CMC of <0.01 mM[108]) is much higher than towards SDS (high CMC of 8 mM[108]).[109] Current reports have found that covalently attached PEG chains decrease amount of bound protein. In our study, however, the existence of a PEG containing polymer actually promoted the HSA interaction. The

binding affinity of Lut to HSA is around 5 times higher than the reported affinity for isolated PEG to HSA.[110] Unlike pure PEG, Lut contains a hydrophobic alkyl chain, and therefore may prefer binding to hydrophobic pockets of HSA. Therefore, some surfactant molecules would have to detach from the particle surface and form complexes with the protein in solution.

The observed trends for the binding parameters are summarized in Figure 4.2.14.

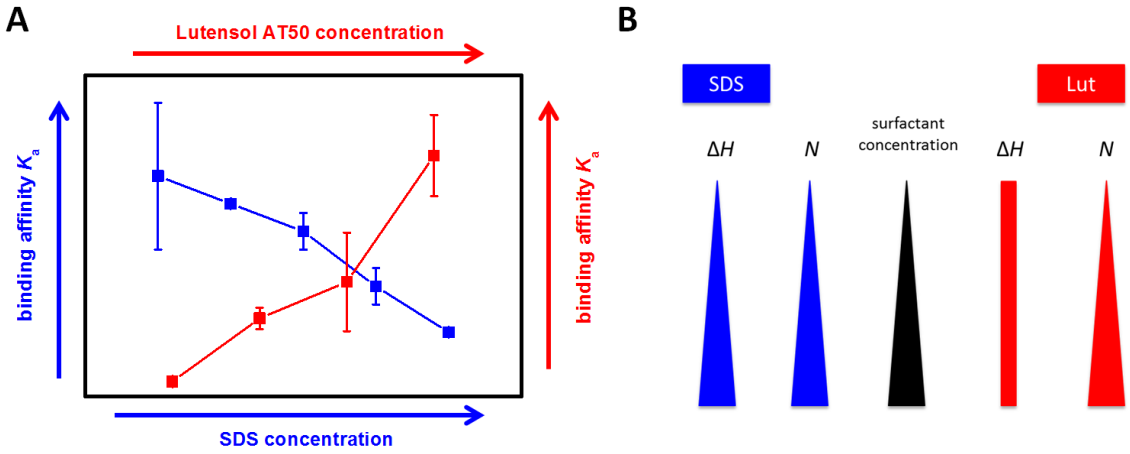

Figure 4.2.14 Illustration of observed trends for binding parameters dependency on surfactant concentration: a) binding affinity trends, b) adsorption enthalpy and stoichiometry trends.

4.2.3 Fate of the surfactant after protein interaction

Thus, the question arises, what happens with the surfactant after the protein interaction. There are three possible scenarios: i) formation of a protein-surfactant-particle complex, ii) formation of a protein-surfactant complex detached from the particle and iii) formation of a protein-particle complex where the surfactant is released into solution (see Figure 4.2.15).

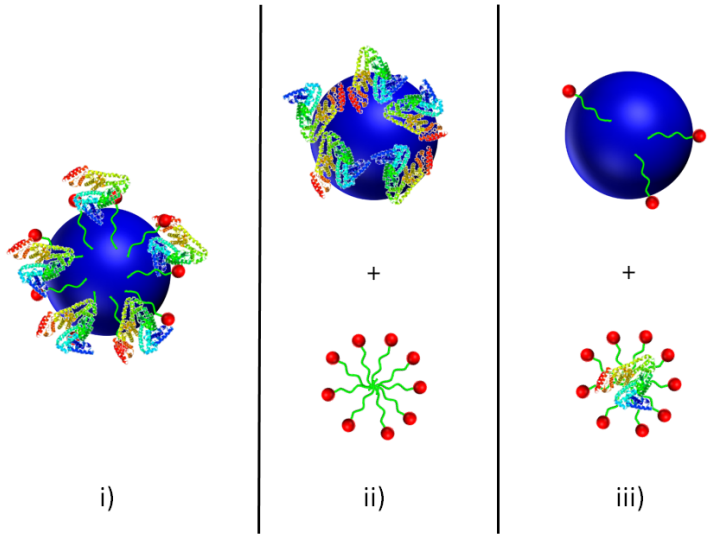

Figure 4.2.15 Schematic representation of species formed after interaction of the protein with the nanoparticle surface.

To address this point, we studied the sample composition after ITC measurements with DLS. In Figure 4.2.16 A the autocorrelation function of SDS-stabilized particles in mixture with HSA is shown. For comparison, the autocorrelation function of pure SDS with HSA is displayed in Figure 4.2.16 B. It can be seen that the SDS-HSA mixture can only be represented by a fit containing an additional aggregate, while the NP containing sample can be described perfectly by the force fit of the individual components. In Figure 4.2.16 B the intensity fraction of the aggregates represents about 60% of the total intensity and yields a hydrodynamic diameter of ~2 µm. This aggregation was also found for mixtures with Lut and HSA (Figure 4.2.17 B). Here, the intensity fraction of the aggregates represents about 70% of the total intensity and yields a hydrodynamic diameter of ~1.2 µm. This aggregation of both pure surfactants was found to be concentration independent. In contrast to the SDS samples, the Lut-stabilized PS-NPs in mixture with HSA cannot be fitted by the force fit (see Figure 4.2.17 A). Additional aggregates are occurring with an intensity fraction of about 45% of the total intensity and a hydrodynamic diameter of ~540 nm. This could be a hint that indeed Lut forms dissolved complexes with HSA, as suspected from the ITC measurements, whereas HSA seems to remain bound to the SDS-stabilized NPs.

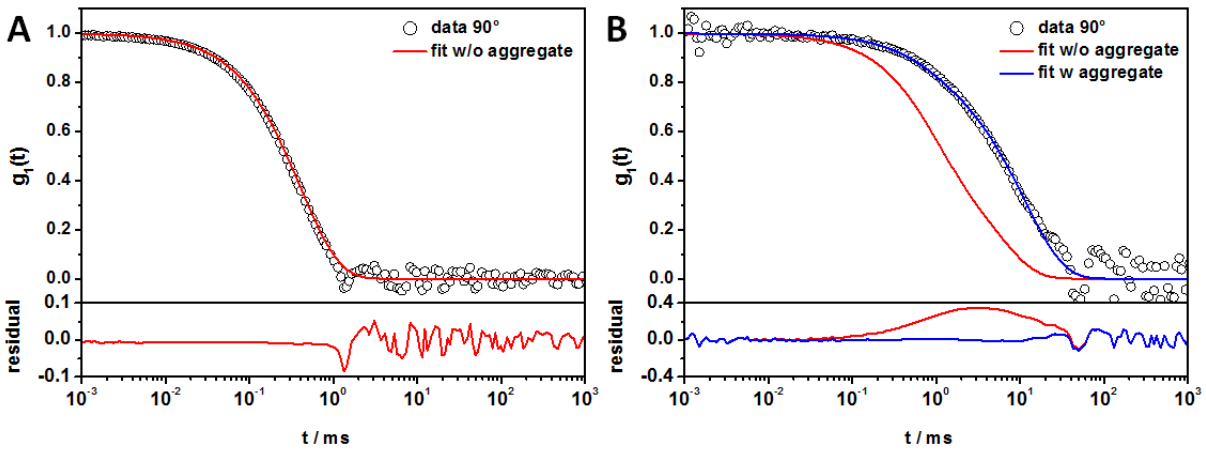

Figure 4.2.16 Exemplary DLS measurement of A) SDS-stabilized nanoparticles containing the highest (13%) surfactant concentration (unpurified) mixed with HSA compared to B) pure SDS (0.25 mM) mixed with HSA (right) at a scattering angle of 90° (q = 0.014 nm^{-1}). Top: Autocorrelation functions $g_1(t)$ (open circles ○) with fits corresponding to the sum of the individual mixture components (red line) and a fit corresponding to additional aggregate formation (blue line). Bottom: residuals from subtraction of the fits from the data points.

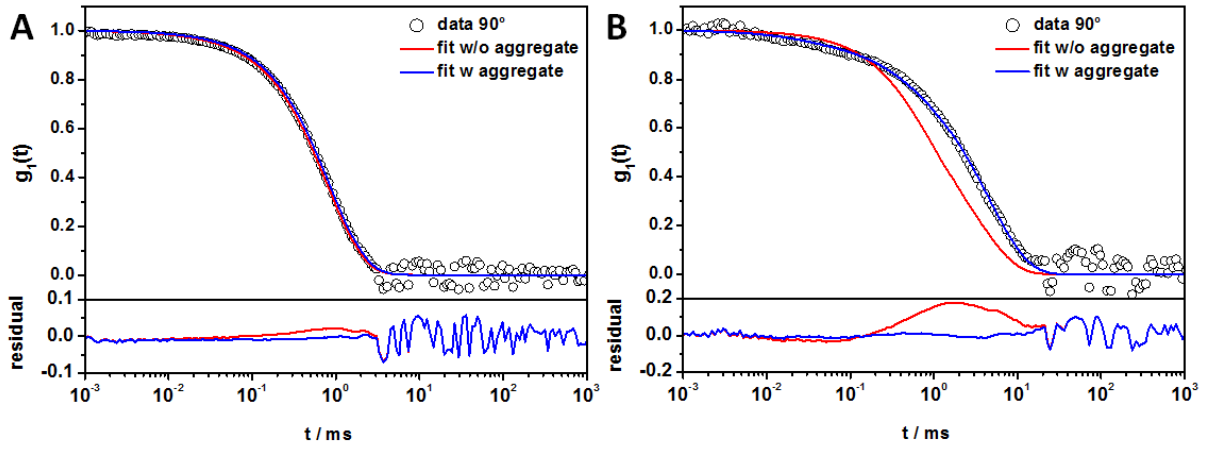

Figure 4.2.17 Exemplary DLS measurement of A) Lut-stabilized nanoparticles containing the highest surfactant concentration (unpurified) mixed with HSA compared to B) pure Lut (0.05 mM) mixed with HSA (right) at a scattering angle of 90° (q = 0.014 nm^{-1}). Top: Autocorrelation functions $g_1(t)$ (open circles ○) with fits corresponding to the sum of the individual mixture components (red lines) and a fit corresponding to additional aggregate formation (blue lines). Bottom: residuals from subtraction of the fits from the data points.

To determine, whether single surfactant molecules, surfactant micelles or small protein-surfactant complexes are released into solution after protein interaction, NMR experiments were performed. Therefore, model PS-NPs, both SDS and Lut stabilized, were synthesized in D_2O miniemulsion by Katja Klein (MPIP Mainz, Germany) and were used without further purification. The nanoparticles formed in the miniemulsion reaction have an R_h of 59 nm. As a control, samples with the same surfactant concentrations in D_2O were prepared. Also, pure HSA as well as mixtures of HSA with SDS and HSA with Lut in D_2O were prepared for comparison. The NMR experiments were performed by Dr. Manfred Wagner, MPIP Mainz, Germany. First, the ^{1}H-NMR and DOSY spectra (both 850 MHz) of SDS are shown in Figures 4.2.18 and 4.2.19.

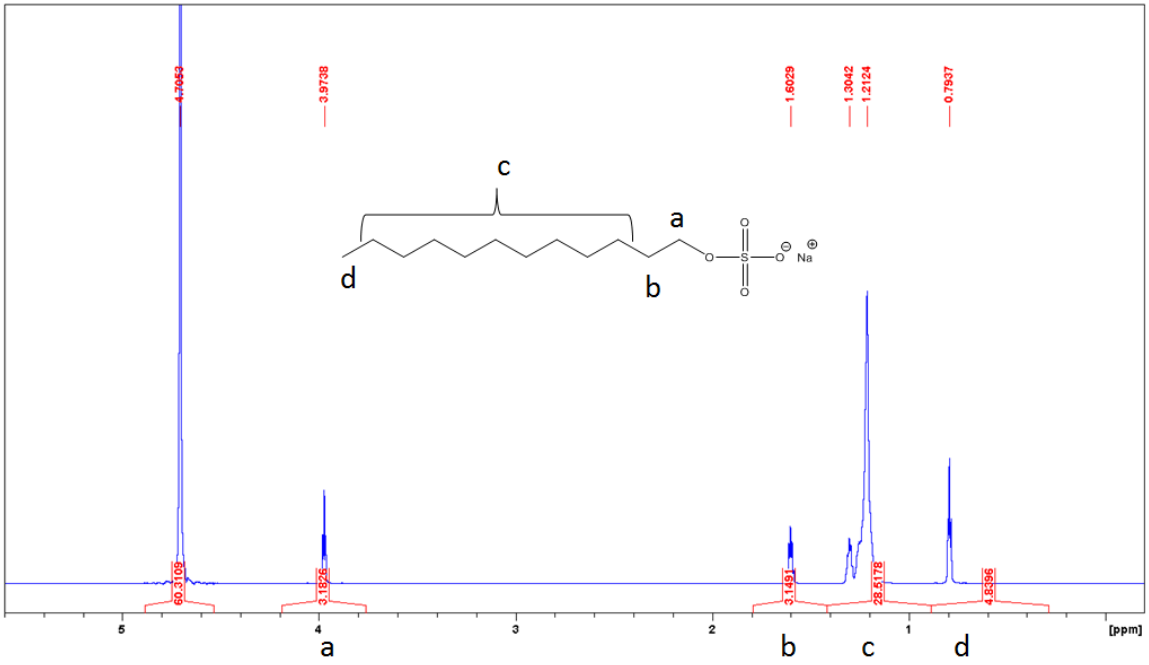

Figure 4.2.18 ^{1}H-NMR spectrum of SDS with the chemical structure and signals assigned accordingly.

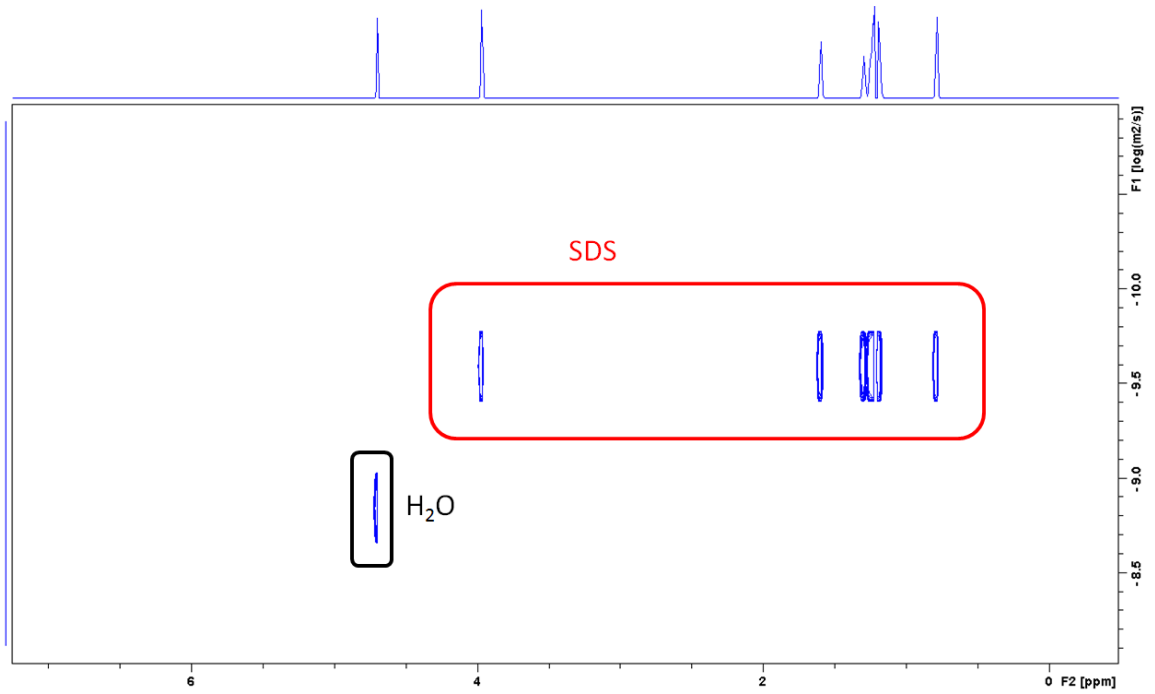

Figure 4.2.19 DOSY spectrum of SDS with signals assigned accordingly.

As it can be seen, SDS gives typical signals at a chemical shift of $\delta = 3.79, 1.60, 1.21$ and 0.79 ppm and the diffusion of SDS can be detected in the DOSY spectrum at a diffusion coefficient of $D = 4.0 \cdot 10^{-10}$ m^2 s^{-1}. This corresponds to an R_h of the diffusing species of 0.5 nm. According to the size of SDS, these species are SDS micelles.

Next, the ^{1}H-NMR and DOSY of SDS-stabilized PS-NPs are analyzed in Figures 4.2.20 and 4.2.21. The nanoparticles formed in the miniemulsion reaction are relatively large in comparison to single molecules or proteins. Therefore they are diffusing very slowly and cannot be detected in the NMR experiments. The signals remaining ($\delta = 7.30$ ppm, $1.46 - 0.64$ ppm,) can probably be assigned to soluble side products formed during the reaction and tetrahydrofuran (THF) ($\delta = 3.66, 1.79$ ppm) used for cleaning. All of the signals observed belong to species diffusing faster than SDS. For comparison both ^{1}H-NMR spectra (SDS and the NP-suspension) are showed in a stacked view in Figure 4.2.22. From the spectra it is clearly visible, that no SDS can be detected in the NP-suspension. This means that most of the SDS molecules probably cover the NP surface and the surface of the NMR tube as well as the air-D_2O interface. For the interaction studies with HSA, this is a good starting point, since SDS being released from the particle surface could be detected in solution.

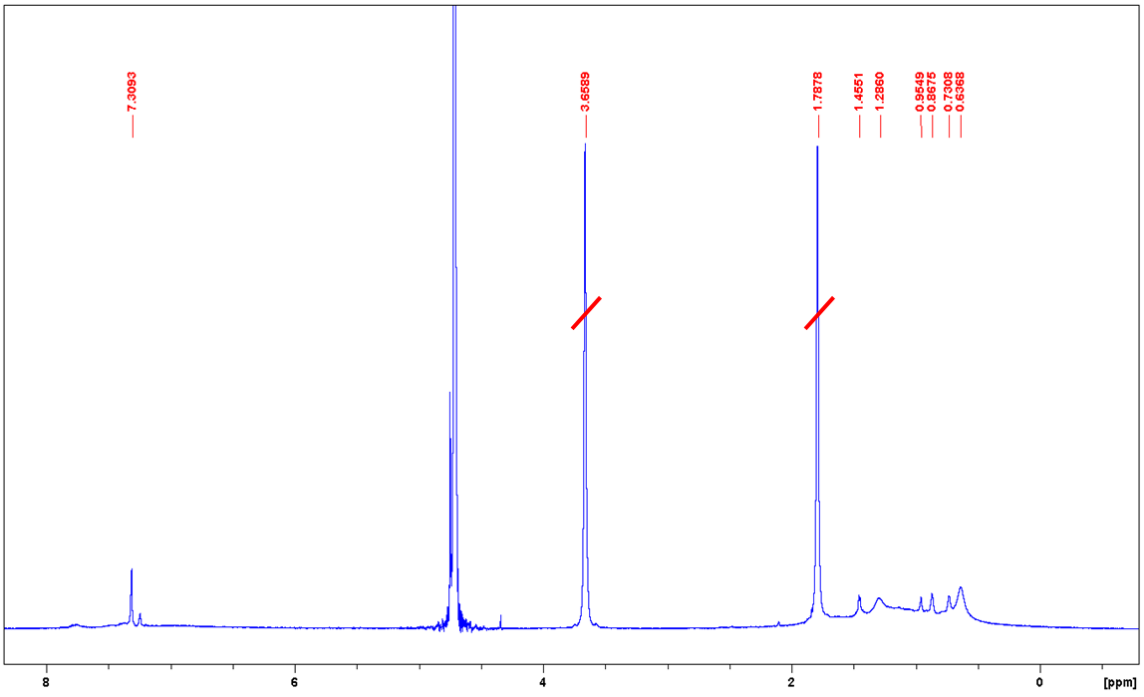

Figure 4.2.20 ^{1}H-NMR spectrum of SDS-stabilized PS-NPs.

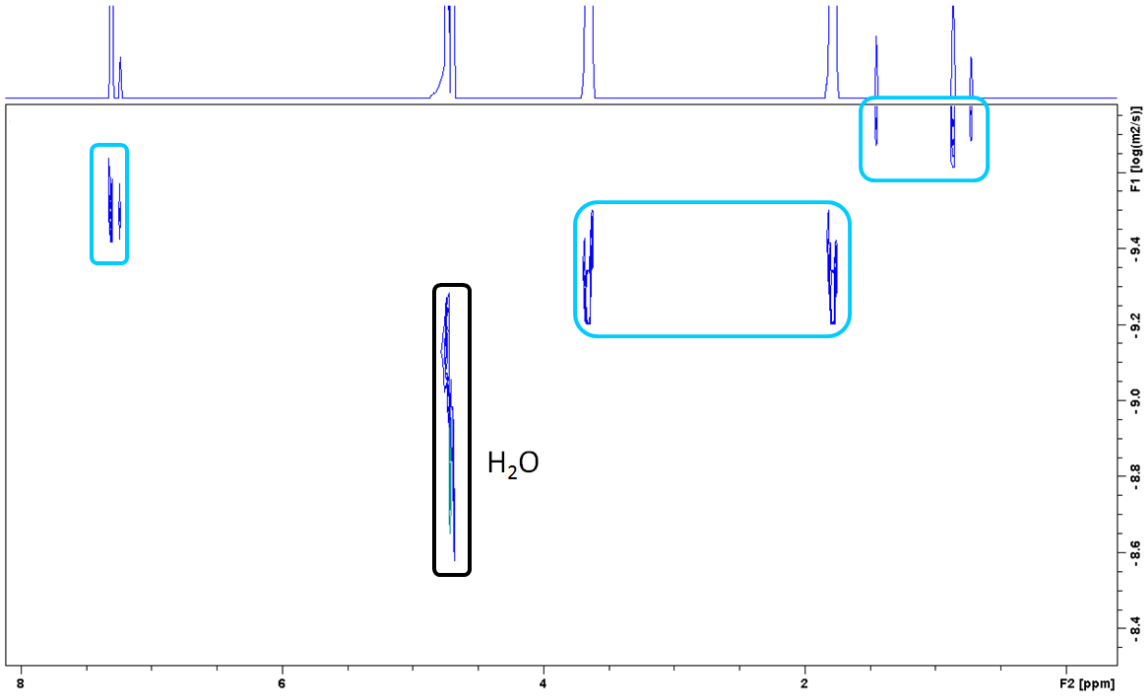

Figure 4.2.21 DOSY spectrum of SDS-stabilized PS-NPs with signals assigned accordingly.

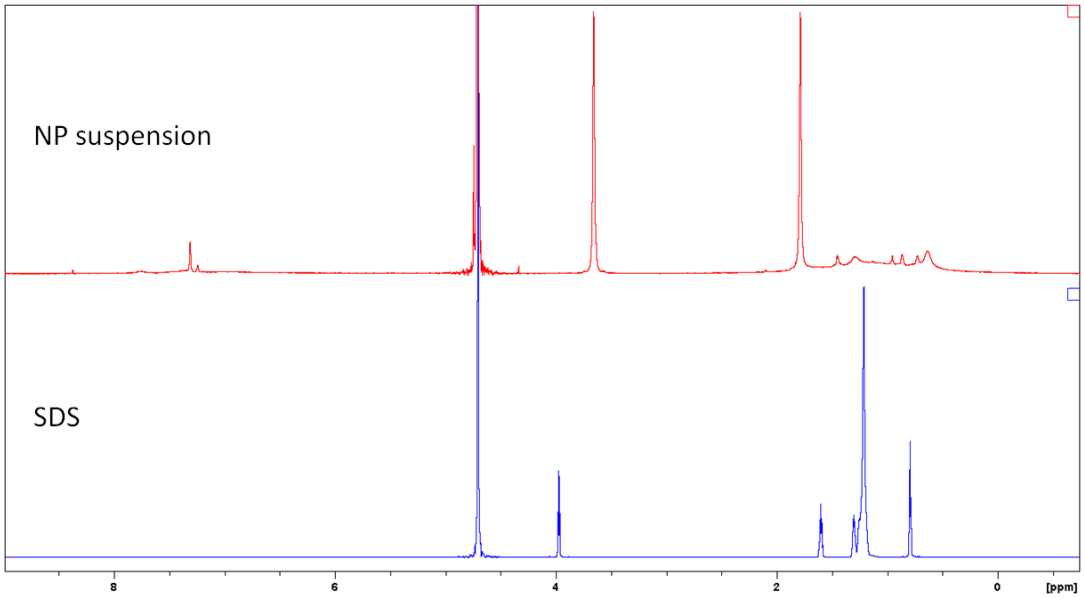

Figure 4.2.22 Stacked ^{1}H-NMR spectra of SDS and SDS-stabilized PS-NPs.

Subsequently, the ^{1}H-NMR (Figure 4.2.23) and DOSY (Figure 4.2.24) spectra were recorded. The signals in the ^{1}H-NMR can be assigned to characteristic structure elements of proteins like protons from aromatic and aliphatic amino acid residues, but also protons on the C_α of the main chain. In the DOSY spectrum HSA can nicely be seen diffusing in its monomeric form. The diffusion coefficient obtained is $D = 5.7 \cdot 10^{-11}$ m^2 s^{-1}, which gives an R_h = 3.8 nm. This is in very good agreement with literature values for the size of HSA.[111]

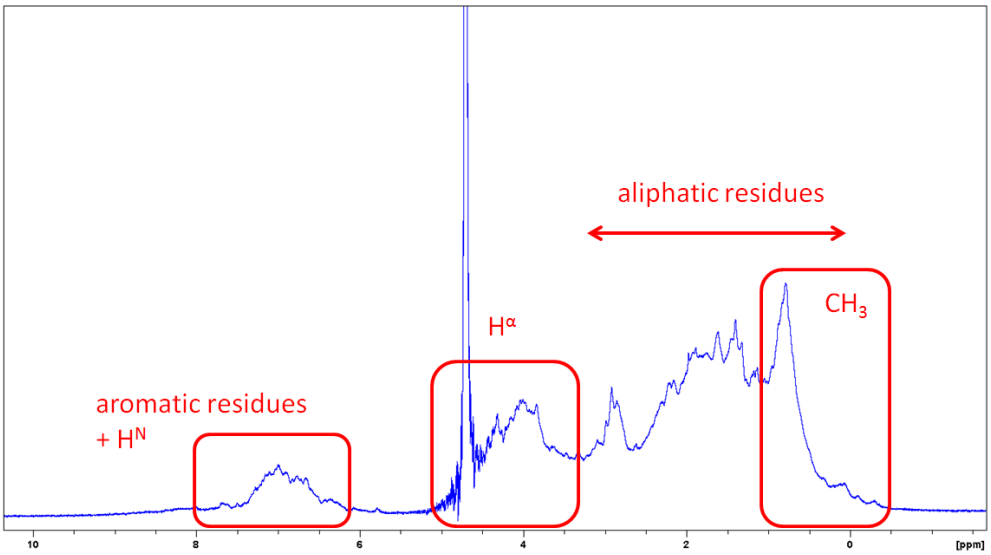

Figure 4.2.23 ^{1}H-NMR spectrum of HSA with signals assigned to characteristic structure elements.

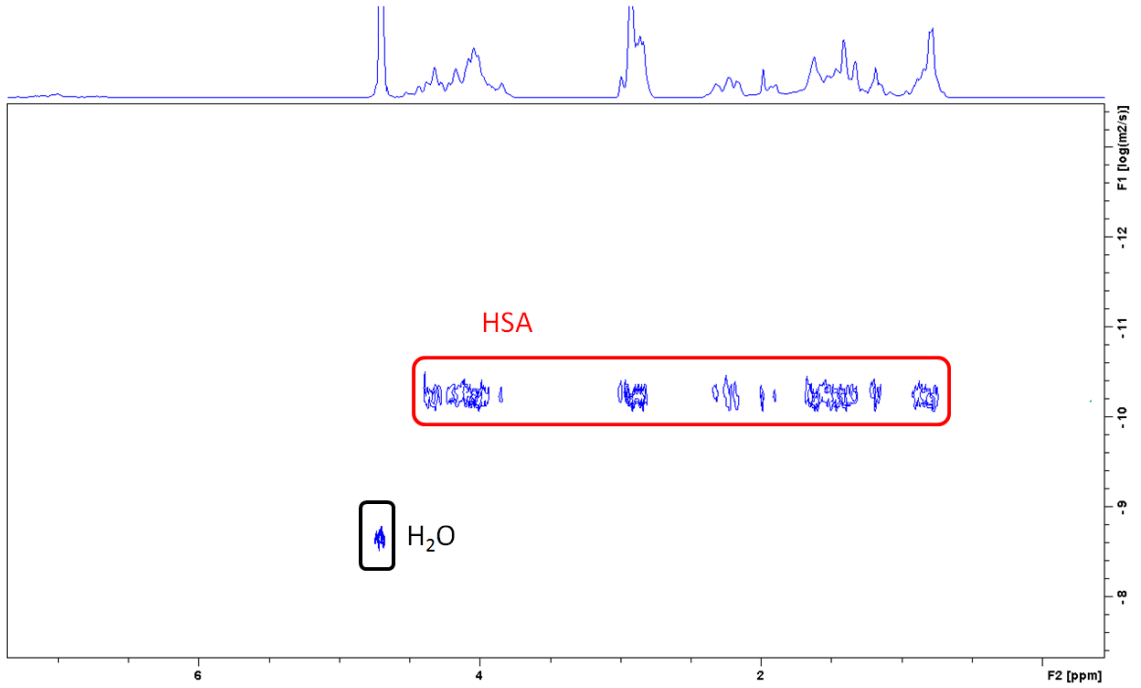

Figure 4.2.24 DOSY spectrum of HSA.

For the next reference spectra needed, solutions of SDS and HSA in D_2O were mixed. As known from the DLS measurements, they form micrometer sized complexes upon mixing. Those aggregates are too large to be detected in NMR, so only aggregates containing one or very few albumin molecules could be seen. In both spectra (Figures 4.2.25 and 4.2.26) the signals of pure SDS and pure HSA are observed at the same time. There seems to be a minor interaction of the SDS with HSA shown in the DOSY spectrum, but mostly the two species are diffusing independently. This confirms the data obtained from DLS and indicates that only very large aggregates are formed.

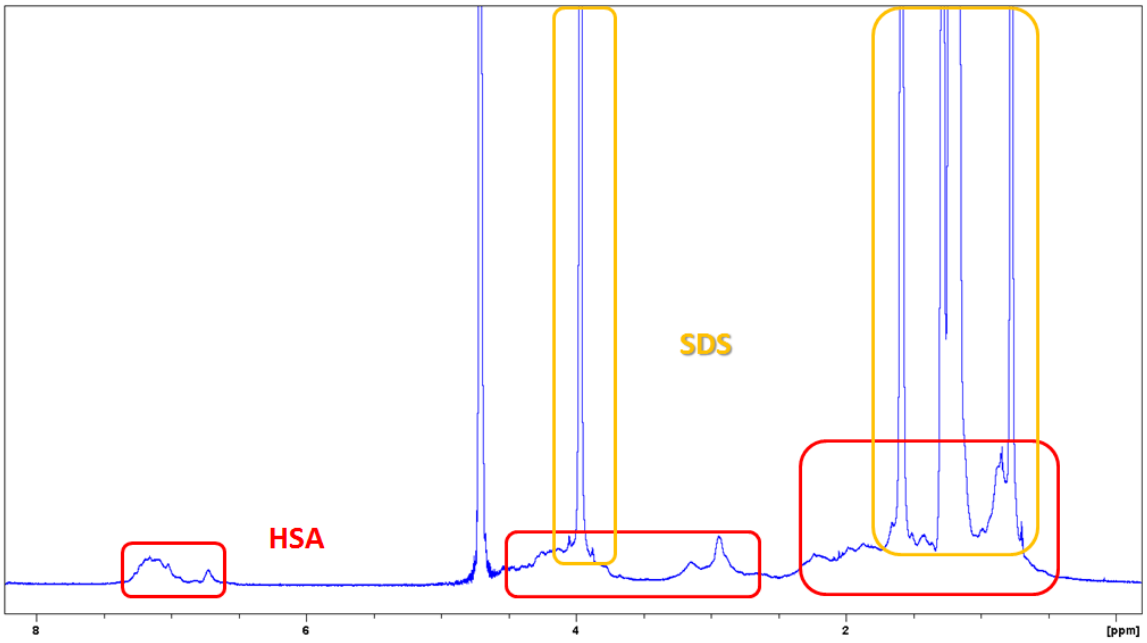

Figure 4.2.25 ^{1}H-NMR spectrum of a mixture of SDS and HSA with signals assigned to each species.

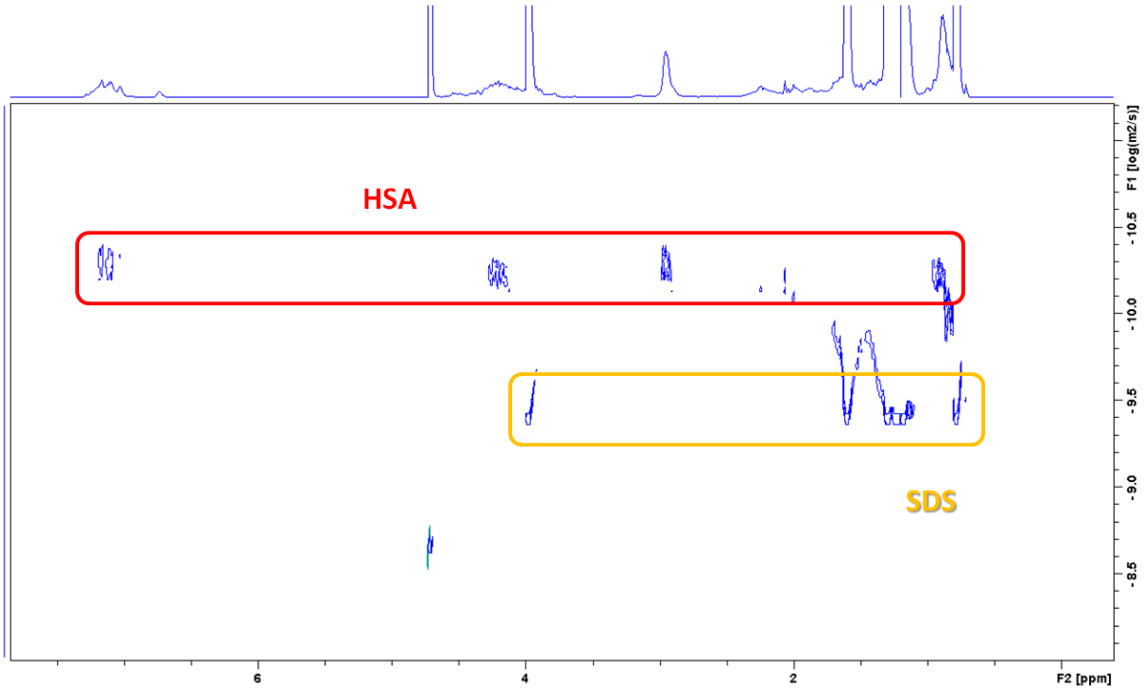

Figure 4.2.26 DOSY spectrum of a mixture of SDS and HSA with signals assigned to each species.

Finally, the mixture of the SDS-stabilized PS-NPs with HSA was analyzed. After interaction of the different species in the sample, in the ^{1}H-NMR spectrum (Figure 4.2.27) as well as the DOSY spectrum (Figure 4.2.28) only the individual components, meaning the pure protein and the signals from the suspension, can be detected. The signal intensity of the HSA signals, however, is much lower than for the same concentration of pure HSA. This can be attributed to the fact that most of the protein is adsorbed onto the particle surface and due to the decreased mobility and therefore decreased T_2 relaxation time are not visible as a sharp peak in the NMR spectra. Interestingly, no SDS signals can be detected after mixing. If SDS molecules detached from the particle surface, they would be observable in solution (due to their mobility). Since in the DLS measurement also no large aggregates were observed, it can be concluded that after adsorption of HSA a particle-surfactant-protein complex is formed.

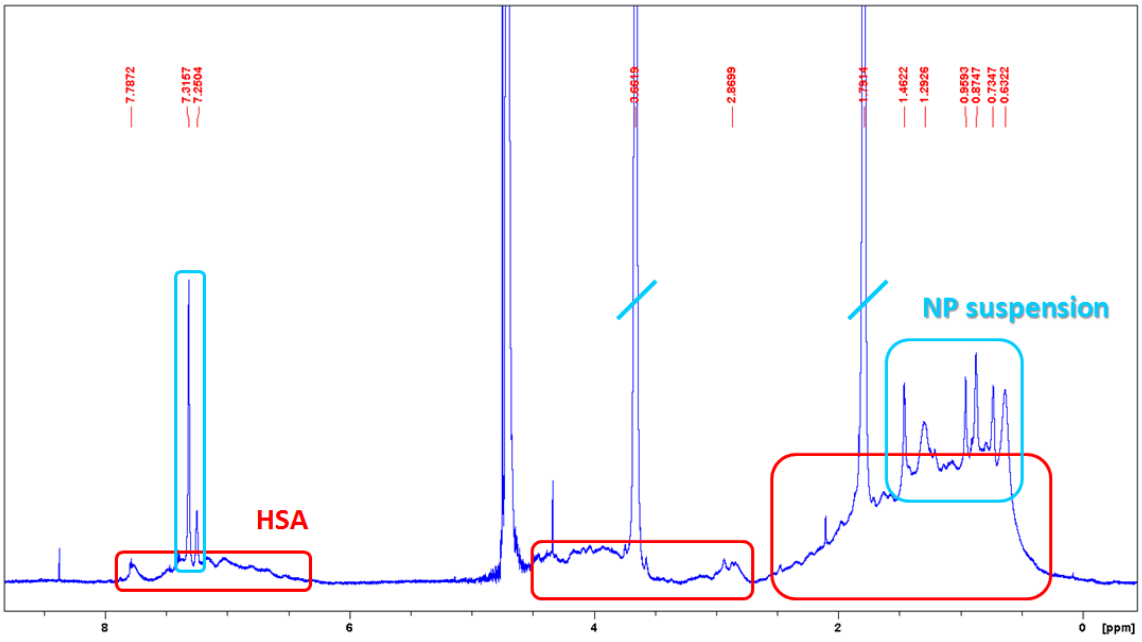

Figure 4.2.27 ^{1}H-NMR spectrum of a mixture of SDS-stabilized PS-NPs and HSA with signals assigned to each species.

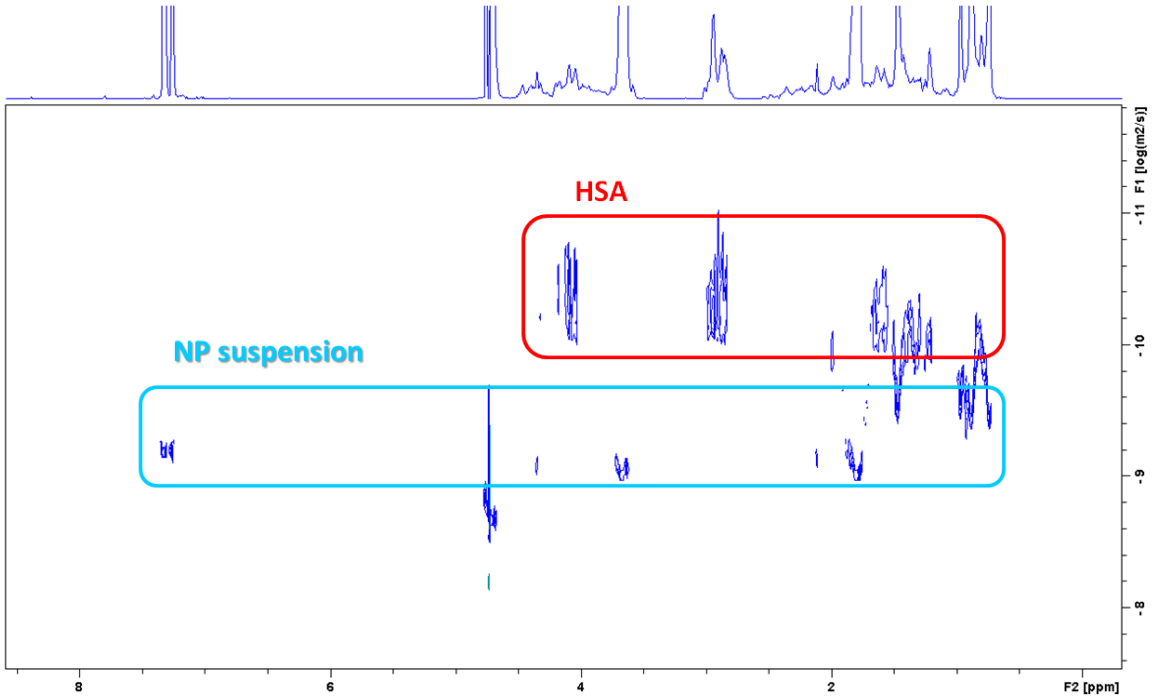

Figure 4.2.28 DOSY spectrum of a mixture of SDS-stabilized PS-NPs and HSA with signals assigned to each species.

The same analysis was performed for the interaction with Lut stabilized particles. Accordingly, the ^{1}H-NMR and DOSY spectra of Lut were measured first (Figures 4.2.29 and 4.2.30). The characteristic signals for Lut can be found at chemical shifts of $\delta = 1.50, 1.23$ and 0.84 ppm (hydrophobic alkyl chain) and $\delta = 3.45 - 3.80, 3.39$ ppm (hydrophilic PEG chain). The diffusion analysis of Lut shows only one diffusing species with a diffusion coefficient of $D = 4.5 \cdot 10^{-11}$ m^2 s^{-1} giving an R_h of 4.8 nm. Considering the length of a Lut molecule, this size corresponds to Lut micelles.

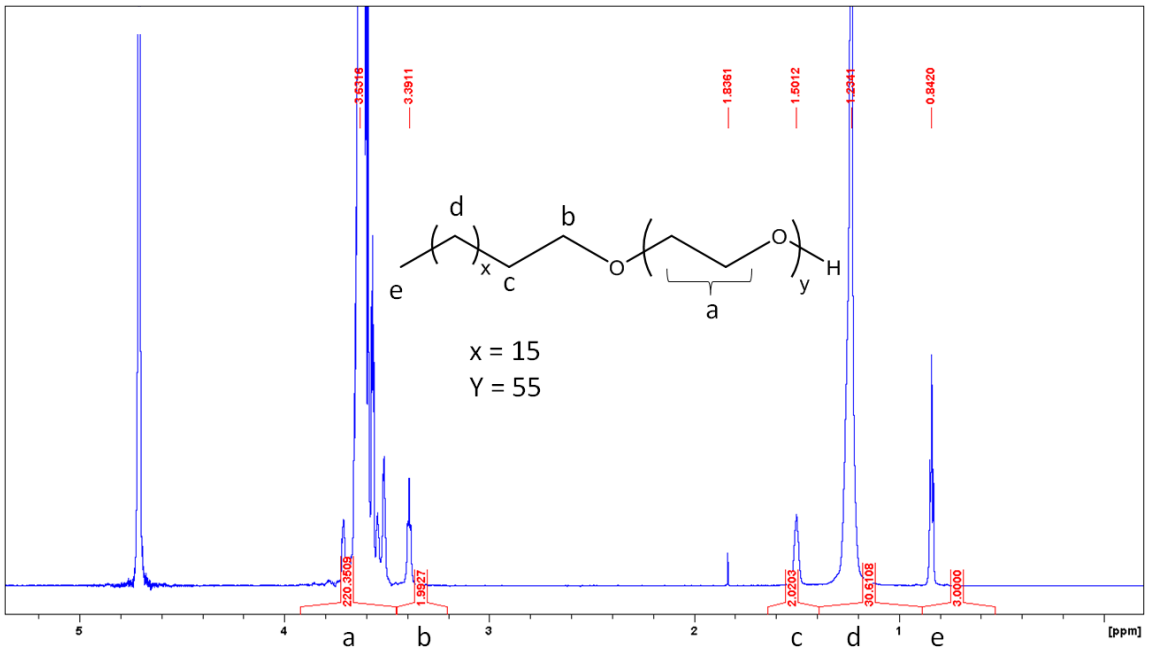

Figure 4.2.29 ^{1}H-NMR spectrum of Lut with the chemical structure and signals assigned accordingly.

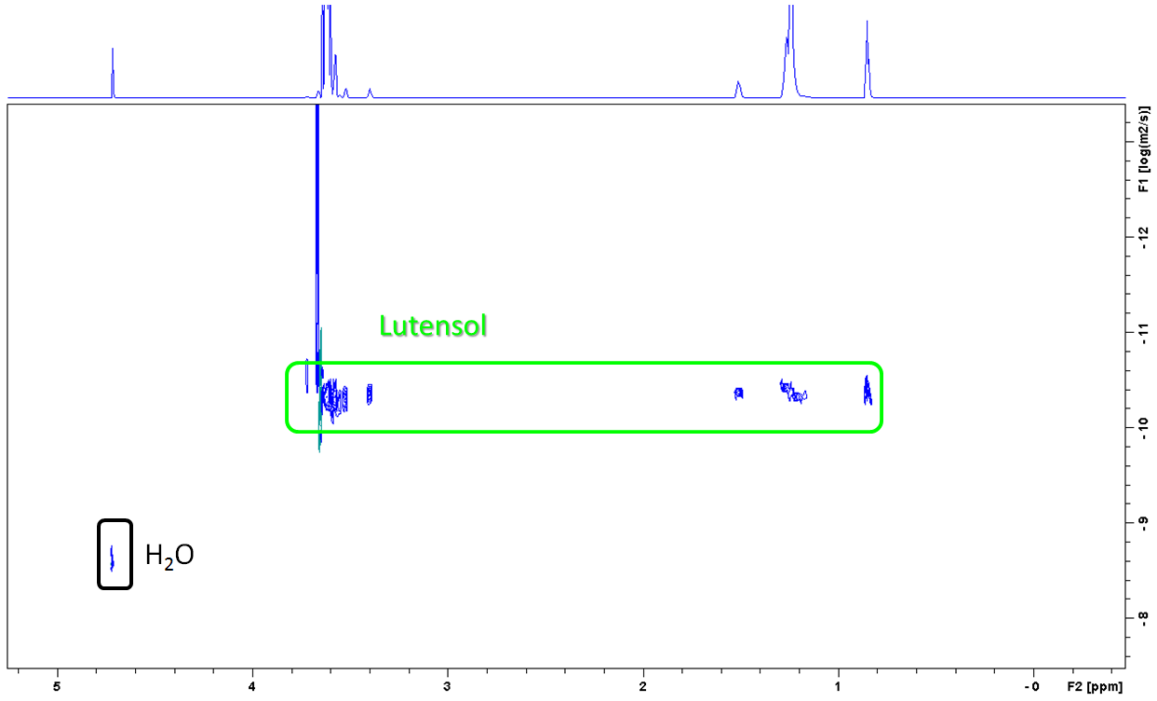

Figure 4.2.30 DOSY spectrum of Lut.

In the next step, the spectra of the Lut-stabilized NP suspension are examined (Figure 4.2.31 and 4.2.32). The same signals like in the SDS-stabilized sample resulting from reaction side products are visible. Additionally, here Lut signals can be detected. However, the integral ratio between the hydrophilic head group and the alkyl chain

suggest, that the alkyl protons are more difficult to detect. A possible reason could be that they are partly immobilized at the particle surface. However, for the mixture with proteins, the fact that free Lut is visible in solution is not ideal. If Lut molecules were released into solution, this would be difficult to detect.

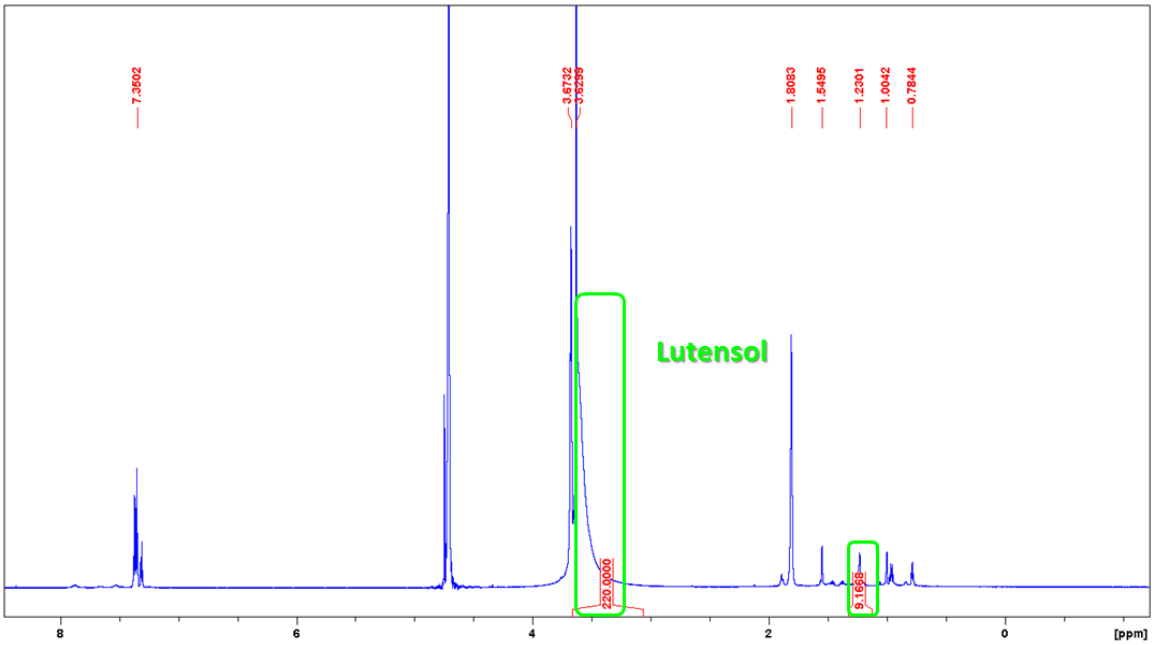

Figure 4.2.31 ^{1}H-NMR spectrum of Lut-stabilized PS-NPs.

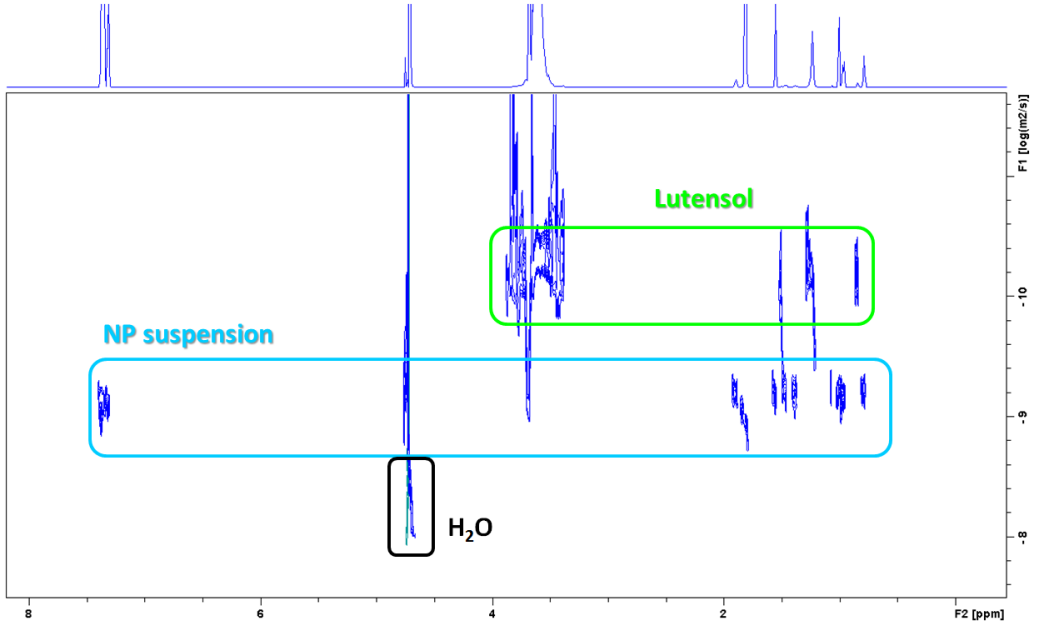

Figure 4.2.32 DOSY spectrum of Lut-stabilized PS-NPs assigned to each species.

Like before, a mixture of Lut and HSA was also measured as additional reference (Figures 4.2.33 and 4.2.34). Again, both single components can be detected. However, unfortunately, HSA molecules and Lut micelles exhibit the same hydrodynamic radius and therefore the same diffusion characteristics. Thus, in the DOSY spectrum it is not possible to distinguish between two separate components or a complex of one HSA molecule with several Lut chains.

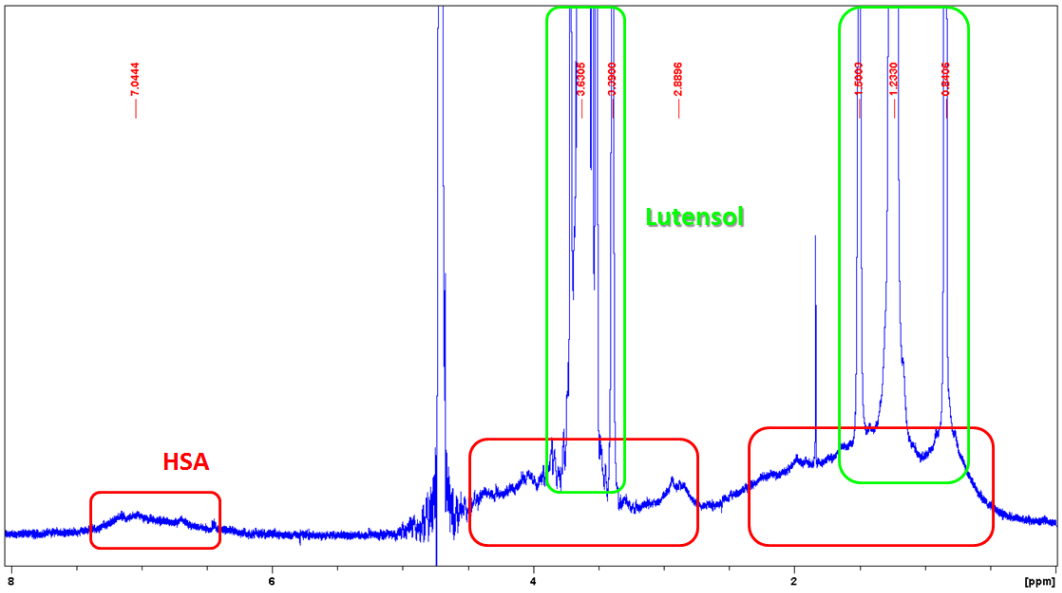

Figure 4.2.33 ^{1}H-NMR spectrum of a mixture of Lut and HSA with signals assigned to each species.

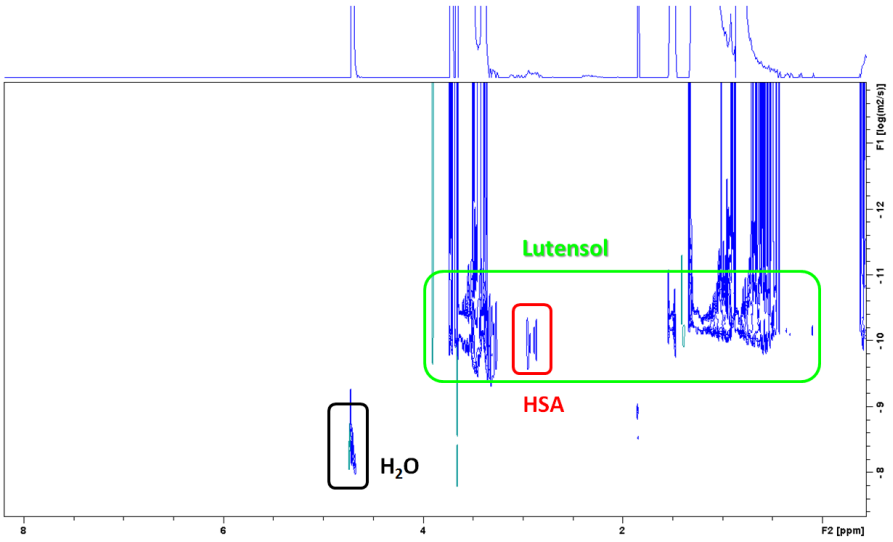

Figure 4.2.34 DOSY spectrum of a mixture of Lut and HSA with signals assigned to each species.

Last, the mixture of Lut-stabilized PS-NPs and HSA was measured. In this case, all components can be detected with the same size they exhibit as separate species (Figures 4.2.35 and 4.2.36). Therefore, conclusions about Lut being released from the particle surface after interaction cannot easily be drawn. Since the intensity of the Lut signal is actually slightly decreasing this seems not to be the case. Rather, a formation of particle-Lut-protein complexes or larger Lut-HSA complexes seems likely. Considering the DLS data, the latter might be the case. However, the information obtained is not fully clear, so that this question remains subject to further investigation.

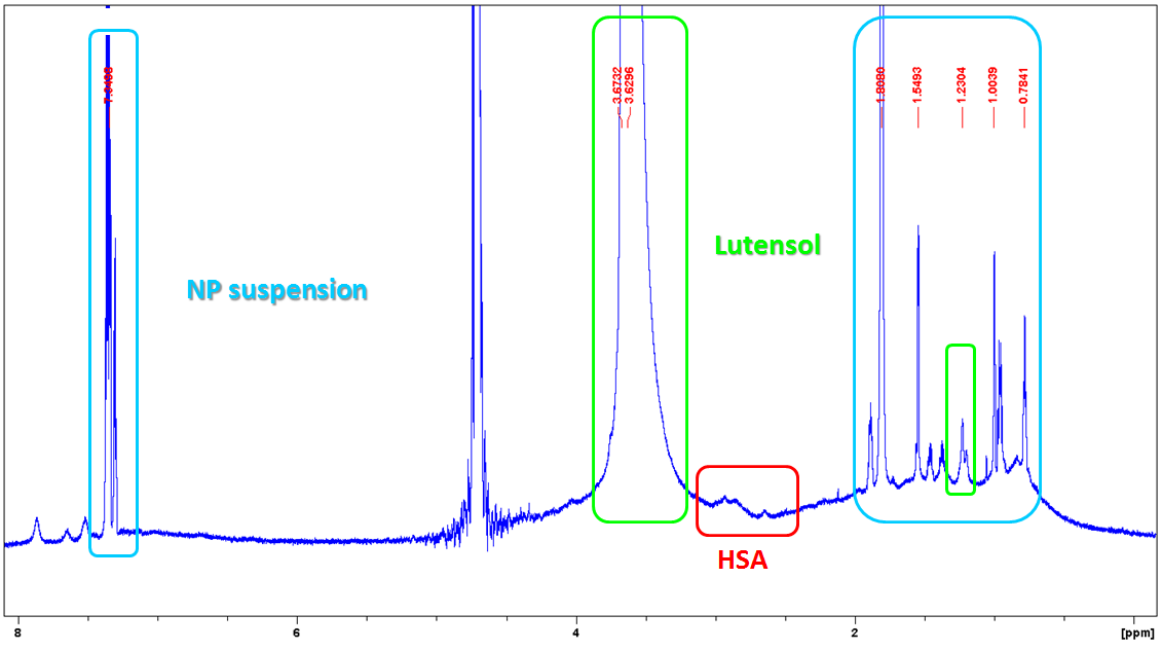

Figure 4.2.35 ^{1}H-NMR spectrum of a mixture of Lut-stabilized PS-NPs and HSA with signals assigned to each species.

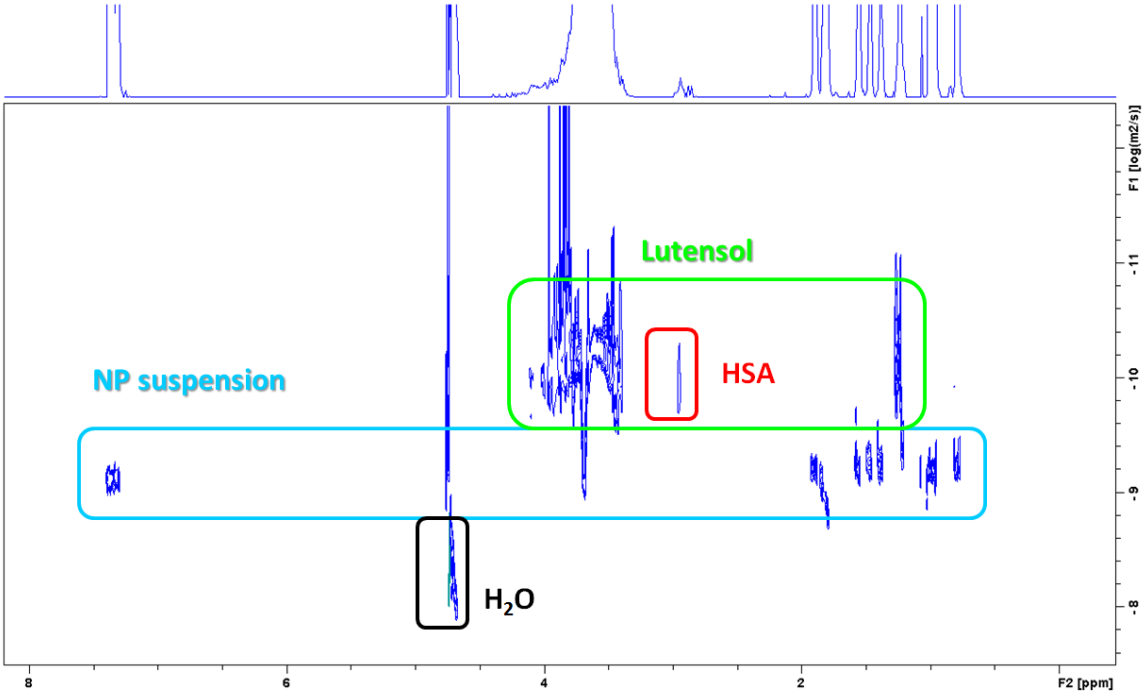

Figure 4.2.36 DOSY spectrum of a mixture of Lut-stabilized PS-NPs and HSA with signals assigned to each species.

4.2.4 Conclusion

In conclusion, the type and amount of available groups on particle surfaces has a significant effect on the protein binding properties. While only small amounts of stabilizing agents may remain, they can have significant adverse effects on protein adsorption and lead to different processes. Until now it was not clear that only very small variations in the number of ‘functional’ groups on the particle surface change the protein binding affinities. It was observed that at high concentrations the surfactant determines the adsorption process, not the particle material. This is of great importance for both surfactant stabilized nanomaterials and covalently attached functional surface groups. It must be ensured that the amount of all groups for a particle is well known and reproducible before studying protein interaction. Additionally, it was observed that the fate of all different molecules involved (surfactant, protein, nanoparticle) may be different after protein adsorption, depending on the type of surfactant used. To avoid formation of additional surfactant complexes it might be necessary to stabilize the nanoparticles with covalently attached functional groups. Thus, the interaction with biological systems becomes less complex.

4.3 SDS quantification in nanoparticle samples

As it was shown that surfactant molecules can dramatically change the surface characteristics of nanomaterials and therefore also their protein binding behavior, a method to quantitate the remaining surfactant in a sample is necessary. In the previous chapter, samples were characterized with regards to surface tension and zeta potential. However those methods allow only qualitative comparison between samples and the absolute concentration of surfactant remains unknown. For nonionic surfactants with not many functional groups it is very difficult to develop direct quantification methods like assays and there is currently no easy way to detect Lutensol. However, for SDS as an ionic molecule there exist different quantification methods, one of which involves complexation of SDS with a cationic dye.[112] Usually this method is used to determine the SDS concentration in biochemical samples containing also proteins, nucleic acids etc. The cationic dye Stains-All[c] shown in Figure 4.3.1 exhibits a fuchsia color in aqueous solution, which gradually turns into yellow upon addition of SDS. Therefore, the SDS induced color change can be observed using UV spectroscopy after establishing a calibration with known SDS concentrations. The specificity of the complex formation was already tested regarding other surfactants (CHAPS[d], Triton X-100[e] and Tween 20[f]), several proteins, buffers, SDS-PAGE reagents, common solvents and even nucleic acids. So far, no additives were found to influence the specificity significantly except some other negatively charged molecules (e.g. some proteins, which form complexes with Stains-All absorbing > 600 nm).[113] Now, the question was whether this quantification method also works in the presence of nanoparticles consisting of different materials and the SDS partially immobilized on the particle surfaces.

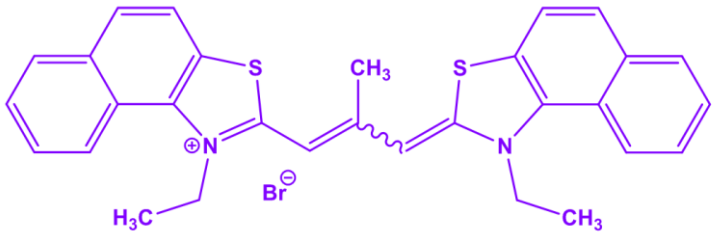

Figure 4.3.1 Chemical structure of Stains-All.

[c] 3,3′-Diethyl-9-methyl-4,5,4′,5′-dibenzothiacarbocyanine
[d] 3-((3-Cholamidopropyl)dimethylammonio)-1-propanesulfonate
[e] Polyethylene glycol *tert*-octylphenyl ether
[f] Polyethylene glycol sorbitan monolaurate

According to the protocol reported in literature, the reaction solution of Stains-All was prepared (see Experimental section). For calibration, aqueous solutions of different SDS concentrations, ranging from 0 - 10 mM, which is the standard concentration for miniemulsion reactions, were prepared. To achieve good precision in low concentrations regimes, more samples between 0.05 and 1 mM were prepared. Of the calibration solutions 2 µL were each added to 200 µL of the Stains-All reactive dye solution and the color change was monitored (see Figure 4.3.2). It can already be seen that a full color change to yellow is achieved in the sample where the 5 mM aliquot was added. Therefore concentrations between 5 and 10 mM SDS can most likely not be distinguished with this method.

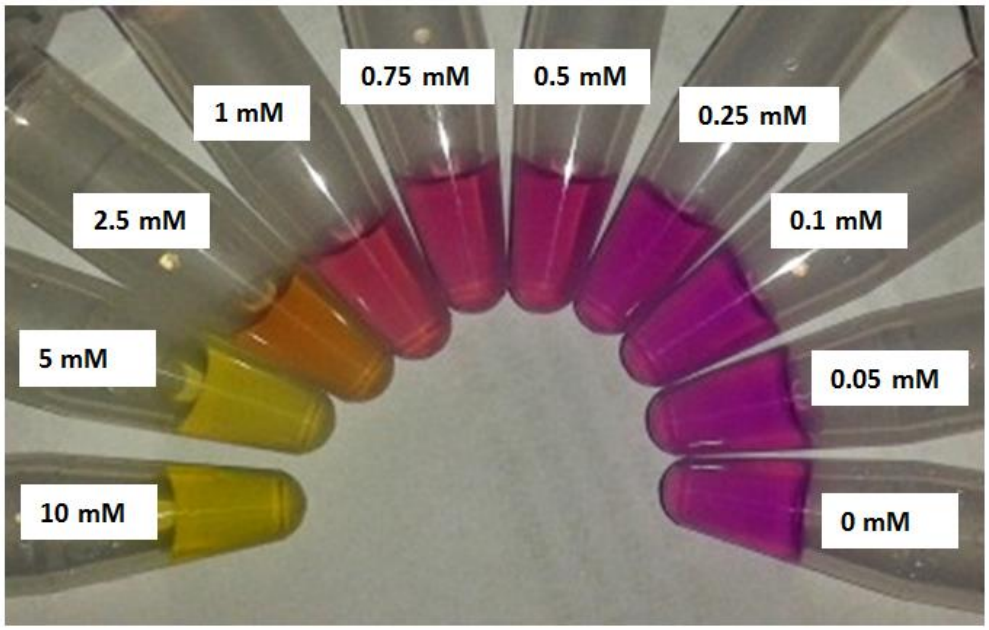

Figure 4.3.2 Samples with different SDS concentrations in Stains-All prepared for calibration.

To evaluate the accuracy of the calibration, all samples were analyzed with a Tecan Plate Reader. For each sample a full absorbance spectrum was recorded in a range between 350 – 750 nm (see Figure 4.3.3). While the absorbance maximum of the free dye is visible at 510 nm, the maximum is shifted to 453 nm when the dye is complexed with SDS as indicated by the straight lines. To quantitate the amount of complexed dye, either the decrease of the absorbance at 510 nm or the increase at 453 nm could be monitored. In the study where this was previously investigated, it was found however, that the best linearity was achieved by monitoring the increase in absorbance not at 438 nm instead of 453 nm (also indicated by a straight line in Figure 4.3.3).

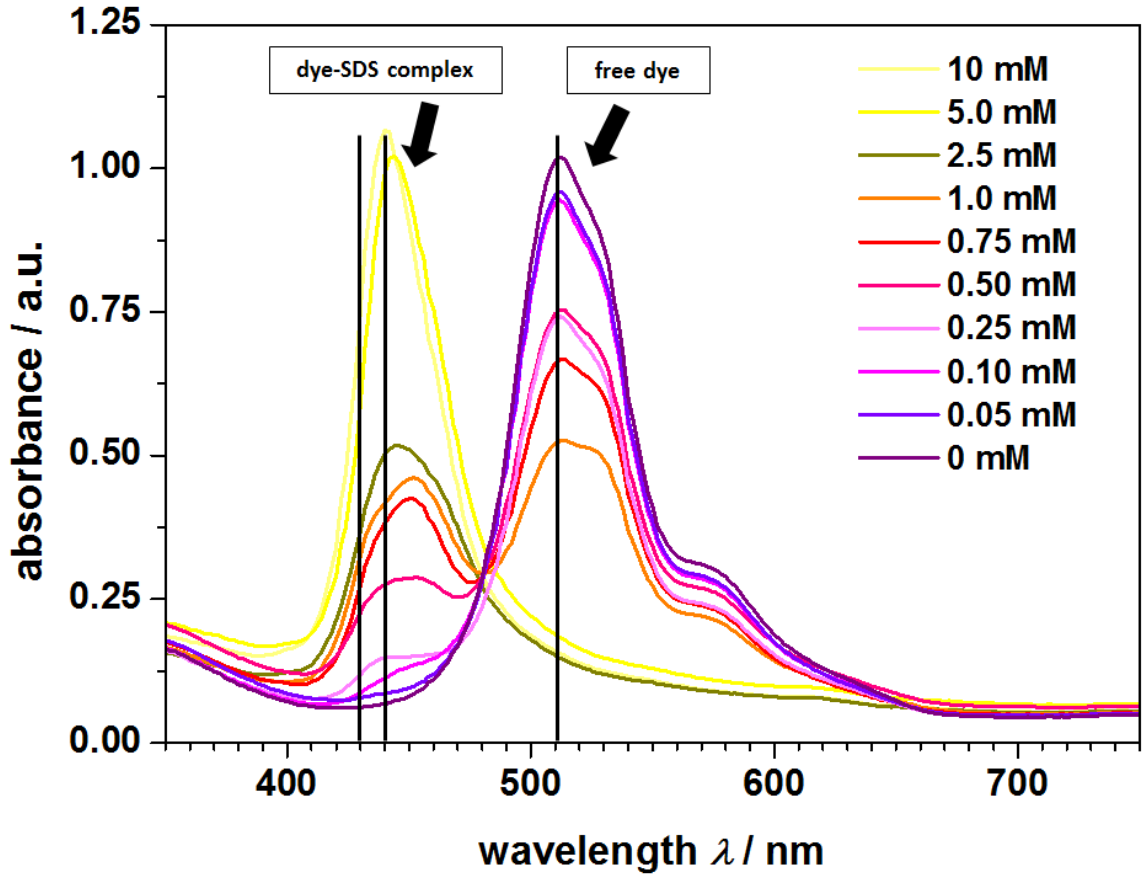

Figure 4.3.3 Absorbance spectra of Stains-All and different concentrations of SDS aliquots added. Straight black lines indicate the wave lengths, which can be used for calibration.

For the identified wave lengths the absorption was plotted against the SDS concentration in the aliquots added (Figure 4.3.4). As it can be seen, for each wave length the three highest concentrations are not in a linear regime any more (red circles). Therefore this calibration cannot readily be used for comparison with samples. It is desirable that also higher SDS concentrations can be quantified. For samples with very small concentrations though, this calibration might be the best to use. In order to increase the accessible concentration range, the calibration was repeated with aliquots of only 1 µL of the SDS solutions.

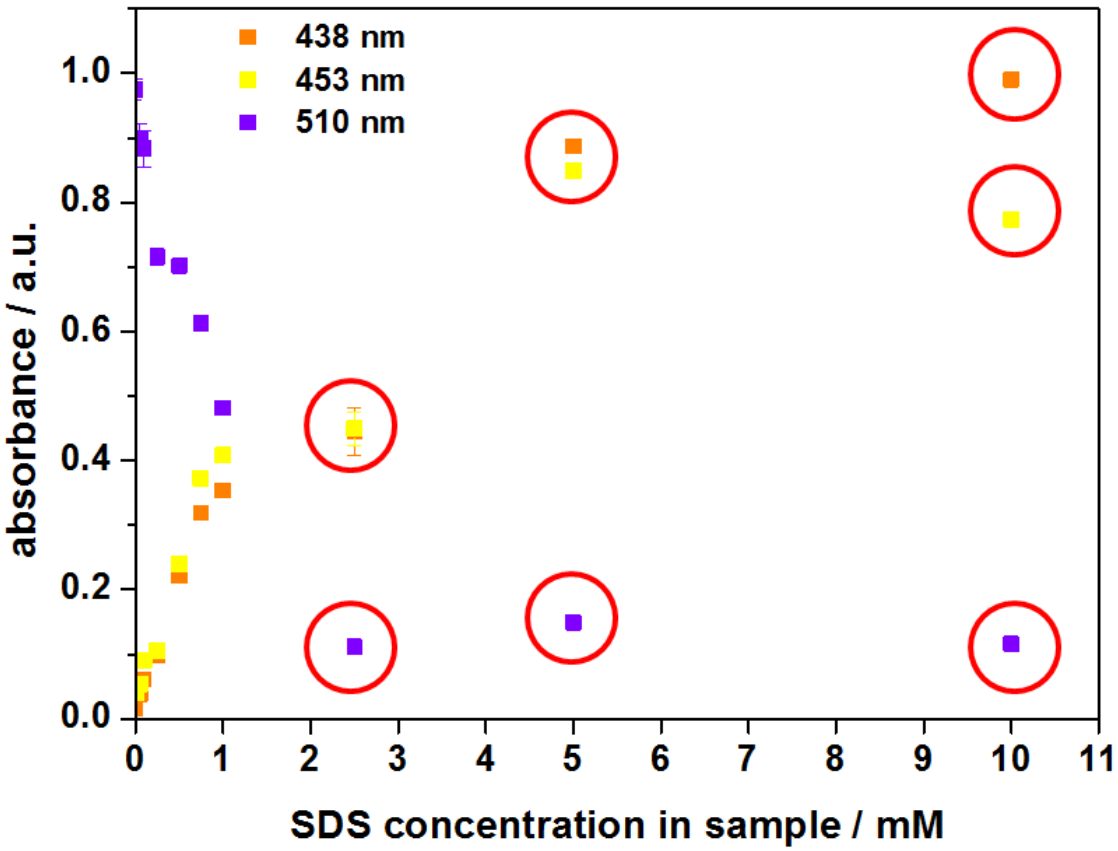

Figure 4.3.4 Absorbance of the calibration solutions at 438, 453 and 510 nm plotted against SDS concentration for 2 µL sample aliquots.

The absorption was again plotted against concentration and indeed a better linearity is being observed (Figure 4.3.5). Then, for each wave length a linear regression was performed and the correlation coefficient *R*, which describes the linearity of the data points, was determined. For all three wave lengths the highest concentration (10 mM) was masked (red squares), as there is still no linear dependency in this range. However all other concentrations can be used. As it was observed in the previous study, the calibration at 438 nm shows the best linearity (R = 0.998) in contrast to 453 nm (R = 0.962) and 510 nm (R = 0.987).

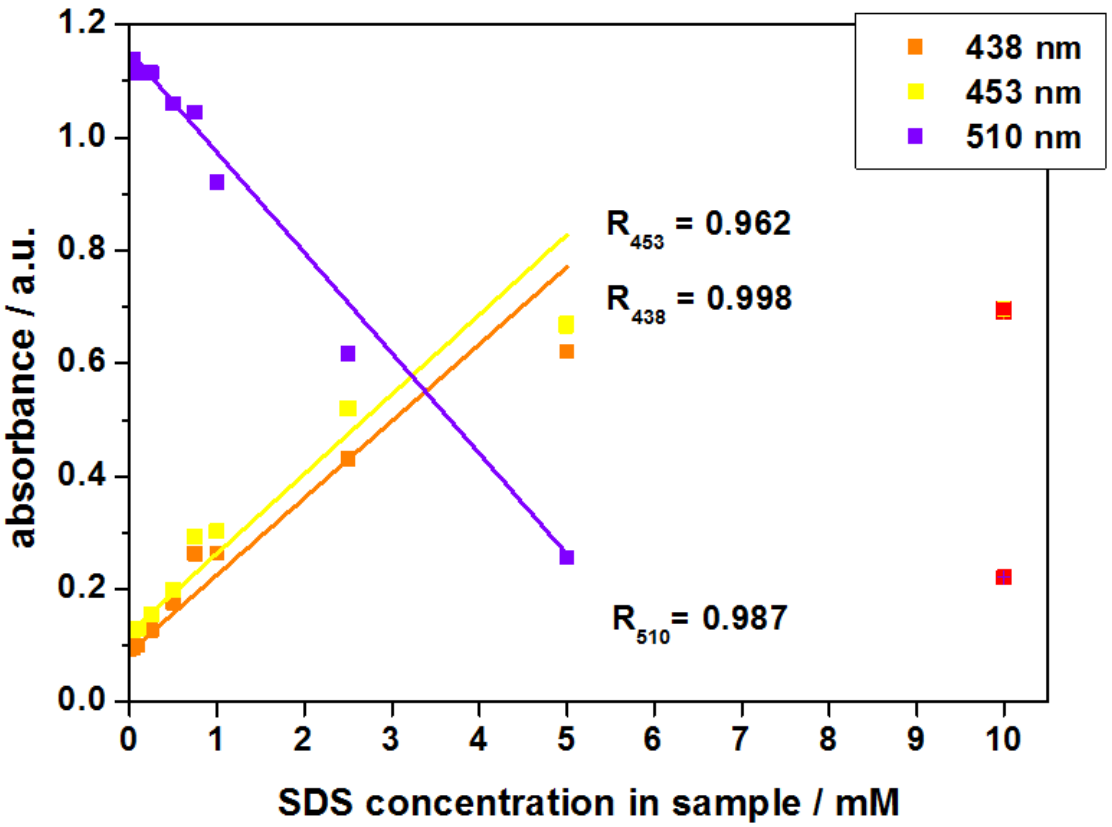

Figure 4.3.5 Absorbance of the calibration solutions at 438, 453 and 510 nm plotted against SDS concentration for 1 µL sample aliquots.

According to the calibration determined, all nanoparticle samples will be compared to the absorbance at 438 nm. With the equation obtained, the SDS concentrations can be calculated for each sample after solving for *c*:

$$Absorbance = 0.13635\ \mathrm{mM}^{-1} \cdot c + 0.08863 \tag{4.3}$$

$$c = \frac{Absorbance - 0.08863}{0.13635}\ \mathrm{mM} \tag{4.4}$$

To measure the SDS concentration in different samples with different materials, nanoparticles obtained from different synthetic procedures and before and after purification were collected in the work group. In Table 4.3.1 the different particle samples are shown along with the main material and surfactant characteristics.

Table 4.3.1 Nanoparticle samples for SDS quantification.

sample	particle material	particle conc. / wt%	surfactant used	purification	estimated SDS conc.
KK83	PS	0.1	Lut AT50	centrifugation	-
KK96	PS	3.0	SDS	-	high
KK94	PS/Bodipy	3.0	SDS	-	high
SW097M	DAB[g]/TDI[h]	0.6	SDS	6 h dialysis	medium
SW089B	HES/TDI	1.0	SDS	24 h dialysis	low
MF21s	PP[i]	0.8	SDS	-	high

Since polystyrene is a very common model particle material, three different samples were chosen. As a control, polystyrene particles stabilized with the nonionic surfactant Lut were used, as they should not give any positive SDS signal. Then, two other samples, each containing the amount of SDS after synthesis, were investigated. One particle type was additionally modified with covalently bound Bodipy dye (Ex. 523 nm / Em. 536 nm), which could interfere with the absorbance spectrum of Stains-All. For each particle type, the absorbance spectrum with and without Stains-All dye was recorded and is shown in Figure 4.3.6.

[g] Diaminobutane
[h] Toluene 2,4-diisocyanate
[i] Polyphosphate

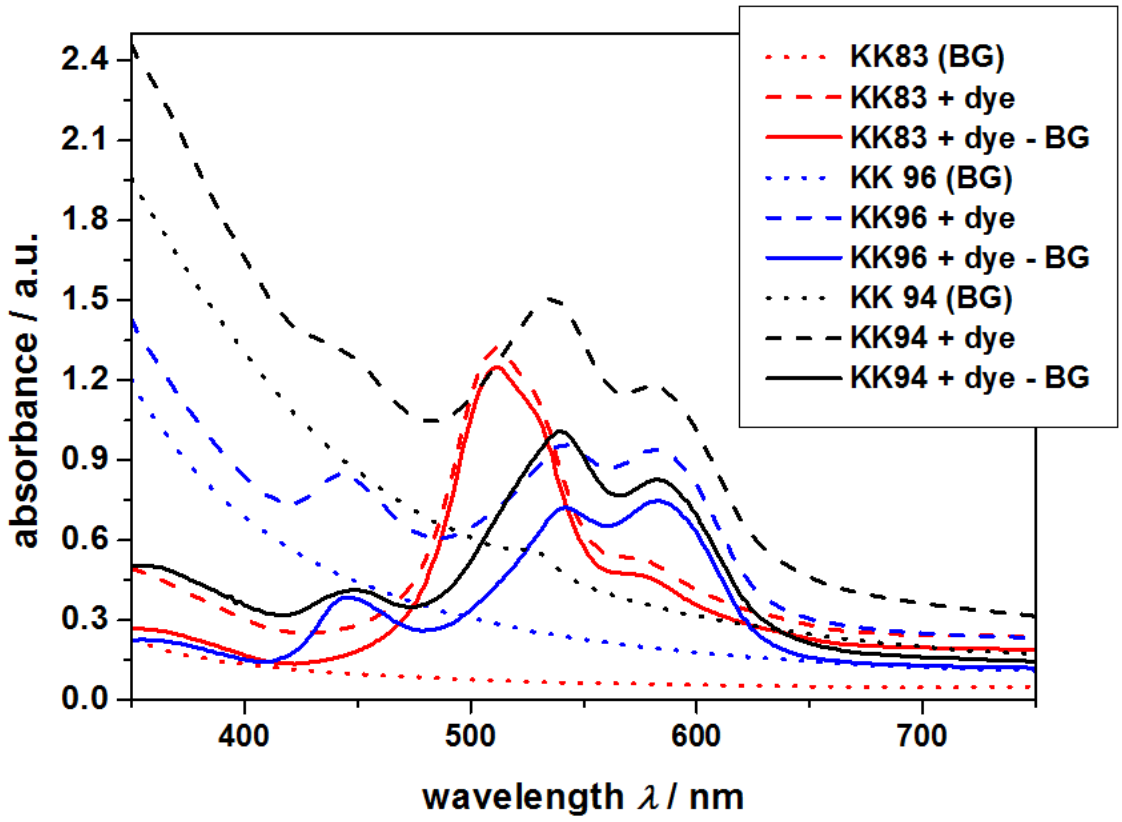

Figure 4.3.6 Absorbance spectra of PS-NP samples in Stains-All solution.

When analyzing the background of each PS-NP sample, it is clearly visible that the absorbance of polystyrene itself interferes with the measurement. Usually the absorbance of polystyrene has its maximum between 200 and 300 nm. Here, a significant absorbance increase towards 300 nm is observed for the higher concentrated sample aliquots (KK94 and KK96). Indeed, this increase is dependent on the particle concentration, but it cannot be avoided completely. Additionally, a new absorbance maximum occurs at 582 nm upon interaction with Stains-All, which in the pure dye is only represented as a shoulder and is referred to as the α-state of Stains-All.[114] This means, that there is some kind of interaction between the particle material and dye. This is supported by the observation, that at higher particle concentrations, insoluble precipitates of dark purple color are formed. In principle, this could be attributed to noncovalent interaction between the aromatic rings of the dye and polystyrene (π-π stacking). Also, in the Bodipy containing particle sample (KK94 BG) the absorbance of Bodipy can be detected at 523 nm. In the SDS-containing samples, the SDS can still be detected and form a complex with Stains-All, but a quantitative measurement is not possible.

To test for other particle materials, the same spectra were recorded for DAB-NCs, HES-NCs and polyphosphate (PP) nanoparticles with different SDS content in each sample. While the sample SW097M was only dialyzed for 6 h after an initial SDS concentration of 3.5 mM during synthesis, SW089B was dialyzed for 24 h with the same initial SDS content. The sample MF21s was not purified after synthesis like the PS-NPs and should still contain an SDS concentration of 7 mM. The recorded spectra are shown in Figure 4.3.7.

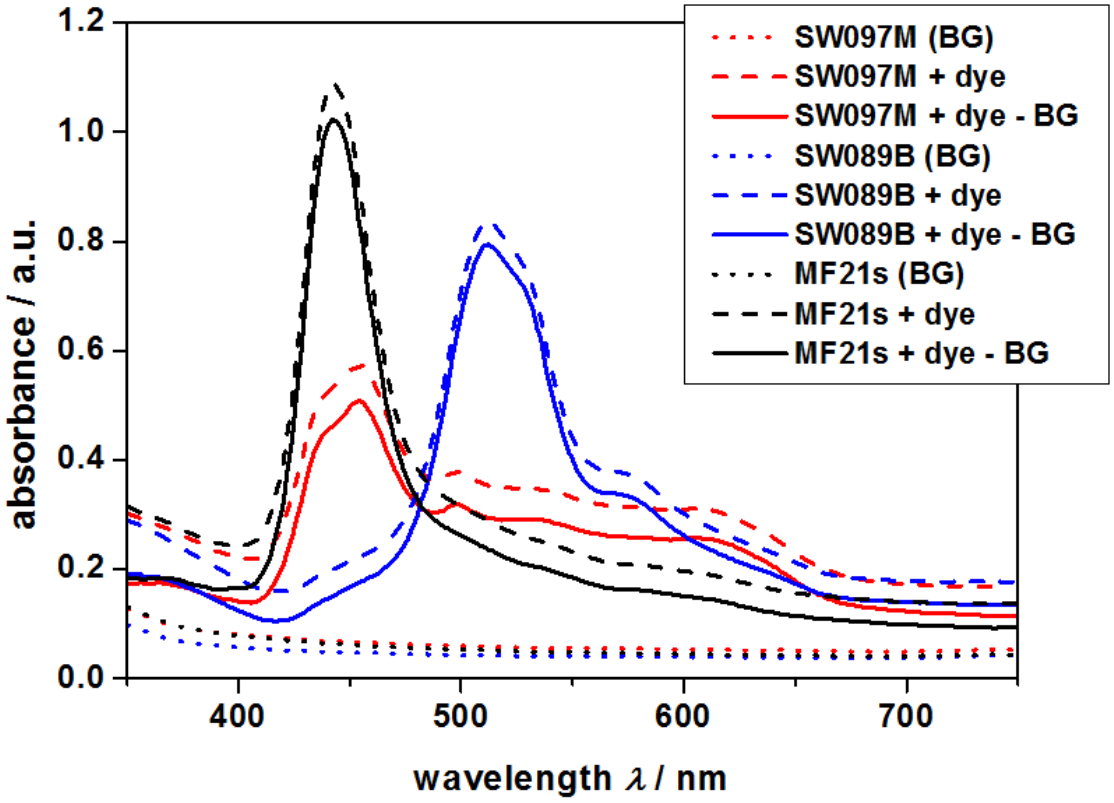

Figure 4.3.7 Absorbance spectra of DAB-NC, HES-NC and PP-NP samples in Stains-All solution.

Here it can be seen, that there is much lower background absorbance, so that the detection of the free dye and SDS-complex is actually possible. In all three samples the corresponding peak maxima can be observed and qualitatively correlate with the estimated SDS content. For quantification, the SDS concentration in the initial samples was then calculated using equation 4.4. The results are shown in Table 4.3.2. The absorbance of the samples is marked either in green or in red, depending on if it is still in the linear range of the calibration or not.

Table 4.3.2 Particle samples with their absorbance at 438 nm and resultant SDS concentration.

sample	absorbance @ 438 nm	SDS concentration / mM
KK83 (PS w/o SDS)	0.1534	0.47
KK96 (PS)	0.3477	1.90
KK94 (PS)	0.3952	2.25
SW097M (DAB)	0.4544	2.68
SW089B (HES)	0.1428	0.40
MF21s (PP)	0.9885	6.60

As it can be seen, almost all samples are within the linear regime of the calibration, except the PP-NP sample. This is expected since the sample was not purified, but still the calculated concentration (6.6 mM) matches the one during synthesis (7 mM) quite well. However, the aim of the assay is not to detect the amount of SDS directly after synthesis, but after several purification steps. Thus, sensitivity in lower concentration regimes is desired. Concerning the PS containing nanoparticles, the calculated SDS concentration can only be used for qualitative comparison. The sample KK83 did not contain any SDS, but still the background was high enough to give a false positive signal. Therefore, also the other two samples cannot be analyzed quantitatively. Interestingly, the trend of the SDS concentration measured in the DAB- and HES-NC samples matches the estimation from the different dialysis times. This shows, that the assay could be used to determine the sufficiency of purification for certain particle materials in very low concentration regimes.

After all, the question remains, whether all of the SDS present in the sample can be detected with the assay. It is not clear if the SDS on the particle surfaces is actually accessible by the dye. Therefore, the two PS-NP samples KK94 and KK96 were centrifuged at a low speed for longer time (see Experimental) to achieve a mild separation of the particles with SDS still attached from the SDS in solution (Figure 4.3.8). Then, the supernatant of each solution was taken for quantification with the Stains-All assay. The absorbance at 438 nm was measured and again the SDS concentration calculated. Then each value was compared with the ones before centrifugation (see Table 4.3.3).

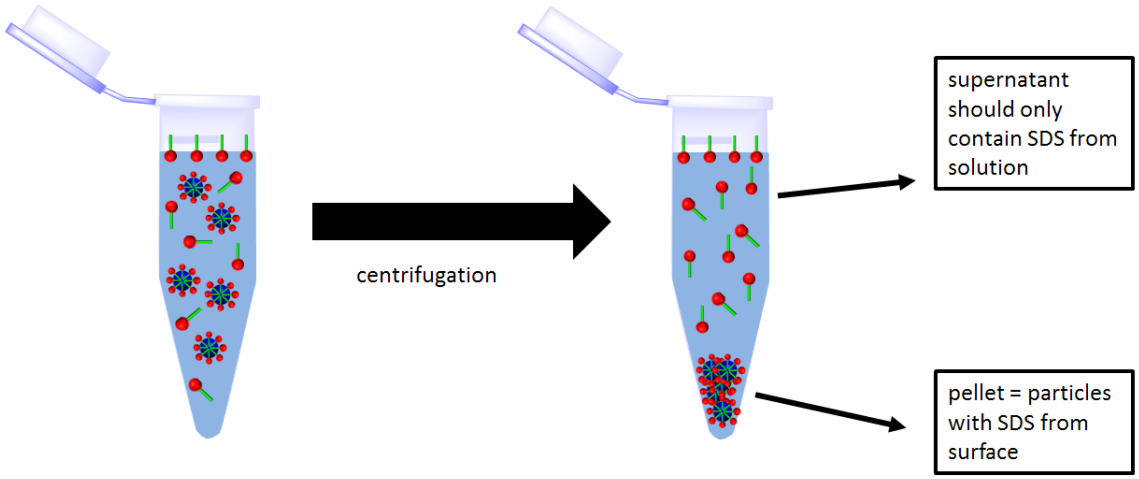

Figure 4.3.8 Schematic representation of the experimental setup for determining, which SDS fraction of the sample can be detected with Stains-All.

Table 4.3.3 Particle samples before and after centrifugation with their absorbance at 438 nm and resultant SDS concentration.

sample	absorbance @438 nm	SDS concentration / mM
KK96 (PS-NP)	0.3477	1.90
KK96 (supernatant)	0.2713	1.34
KK94 (PS-NP)	0.3952	2.25
KK94 (supernatant)	0.1582	0.51

Interestingly, the supernatant after centrifugation exhibits a lower absorbance after background subtraction for both samples. This could be a hint, that some of the SDS was still attached to the particle surface and now is not recognized in the assay. Thus, initially all the SDS present in the sample would have been detected. However, since the test was performed with PS nanoparticles, the influence of the particle material is not clear. Therefore, the different absorbance before and after centrifugation could also just result from the removal of the polystyrene itself. Accordingly, more samples need to be tested to verify the results obtained here.

4.3.1 Conclusion

In summary, the investigated method to quantify SDS in solution could successfully be adapted to nanoparticle suspensions. Although only a few different materials were tested, the qualitative trend of the expected SDS concentrations could be verified. The tested calibration rows can be used for very small SDS concentrations, so that all interesting concentration ranges can be detected. Larger SDS concentrations could also be detected with prior dilution of the sample of interest. To determine the factors limiting the sensitivity of the dye, more materials have to be tested. In this test, only polystyrene was found to influence the complexation of SDS. Also, additional fluorescent dyes present can interfere with the absorbance spectra. It also has to be clarified, if all SDS present in the sample can be detected readily. Therefore the centrifugation experiments would have to be repeated with other materials or the particle materials has to be dissolved in an organic solvent. Generally speaking, this assay provides a promising tool to quantitate SDS in nanomaterial dispersions.

4.4 Influence of protein fluorescence labels on the protein adsorption on hydrophilic vs. hydrophobic materials

Using fluorescent proteins allows characterizing different aspects of the protein corona formation and properties by applying highly sensitive and selective techniques like e.g. microscale thermophoresis or fluorescence correlation spectroscopy (FCS).[115, 116] Fluorescent proteins are generally used either as genetically encoded fluorophores (e.g. green fluorescent protein family - GFP)[49] or proteins with a subsequently attached label. GFP provides a great tool to study protein expression, interaction and many other cellular processes *in vivo*. As the native plasma proteins do not show intrinsic fluorescence, they have to be labeled by a covalent attachment of small molecule fluorophores.

For the protein corona analysis FCS has become an important technique. It is most suitable for the interaction of very small nanomaterials like quantum dots with proteins, which has been demonstrated by U. Nienhaus and coworkers.[76, 77, 117, 118] However, it is more difficult to investigate larger structures like drug carrier systems. The carriers can be fluorescently labeled, but the size change caused by a monolayer of adsorbed proteins will not be visible any more due to the experimental error. Protein adsorption with labeled proteins or peptides has been studied on flat surfaces[119] as well as spherical particles[120] without an estimation of the label influence. However, it has been observed in several studies the attached label can change the physico-chemical properties of the used proteins.[121-123] It was also found that these changes further affect the behavior of the proteins *in vitro* and *in vivo*, for example the binding of labeled proteins to cell surfaces.[124] Accordingly, Guan *et al.* observed that the adsorption of fluorescently labeled bovine serum albumin (BSA) to a hydrogel was increased in comparison to native BSA.[125]

In this chapter, the effect of fluorescence labels on the protein adsorption to hydrophilic nanomaterials was investigated. In the first chapter (see chapter 4.1), it was discussed that due to its hydrophilic nature HES-NCs exhibit a relatively low protein affinity compared to other, more hydrophobic nanomaterials. Here, we compared the impact of different fluorescence labels attached to bovine and human serum albumin (HSA) on the interaction of these proteins with HES-NCs.

4.4.1 Characterization of materials used for adsorption experiments

In order to compare the influence of the label's chemical structure, three different fluorescent dyes, namely Alexa Fluor® 488 (AF488), Bodipy® FL (BP) and Fluorescein (FITC) were chosen. The dyes exhibit different characteristics like polarity and excitation and emission maxima (see Table 4.4.1). Their dipole moments were calculated using the ChemBio 3D Ultra GAMESS Interface and are shown in Figure 4.4.1 together with the respective chemical structures. Commercially available conjugates of those dyes with BSA were purchased, while an additional BP-HSA conjugate was synthesized and purified (see Experimental Part).

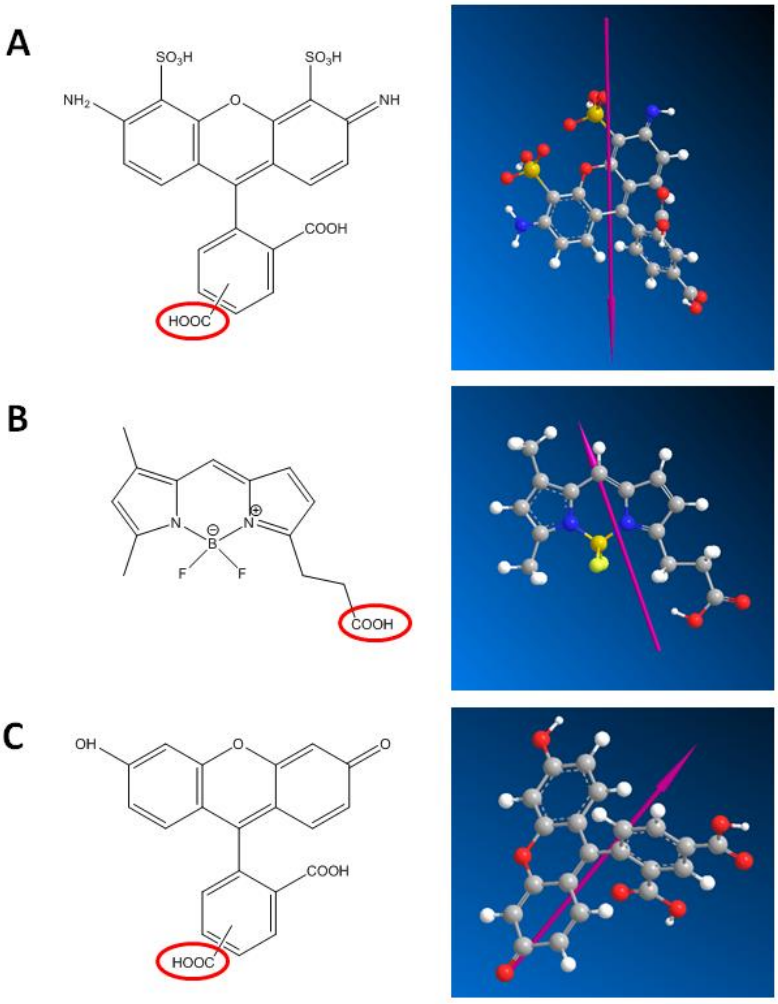

Figure 4.4.1 Chemical structures of the fluorescent dyes used (left) with a red circle indicating the carboxylic acid group coupled to the protein as amide bonds. For each structure the 3D orientation and dipole moment is displayed (right) using a magenta arrow. The length of the arrow corresponds to the value of dipole moment. A) Alexa Fluor® 488, B) BODIPY® FL, C) Fluorescein.

Table 4.4.1 Fluorescent dyes characteristics.

Dye	Dipole moment[a] / debye	Excitation Maximum[b] / nm	Emission Maximum[b] / nm
Alexa Fluor® 488	18.76	490	525
Bodipy® FL	10.59	503	512
Fluorescein	11.14	490	525

[a] calculated with ChemBio 3D Ultra GAMESS Interface
[b] as given by the supplier

The labeling of HSA was performed to obtain a protein with only one fluorescence label attached, since all commercially available conjugates feature several dye molecules per protein, as confirmed by FCS (see Table 4.4.2). BP was chosen for the conjugation because it gave the best coupling yield compared to the other dyes. The BP-HSA conjugate was characterized with high performance liquid chromatography (HPLC) by Beate Müller (MPIP Mainz, Germany) to ensure complete conversion of the HSA (see Figures 4.4.2-4.4.4). The conjugate can be seen at an elution time of ca. 4.4 min while an impurity is detected at ca. 4.9 min. From the polarity and the absorption characteristics, the impurity is suspected to be the corresponding free carboxylic acid of Bodipy FL, which could not be fully removed during purification. Using FCS, the number of dye molecules per protein was determined to be one.

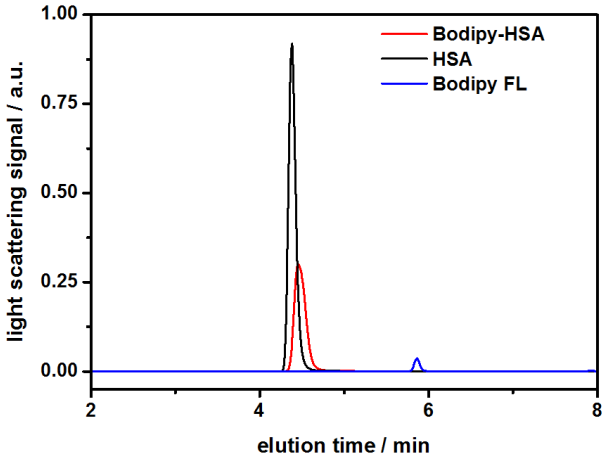

Figure 4.4.2 HPLC analysis of the Bodipy-HSA conjugate displaying the light scattering signal: Bodipy-HSA (red line), unmodified HSA (black line) and pure Bodipy FL succinimidyl ester (blue line).

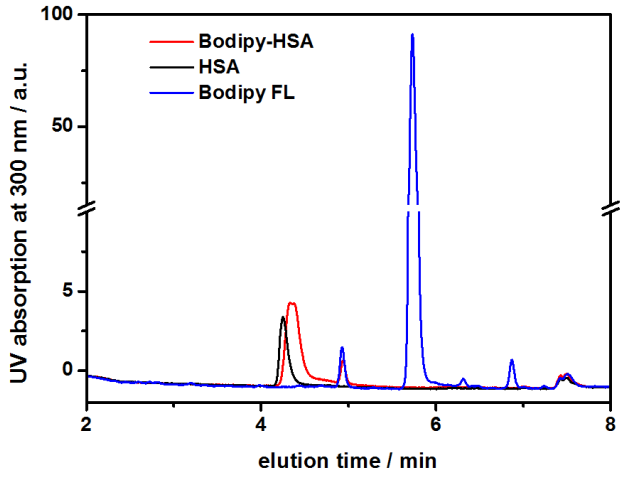

Figure 4.4.3 HPLC analysis of the Bodipy-HSA conjugate displaying the UV signal at a wavelength of 300 nm: Bodipy-HSA (red line), unmodified HSA (black line) and pure Bodipy FL succinimidyl ester (blue line).

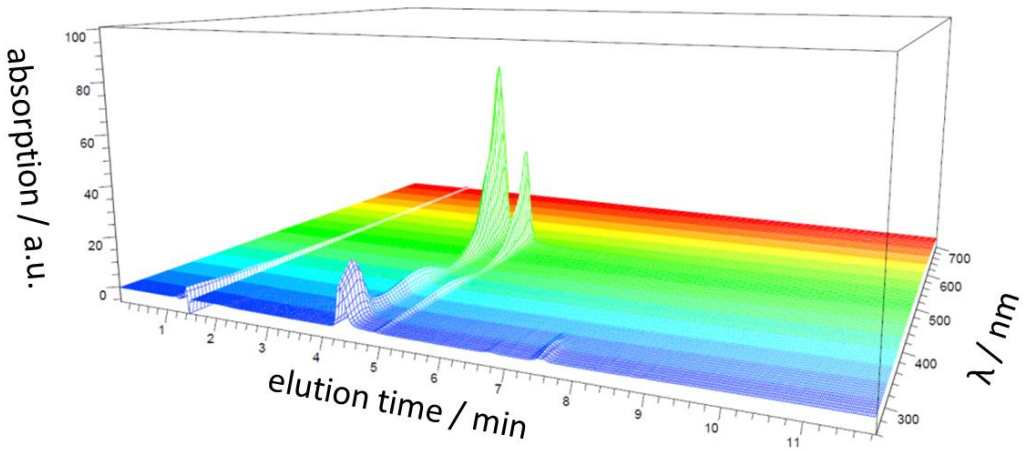

Figure 4.4.4 HPLC 3D plot displaying the absorption spectra for the eluted Bodipy-HSA conjugate.

Hydrophilic HES-NCs with an R_h of 128 ± 13 nm and hydrophobic polystyrene nanoparticles (PS-NPs) with an R_h of 59 ± 6 nm (sizes determined by DLS) were synthesized according to previously published procedures.[86, 100] Detailed characterization of the nanomaterials can be found in chapter 4.1 and 4.2. Although the sizes of the nanomaterials are different, the surface curvature should not influence the adsorption characteristics dramatically. To account for this difference, the adsorption of unlabeled albumin was also examined.

4.4.2 FCS measurements

The adsorption of all conjugates to HES-NCs was investigated using FCS experiments together with Dr. Kaloian Koynov (MPIP Mainz, Germany) and ITC. In an FCS experiment, the temporal fluorescence intensity fluctuations caused by e.g. the diffusion of the studied fluorescent species through a small observation volume are monitored and used to evaluate their diffusion coefficient, hydrodynamic radius R_h, concentration and fluorescence brightness.[126] A binding of a fluorescent protein to a non-fluorescent (at the same excitation wavelength) nanocapsule is manifested by an increase of the measured hydrodynamic radius. In addition, ITC provides quantitative information about the binding process between the nanomaterial and the proteins by determining the thermodynamic properties of the reaction. Like this, the binding affinities of labeled and unlabeled proteins can be compared. To enable independent monitoring of the HES-NCs, they were synthesized with encapsulated sulforhodamine dye (SR101) with ex. / em. maxima of 580 / 610 nm. Figure 4.4.5 A shows the normalized FCS autocorrelation curves measured at excitation wavelength of 488 nm in aqueous solution of pure AF488-BSA and in a (6 : 1 molar ratio) mixture of HES-NCs with AF488-BSA. The FCS autocorrelation curve measured upon direct excitation of the nanocapsules' fluorescence at 543 nm is also shown for comparison. All autocorrelation curves were fitted with equation 3.16 to obtain the hydrodynamic radii of the corresponding fluorescent species. For the sample that contained the pure labeled protein, a hydrodynamic radius of R_h = 4.4 nm was obtained, which matches the literature values reported for single serum albumin molecules.[111] Any binding of AF488-BSA to the HES-NCs should result in a strong shift of the autocorrelation curve to longer lag times, reflecting the appearance of much larger, slowly diffusing fluorescent in the size range of the HES-NCs. However, the autocorrelation curve measured upon 488 nm excitation in the mixture of both components was identical to that observed in the solution of pure AF488-BSA. Similar results were obtained upon various HES-NCs to AF488-BSA mixing ratios (see Experimental for details). The presence of HES-NCs in the mixture could be detected with FCS only upon direct excitation (of SR101) at 543 nm (Figure 4.4.5 A). The fit to the corresponding autocorrelation curve revealed an R_h value of 133 nm, which is in good agreement with that measured with DLS. These findings suggest that the capsules and proteins are not interacting with each other at all.

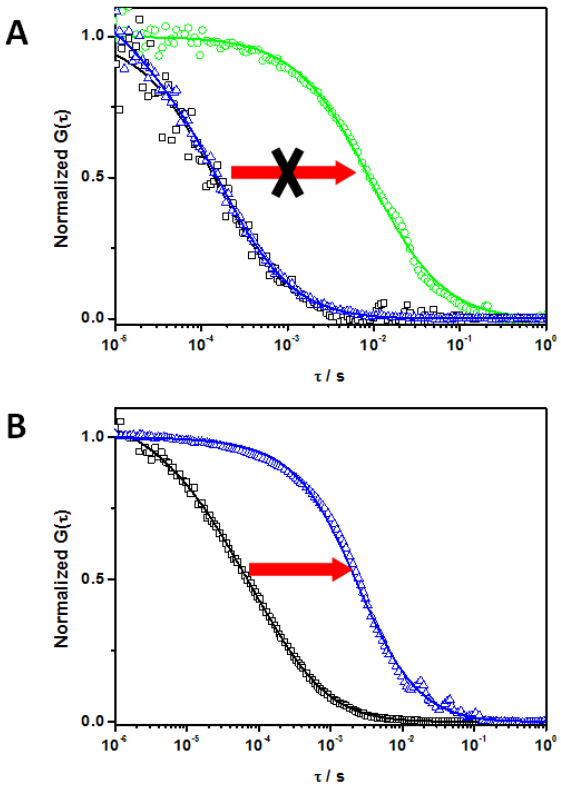

Figure 4.4.5 Normalized FCS Autocorrelation curves (symbols) and corresponding fits (straight lines). A) pure AF488-BSA at 488 nm excitation (black squares □), AF488-BSA in the presence of HES-NCs at 488 nm excitation (blue triangles Δ) and SR101-labeled HES-NCs in the presence of AF488-BSA at 543 nm excitation (green circles ○). B) pure BP-HSA (black squares □) and BP-HSA in the presence of PS-NPs (blue triangles Δ) both at 488 nm excitation. The red arrows indicate the existing or non-existing shift to slower diffusion coefficients of the proteins adsorbed on the NPs.

The same experiments were performed for the other commercial conjugates with the same result, although the dyes used for fluorescence labeling exhibit different polarities (Table 4.4.1). Also, the in house prepared BP-HSA conjugate that was labeled with only one dye per protein (compared to ~5 dyes per protein for the commercial counterparts, Table 4.4.1) did not show any adsorption to the HES-NCs in the FCS experiments. Since HES is a very hydrophilic material, PS-NPs were used as a hydrophobic reference material. Exemplarily, the PS-NPs were mixed with BP-HSA (at 340 : 1 molar ratio) and studied with FCS. Since the PS-NPs were not labeled themselves, only the autocorrelation curves obtained at 488 nm excitation wavelength were recorded (see Figure 4.4.5 B). Here it can be clearly detected that the proteins attach to the nanoparticles because the R_h of the fluorescent species shifted from 4.4 nm in the solution of pure BP-HSA to 48 nm in the mixture, which is in the size range of the PS-NPs.

4.4.3 ITC measurements and isoelectric focusing of dye-protein conjugates

To obtain quantitative information about the different adsorption characteristics of labeled and non-labeled albumin, these processes were investigated with ITC. The investigated HES-NCs were placed in the measurement cell and titrated with pure BSA, HSA and all dye-albumin conjugates. As a reference, all proteins were also titrated into pure water to determine the heat of dilution, which was then subtracted from the adsorption measurements. For each titration the so-called adsorption isotherms are obtained after integrating the baseline-corrected heat rates. Exemplarily, the adsorption isotherms for AF488-BSA and BSA on HES-NCs are shown in Figure 4.4.6 A. While for BSA an exothermic signal is obtained, the signals for the labeled BSA fluctuate around zero.

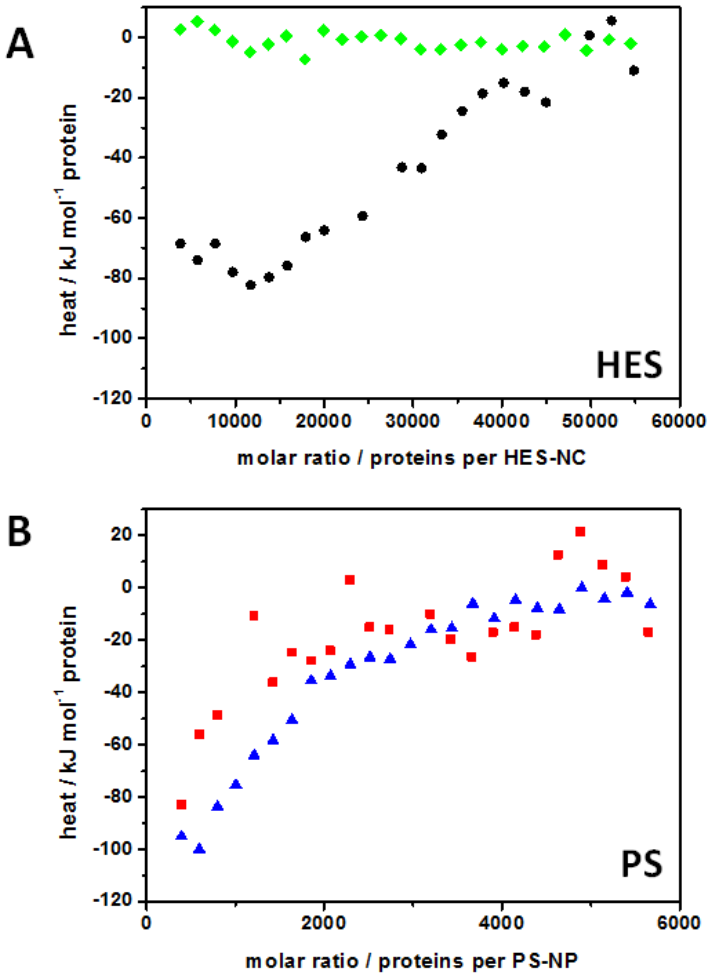

Figure 4.4.6 ITC adsorption isotherms obtained from the titration of A) HES-NCs with AF488-BSA (green diamonds ♦) and B) PS-NPs with BP-HSA (red squares ■). For comparison the corresponding isotherms for BSA (black circles ●) and HSA (blue triangles ▲) are shown.

For both BSA and HSA, this is the expected adsorption behavior and in good agreement with previously reported results.[86] In contrast, the labeled albumin does not show any kind of interaction with the NCs that involves the absorption or release of heat. Therefore, if any interaction is taking place it must be enthalpically neutral and only driven by entropy. Taking the FCS results into account, this is not the case and both methods agree in the finding that the fluorescence labeling completely suppresses the protein adsorption. As in the FCS experiments, the ITC data were compared with titrations of PS-NP (Figure 4.4.6 B). Again, the measurements support the previously obtained results and reveal that between the adsorption of BP-HSA and pure HSA to PS-NP no differences are noticeable. Both proteins show an exothermic adsorption behavior. The same adsorption characteristics as for AF488-BSA were found for all other dye-protein conjugates on HES-NCs (see Figure 4.4.7).

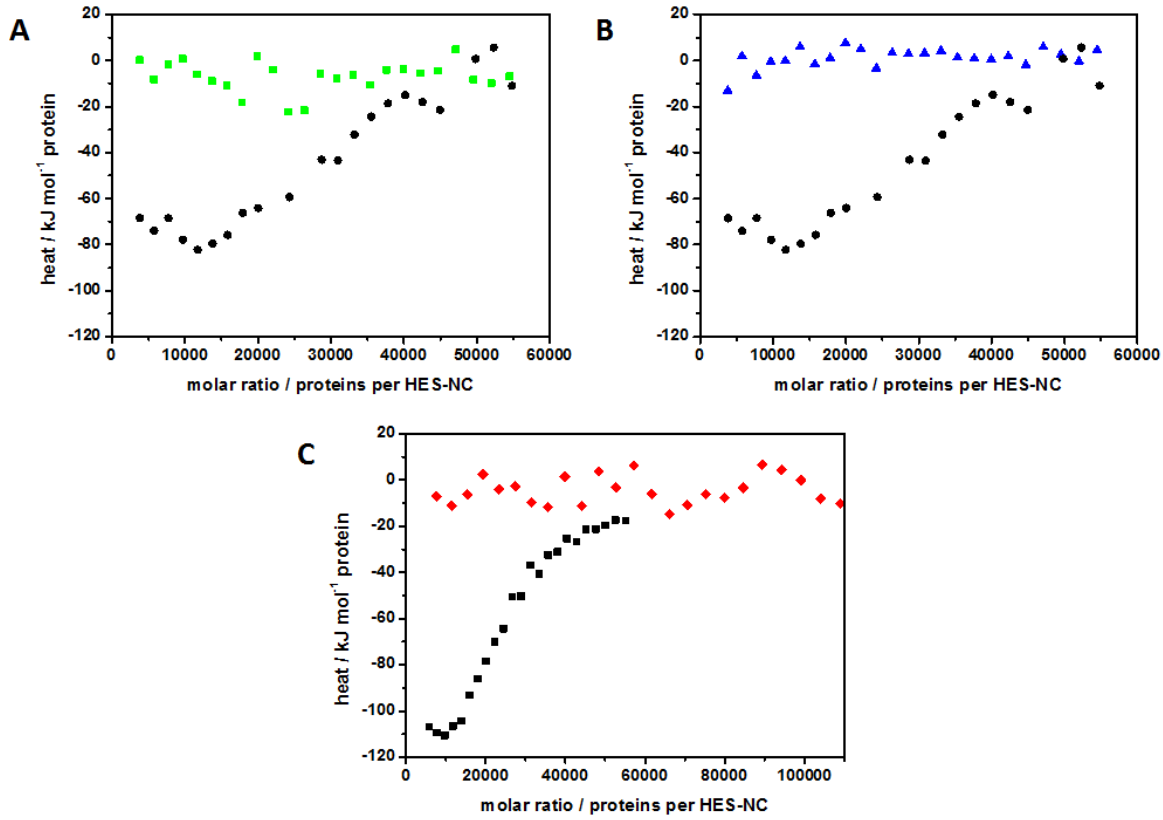

Figure 4.4.7 ITC adsorption isotherms obtained from the titration of A) HES-NCs with BP-BSA (green squares ■), B) HES-NCs with FITC-BSA (blue triangles ▲) and C) HES-NCs with BP-HSA (red diamonds ♦). For comparison the corresponding isotherms for HES-NCs with unlabeled BSA (black circles ●) and HSA (black squares ■) are shown.

Based on these findings, it can be concluded that a covalently attached fluorescent label influences the interaction of a protein with a hydrophilic surface material like HES much stronger than with a hydrophobic one like PS. This suggests that the used modifications of the albumin molecule primarily interfere with the electrostatic interactions of the protein with any kind of surface – independent from their polarity – while hydrophobic interactions are not influenced significantly. To further examine the changes in electrostatic characteristics of the proteins, the isoelectric points of all dye-protein conjugates and the unmodified proteins were determined by Dr. Susanne Schöttler, MPIP Mainz, Germany (see Figure 4.4.8 and 4.4.9, Table 4.4.2).

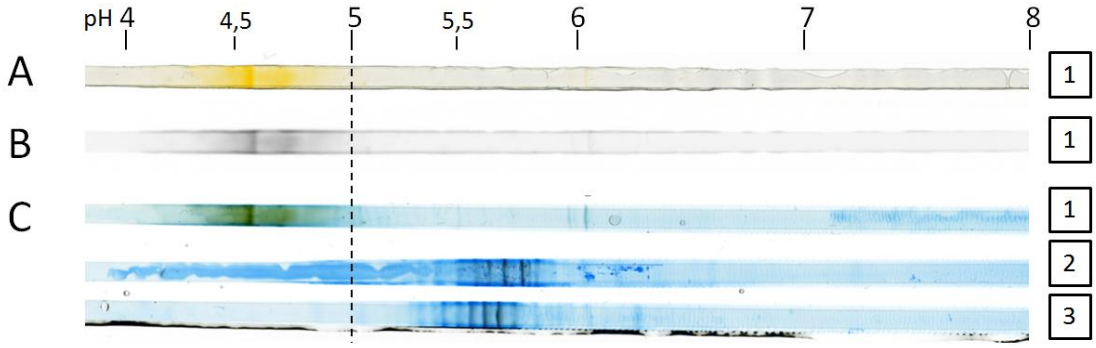

Figure 4.4.8 Isoelectric focusing run 1. A) Scan before staining at visible light, B) Scan before staining at 488 nm wavelength, C) Scan after staining with Coomassie Brilliant Blue. Lane 1: AF488-BSA, Lane 2: HSA, Lane 3: BSA. The dotted line at pH 5 is introduced as a guide to the eye.

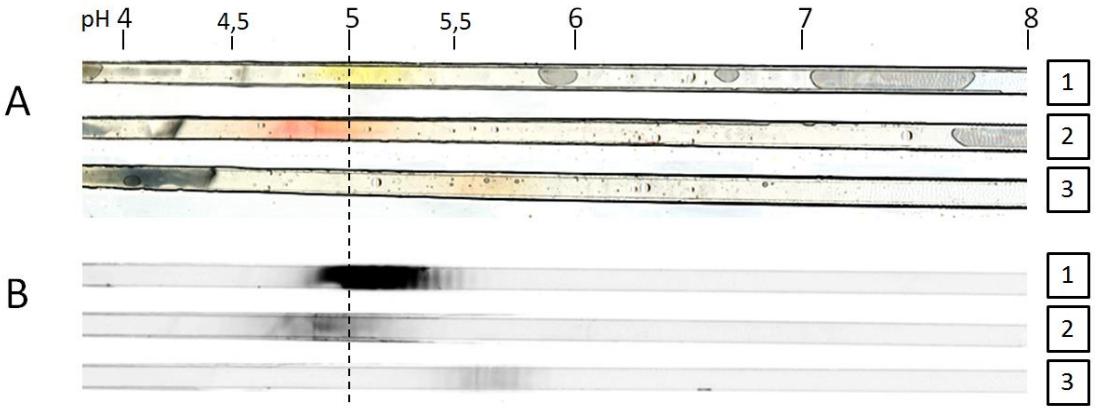

Figure 4.4.9. Isoelectric focusing run 2. A) Scan at visible light, B) Scan at 488 nm wavelength. Lane 1: FITC-BSA, Lane 2: BP-BSA, Lane 3: BP-HSA. The dotted line at pH 5 is introduced as a guide to the eye.

Table 4.4.2 Isoelectric focusing data of labeled and unlabeled albumin.

Protein	Number of attached dye molecules per protein[a]	IEP range of bands	IEP mean value
BSA	-	5.3-5.7	5.5
HSA	-	5.4-5.8	5.6
AF488-BSA	5	4.4-4.6	4.5
FITC-BSA	5	4.9-5.3	5.1
BP-BSA	5	4.7-5.1	4.9
BP-HSA	1	5.4-5.8	5.6

[a] as given by the supplier and roughly confirmed with FCS

As it can be seen, the isoelectric points (IEP) of BSA and HSA are in agreement with those reported in literature.[127] The attached fluorescence labels significantly reduce the IEP for the commercial conjugates. The only exception is the additionally synthesized BP-HSA conjugate with only one dye molecule per protein, which has the same IEP like pure HSA. However, one dye molecule was still enough to prevent adsorption to HES-NCs. To this extent, it is unlikely that the influence on the adsorption is caused by the small change of the IEP of the protein. Rather, it also has to do with the position of the fluorescence label. The pH during the synthesis of the BP-HSA conjugate was adjusted to yield HSA with the fluorescence label at the N-terminus of the protein. This can be achieved at a pH of 7.4, where the terminal amino group should not be protonated in contrast to the ε-amino groups of lysine residues, because those have a higher pK_a value.[128] Accordingly, the N-terminus of the protein or the residues in direct proximity have to be significantly involved in the electrostatic interaction with hydrophilic materials. Since albumin has some hydrophobic patches that normally are not solvent accessible (hydrophobic pocket), it is likely that these patches are responsible for binding to hydrophobic materials via Van-der-Waals interactions. These hydrophobic patches are not influenced by any fluorescence labels coupled to amino groups on the protein surface, so they are available after reorganization of the protein structure.

4.4.4 Conclusion

In conclusion, the influence of different fluorescence labels on the interaction of albumin with hydrophilic vs. hydrophobic nanomaterials was investigated. Interestingly, in all cases, the fluorescence label completely suppressed the interaction with the hydrophilic HES-NCs. In contrast the adsorption on PS-NPs was not affected in any way. Additionally, it was shown that the polarity of the dye as well as the number of attached molecules did not change the binding properties of the protein. From these findings it was derived that the fluorescent labels interfere with the electrostatic interactions of the protein since they are coupled to lysine residues or the N-terminus. For future investigations, if a protein label is necessary e.g. for FCS studies involving large particles, it should be carefully chosen so that it does not block the primary interaction processes. Therefore, the interaction processes have to be known or experiments with different label types have to be conducted. Nonetheless, the obtained data should always be verified using methods, which do not involve a modification of one of the materials.

4.5 Evaluation of the temperature effect on protein adsorption characteristics

When protein adsorption on nanocarriers for biomedical application is being investigated, most of the time this is being done at one fixed temperature. Typically, this is either 37 °C since this is body temperature, or 25 °C for better experimental conditions. While it is often not considered, it has been shown that the temperature during the time the protein corona is formed has a significant influence on the protein composition found later.[129] It could now be argued, that all protein adsorption experiments should thus be performed at 37 °C since this is the biologically relevant temperature. However, a protein corona can not only be formed inside the body, but also *in vitro* e.g. for preincubation of nanoparticles for a certain application.[19] Consequently, it is important to obtain an understanding of the influence of temperature, to be able to use this information for a better understanding of the nature of protein adsorption. Therefore, model polystyrene nanoparticles (PS-NPs) stabilized with small amounts of Lutensol AT50 (Lut) were used to study their interaction with several single plasma proteins at 25 °C and 37 °C each. To ensure that the interaction considered is not influenced significantly by the surfactant, the particles were thoroughly purified by centrifugation and the zeta potential was measured afterwards. A value of -14.6 ± 1 mV was obtained, which indicates a very low coverage with Lut. Additionally, the size of the PS-NPs was determined to be R_h = 53 ± 5 nm.

4.5.1 PS-NP interaction with human serum albumin (HSA)

First, the interaction between HSA and PS-NPs was investigated, since the parameters obtained can then be compared to the data regarding the influence of different surfactant coverages. The titrations of PS-NPs with HSA at 25 °C and 37 °C are shown in Figure 4.5.1. For both temperatures an exothermic adsorption process could be observed and the obtained binding isotherms could be fitted according to an independent binding model. In Table 4.5.1 the calculated fitting parameters are shown for both temperatures.

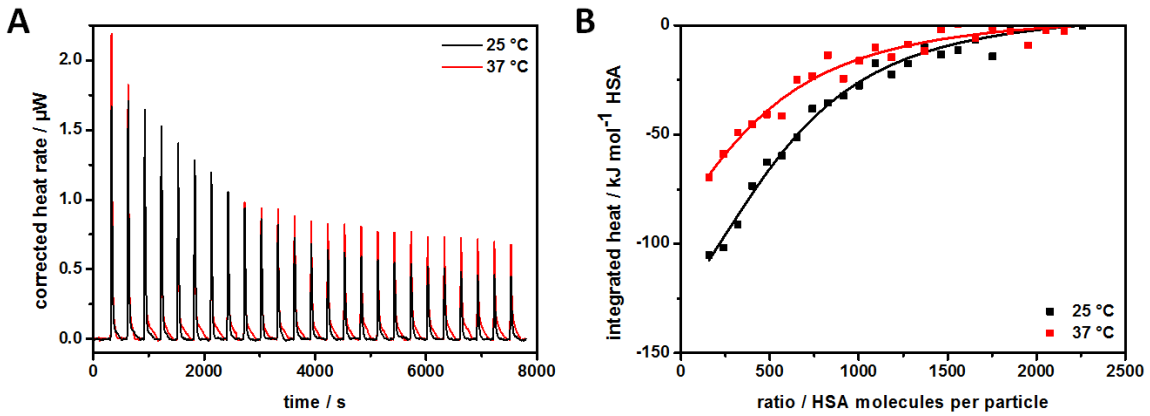

Figure 4.5.1 A) ITC raw data of PS-NP titrated with HSA: baseline corrected heat rates of the titration performed at 25°C (black line −) and 37 °C (red line −). B) Integrated heats from each titration after subtraction of dilution heat with a corresponding fit according to an independent binding model. The titrations were performed with a particle concentration of 10 g·L^{-1} (2.22·10^{-5} mM) and a HSA concentration of 10 g·L^{-1} (0.15 mM).

Table 4.5.1 Parameters obtained from fits of ITC measurements of PS-NPs with HSA at different temperatures according to an independent binding model.

Temperature / °C	K_a / 10^5 L·mol^{-1}	N	ΔH / kJ·mol^{-1}
25	1.3 ± 0.2	624 ± 195	-183 ± 30
37	0.8 ± 0.1	347 ± 122	-263 ± 90

Errors represent the mean standard deviation of values obtained from 3 or more individual experiments

Comparing the parameters obtained at 25 °C with those in chapter 4.2, it can be seen that they match the data obtained previously with Lut-stabilized PS-NPs. Regarding the trends of K_a and N, the values for this system are lying between those for completely purified (K_a, N not measureable) and completely unpurified PS-NPs (K_a = 1.4 ± 0.1·10^5 L·mol^{-1}, N = 7,629 ± 1,258, ΔH = -184 ± 8 kJ mol^{-1}) interacting with HSA, while ΔH remains constant. This correlates quite well with the amount of Lut expected in the sample from the purification and zeta potential measurements. Also it shows that different particle batches exhibit similar adsorption characteristics when it is ensured that surfactant coverage is comparable.

When the temperature is raised to 37 °C, the adsorption isotherm is shifted. While the adsorption enthalpy obtained at both temperatures T remains constant within the accuracy of the measurement, N and K_a decrease with increased T. Considering the assumption of an equilibrium that is made when applying an independent binding model,

the binding affinity equals the equilibrium constant and can be written in the following way:

$$K_a = \frac{[protein{-}particle{-}complex]}{[protein]\cdot[particle]}$$

When the adsorption is an exothermic process, the equilibrium is accordingly shifted towards the side of the single components upon increasing *T*. Consequently, K_a becomes smaller as long as the reaction is reversible. In this case, the adsorption of HSA onto PS-NPs seems to satisfy the assumption of an equilibrium reaction and therefore the adsorption is decreased with higher temperatures. Also when more free protein is in solution, a smaller number is adsorbed onto one particle and thus the decreased stoichiometry *N* is also in agreement with a reversible reaction.

4.5.2 PS-NP interaction with coagulation proteins: fibronectin, fibrinogen, plasminogen

Further, the interaction of PS-NPs with coagulation proteins was studied. Therefore fibronectin, fibrinogen and plasminogen were used for the titrations since they are readily available. The ITC data obtained from the titration of PS-NPs with fibronectin is shown in Figure 4.5.2 and the parameters summarized in Table 4.5.2. Here, it can also be seen (Figure 4.5.2 B) that the adsorption isotherm changes when the adsorption takes place at a higher temperature.

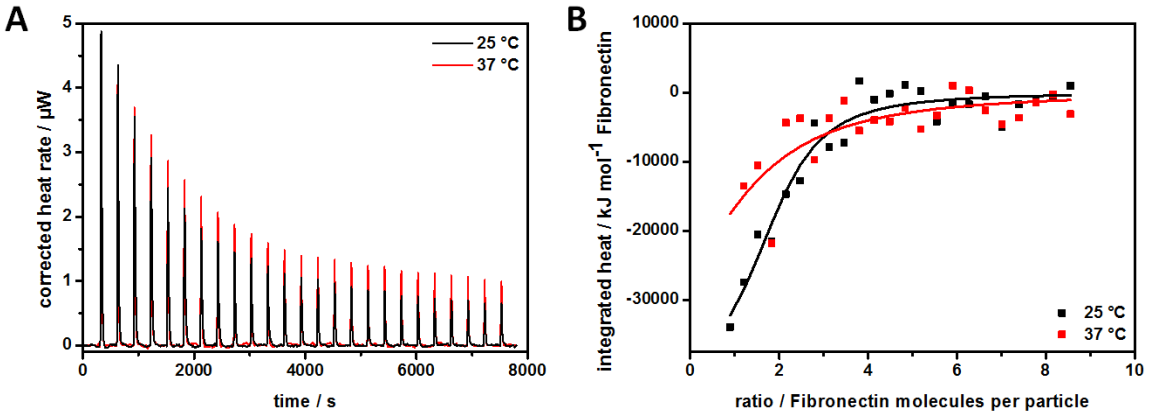

Figure 4.5.2 A) ITC raw data of PS-NP titrated with fibronectin: baseline corrected heat rates of the titration performed at 25°C (black line −) and 37 °C (red line −). B) Integrated heats from each titration after subtraction of dilution heat with a corresponding fit according to an independent binding model. The titrations were performed with a particle concentration of 10 g·L^{-1} (2.22·10^{-5} mM) and a fibronectin concentration of 0.25 g·L^{-1} (0.0006 mM).

Table 4.5.2 Parameters obtained from fits of ITC measurements of PS-NPs with fibronectin at different temperatures according to an independent binding model.

Temperature / °C	K_a / 10^8 L·mol^{-1}	N	ΔH / kJ·mol^{-1}
25	2.2 ± 0.4	2.0 ± 0.2	-36,800 ± 6,200
37	0.7 ± 0.5	1.1 ± 0.1	-37,950 ± 25,600

Errors represent the mean standard deviation of values obtained from 3 or more individual experiments

In the case of fibronectin it was not possible to perform the titrations with lower protein concentration or higher particle concentration. Therefore, the isotherm obtained at 37 °C is not very accurate and the resulting error from the fit is quite large (see Table 4.5.2). For both temperatures a very high heat in relation to the small protein concentration used was measured. Additionally, the number of proteins interacting with a particle is very small. Here, it has to be taken into account that the calculation of the particle concentration is based on several assumptions, so that the actual number of proteins per particle might be a bit higher. However, it is indicated that only a few fibronectin molecules are covering the particle surface immediately after contact. As fibronectin is a very large molecule (M_w = 460,000 g·mol^{-1}), the small number might be able to cover the surface completely or at least prevent the rest of the free surface from being available for interaction. As already observed with HSA, K_a and N decrease when T rises. This is again in agreement with the assumption that this exothermic reaction is reversible and in equilibrium.

Next, PS-NPs were titrated with fibrinogen (Figure 4.5.3) and plasminogen (Figure 4.5.4). For both proteins, the titrations gave no heat change regardless of the temperature. Since there is no enthalpy contribution involved in potential interactions, temperature will not change the heat output of the titration experiments. For both proteins this means, that either there is no interaction taking place or the interaction is purely entropy driven. In the latter case, a temperature increase also increases the entropy contribution to the overall free energy, so that ΔG for the adsorption becomes more negative. This means that adsorption is favored at higher temperatures for purely entropy driven interaction processes.

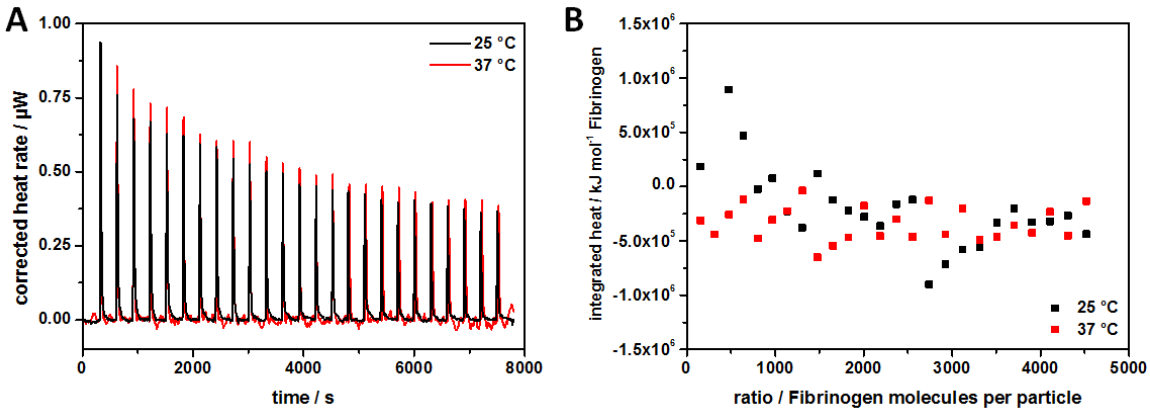

Figure 4.5.3 A) ITC raw data of PS-NP titrated with fibrinogen: baseline corrected heat rates of the titration performed at 25°C (black line −) and 37 °C (red line −). B) Integrated heats from each titration after subtraction of dilution heat with a corresponding fit according to an independent binding model. The titrations were performed with a particle concentration of 1 g·L^{-1} (2.22·10^{-6} mM) and a fibrinogen concentration of 10 g·L^{-1} (0.03 mM).

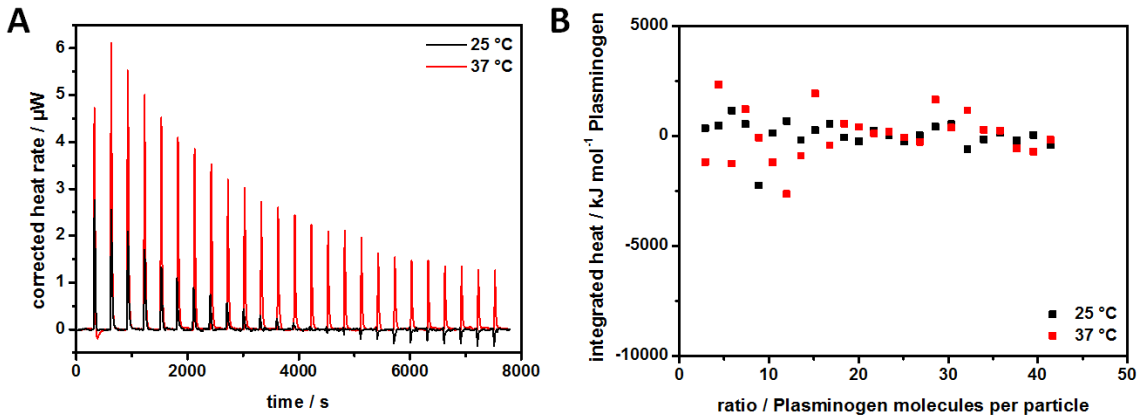

Figure 4.5.4 A) ITC raw data of PS-NP titrated with plasminogen: baseline corrected heat rates of the titration performed at 25°C (black line −) and 37 °C (red line −). B) Integrated heats from each titration after subtraction of dilution heat with a corresponding fit according to an independent binding model. The titrations were performed with a particle concentration of 10 g·L^{-1} (2.22·10^{-5} mM) and a plasminogen concentration of 0.25 g·L^{-1} (0.003 mM).

4.5.3 PS-NP interaction with apolipoproteins: apolipoprotein A-I (ApoA-I), apolipoprotein E (ApoE)

Additionally, the interaction of the PS-NP with available apolipoproteins was tested via ITC. The two proteins available (ApoA-I and ApoE) are relatively similar in size (28 and 34 kDa) but possess different roles in the lipoprotein transport pathways (see

Theory). The titrations of PS-NP with ApoA-I and ApoE at the two different temperatures are shown in Figures 4.5.5 and 4.5.6. As for fibrinogen and plasminogen, no significant heat changes other than the heat of dilution of each protein were detected. For ApoE, the heats of dilution were quite large, which can be attributed to the salts the protein is stabilized with. This also explains the large difference in the heat rate for both titrations (Figure 4.5.6 A). The difference is due to the temperature dependent dilution of the salts. To avoid those kinds of effects (also called 'buffer mismatch'), the same salt concentration would have to be ensured in the NP sample. However, at such high salt concentrations some particles are not stable any more (see Theory). Nevertheless, surprisingly no enthalpy driven interaction can be found, since apolipoproteins were found in hard protein coronas and ApoA-I was also found to bind to HES-capsules. They are believed to interact with more hydrophobic materials mainly because they usually form complexes with the amphiphilic lipids and cholesterol in the blood plasma. In this work, lipid free apolipoproteins were used for the titrations. So instead of complexing lipids it might be the case that they favor the interaction with other amphiphilic molecules like surfactants. The PS-NPs used here have very low surfactant coverage, so that this interaction might be suppressed. Otherwise, the interaction with the particle material could be of entropic nature, which cannot be seen here.

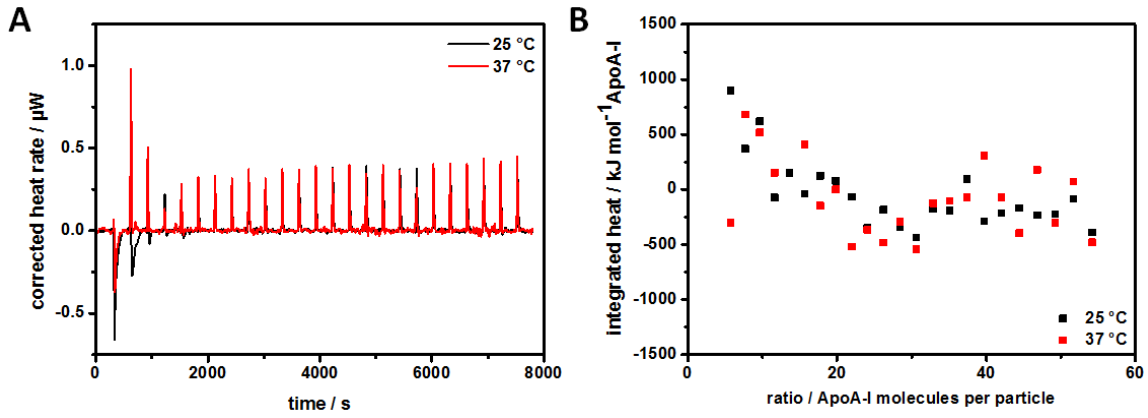

Figure 4.5.5 A) ITC raw data of PS-NP titrated with ApoA-I: baseline corrected heat rates of the titration performed at 25°C (black line −) and 37 °C (red line −). B) Integrated heats from each titration after subtraction of dilution heat with a corresponding fit according to an independent binding model. The titrations were performed with a particle concentration of 10 $g \cdot L^{-1}$ ($2.22 \cdot 10^{-5}$ mM) and an ApoA-I concentration of 0.1 $g \cdot L^{-1}$ (0.0036 mM).

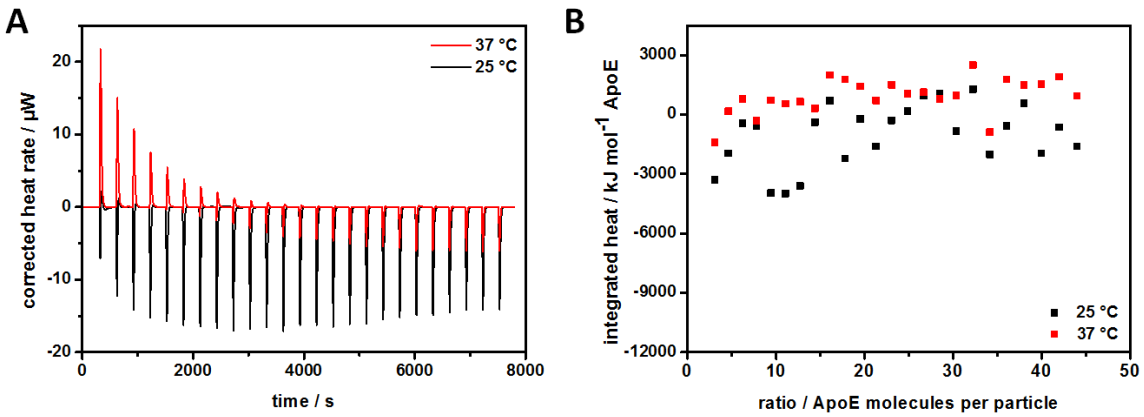

Figure 4.5.6 A) ITC raw data of PS-NP titrated with ApoE: baseline corrected heat rates of the titration performed at 25°C (black line −) and 37 °C (red line −). B) Integrated heats from each titration after subtraction of dilution heat with a corresponding fit according to an independent binding model. The titrations were performed with a particle concentration of 10 g·L^{-1} (2.22·10^{-5} mM) and an ApoE concentration of 0.1 g·L^{-1} (0.003 mM).

4.5.4 PS-NP interaction with Immunoglobulin G (IgG)

As it is also one of the major plasma proteins, the interaction of PS-NPs with IgG was also studied. Usually IgG as an antibody binds to specific antigens with its antigen binding sites. This interaction is specific and very strong. A reaction similar to this antigen recognition should not happen on nanoparticle surfaces. However, also unspecific adsorption with other parts of the antibody could occur on different surfaces. This would mean that the particles are recognized as foreign objects and cleared by the immune system, so it is very important to determine antibody adsorption on nanoparticles.

The titration experiments at 25 °C and 37 °C are shown in Figure 4.5.7. Again, no interaction involving released or absorbed heat can be observed. This means that no specific binding of IgG is occurring. This kind of titrations could serve as an easy test for the recognition of nanoparticles by antibodies. If adsorption is taking place, it has to be entropy driven. When this is the case, the temperature increase to 37 °C is also enhancing the protein adsorption.

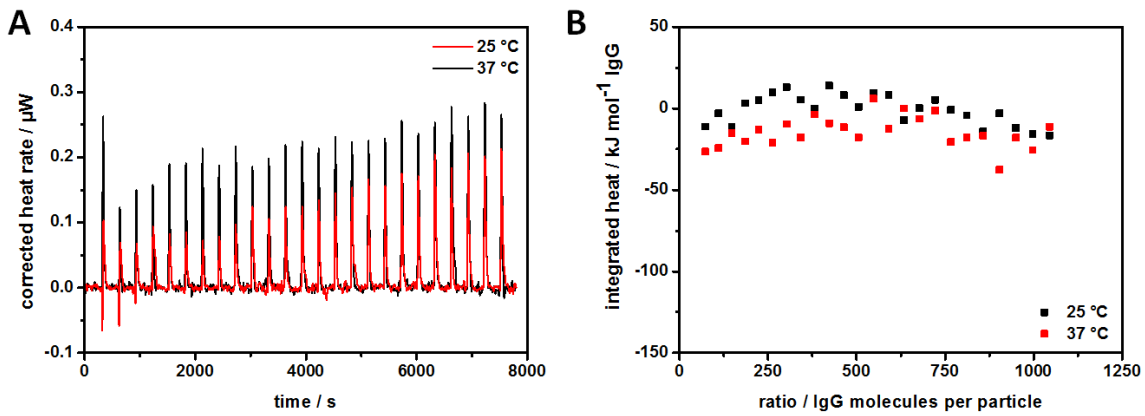

Figure 4.5.7 A) ITC raw data of PS-NP titrated with IgG: baseline corrected heat rates of the titration performed at 25°C (black line −) and 37 °C (red line −). B) Integrated heats from each titration after subtraction of dilution heat with a corresponding fit according to an independent binding model. The titrations were performed with a particle concentration of 10 g·L^{-1} (2.22·10^{-5} mM) and an IgG concentration of 10 g·L^{-1} (0.035 mM).

4.5.5 PS-NP interaction with Transferrin

The last tested protein in the titration measurements was transferrin. The obtained titration data is shown in Figure 4.5.8. Again, no enthalpy driven adsorption process could be detected. Since Transferrin was proven to bind to PS-NPs, it is unlikely that here no interaction is occurring. Potentially, again there is only an entropy driven adsorption process like it is probably for the other investigated proteins.

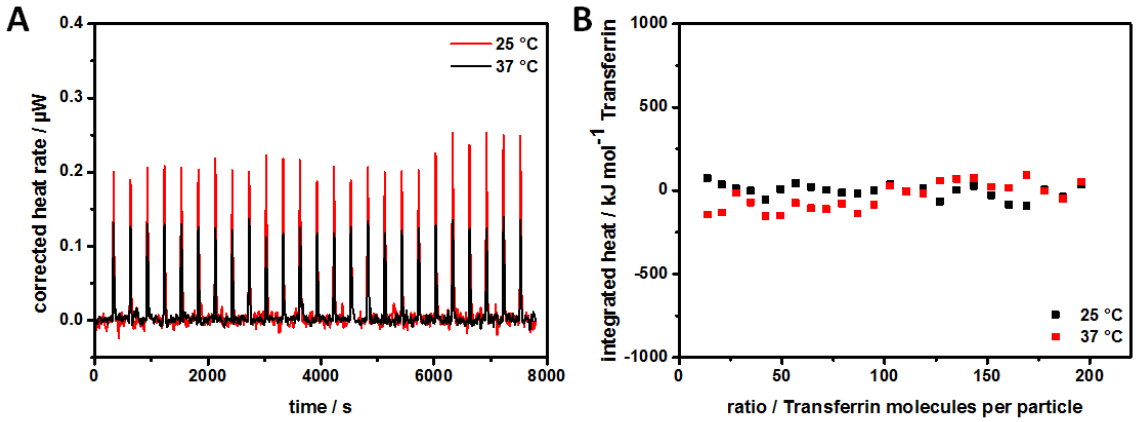

Figure 4.5.8 A) ITC raw data of PS-NP titrated with transferrin: baseline corrected heat rates of the titration performed at 25°C (black line −) and 37 °C (red line −). B) Integrated heats from each titration after subtraction of dilution heat with a corresponding fit according to an independent binding model. The titrations were performed with a particle concentration of 10 g·L^{-1} (2.22·10^{-5} mM) and a transferrin concentration of 1 g·L^{-1} (0.013 mM).

4.5.6 DLS and Zeta-potential measurements of all investigated proteins

All protein-NP mixtures obtained from ITC were also analyzed with DLS and zeta potential measurements. DLS allows determining, whether aggregate formation can be observed after the mixing. All particle protein mixtures except PS-NPs + plasminogen at 37 °C could be analyzed (see Figure 4.5.9 and 4.5.10).

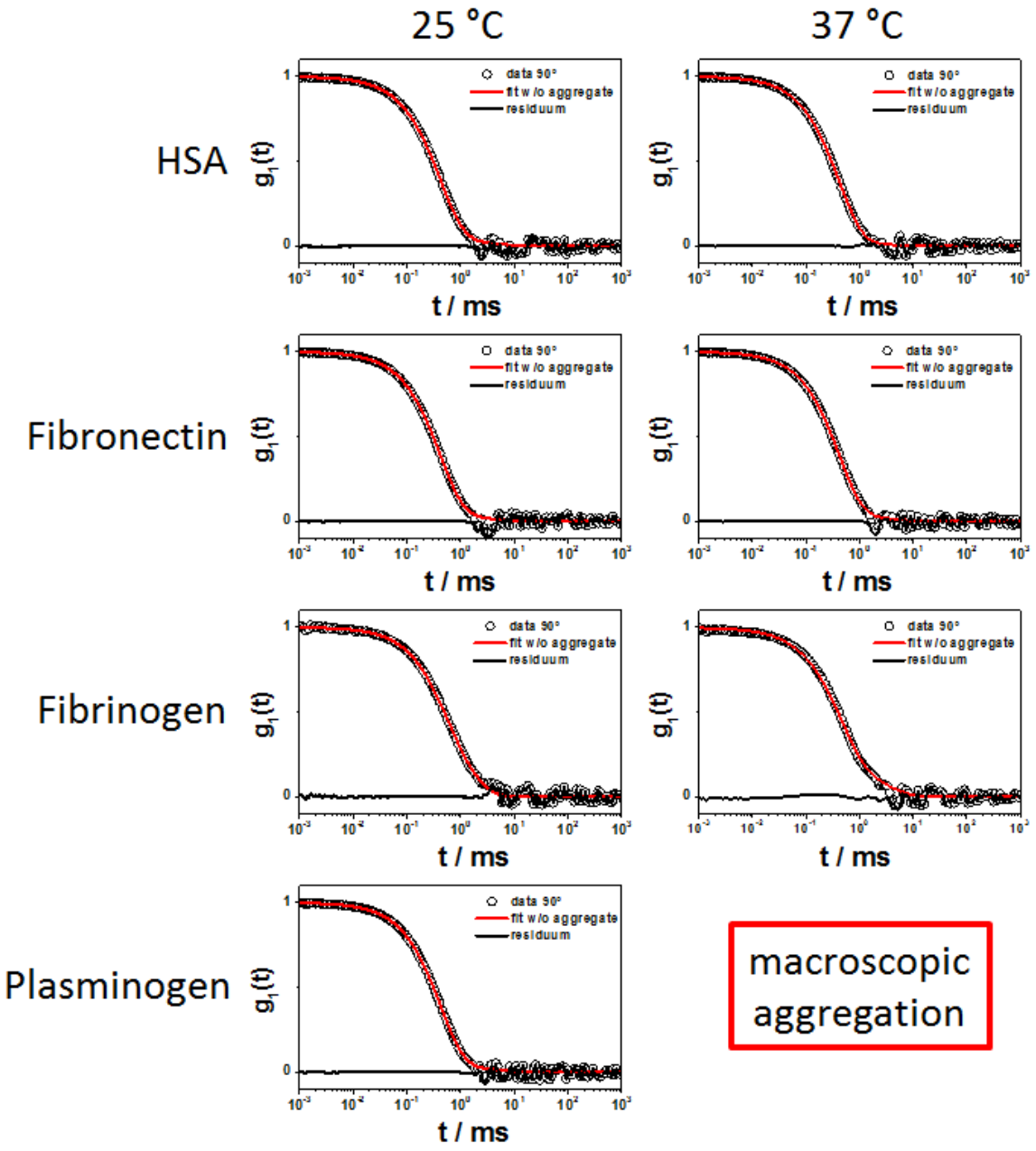

Figure 4.5.9 Normalized field autocorrelation functions $g_1(t)$ of particle-protein mixtures together with a force fit consisting of the sum of the individual components (red line) and the corresponding residuum after subtraction of the fit from the data (black line). The curves are displayed for a scattering angle of 90° and temperatures of 25 °C and 37 °C.

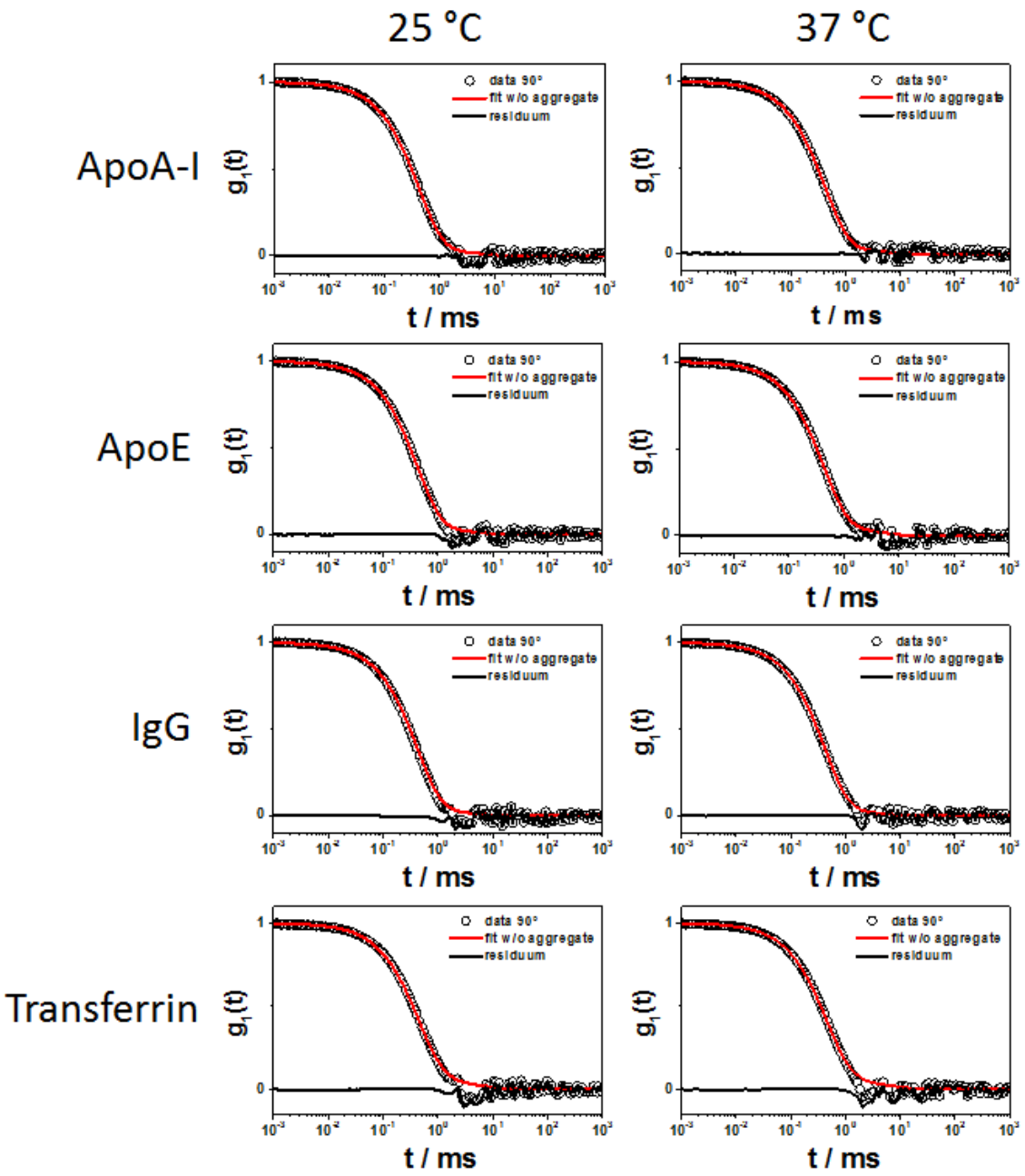

Figure 4.5.10 Normalized field autocorrelation functions $g_1(t)$ of particle-protein mixtures together with a force fit consisting of the sum of the individual components (red line) and the corresponding residuum after subtraction of the fit from the data (black line). The curves are displayed for a scattering angle of 90° and temperatures of 25 °C and 37 °C.

The PS-NP + plasminogen sample formed macroscopic structures several hours after mixing at 37 °C, so that these structures were already too large for light scattering. The fact that the PS-NPs aggregated in the presence of plasminogen only after the mixing at 37 °C and not 25 °C gives a hint that actually an entropy driven adsorption process is

taking place. This process is enhanced at higher temperatures. In all other samples no aggregation could be detected.

Also, the zeta potential of each mixture was determined after the reaction at the different temperatures and compared to the values for the pure protein as well as the bare nanoparticles. The obtained values are displayed in Figure 4.5.11. All proteins exhibit negative zeta potentials except IgG. This is excepted since IgG has an isoelectric point between pH 7.2 and 8.6 depending on the fractions of IgG subclasses,[130] so it has a slightly positive charge at pH 7. In the most cases, the zeta potentials of the protein-particle mixtures differ from the values for the pure proteins and the bare particles. Also, differences between samples mixed at 25 °C and at 37 °C can be seen for HSA, fibronectin and fibrinogen. Usually, it is believed that the coverage of a particle with proteins results in an overall zeta potential similar to the one of the protein, because the proteins cover the surface charges of the particle. However, here many of the mixtures actually exhibit more negative zeta potentials than the individual components. It is not quite clear, why this is the case, but it suggests that some kind of interaction is occurring between the proteins and the particle. Otherwise, bimodal distributions of zeta potential would be observed with maxima at the values for each the protein and the particle. It could be assumed, that those negative potentials develop when proteins adsorb to the particle surface and subsequently change their tertiary structures to reveal more negatively charged patches. It has to be noted that only for the cases of HSA and fibronectin an adsorption stoichiometry could be determined. So for all other mixtures it is not clear, how much of the particle surface is actually covered by proteins. For most of the potentially entropy driven reactions (except fibrinogen) the difference between the two temperatures is not significant. Only the fibrinogen mixture exhibits a less negative potential at 37 °C than at 25 °C, but it cannot determined whether this indicates more or less protein adsorption. The same is true for the mixtures with HSA and fibronectin. Clearly, the interactions are temperature dependent, but result in different zeta potential changes. While the potential of the HSA-covered particles decreases, the one of fibronectin-covered particles increases at higher temperature. It is thus not possible to completely understand the processes going on for each protein from the ITC, DLS and zeta potential measurements, but the expected influence of temperature change could still be shown.

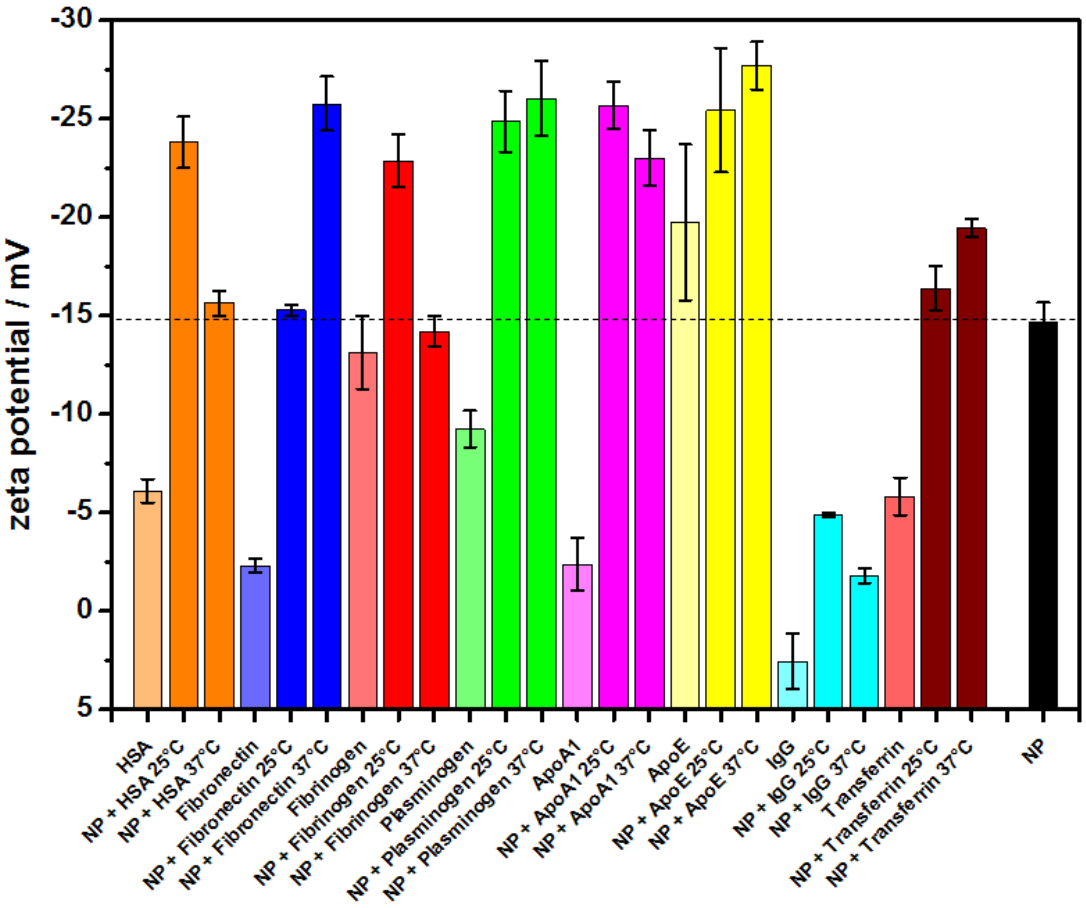

Figure 4.5.11 Zeta potential measurements of PS-NPs after mixing with different proteins compared to single proteins and particles. The dotted line represents the zeta potential of the bare nanoparticles (black column on the right).

4.5.7 Conclusion

In conclusion, the effect of different temperatures during the process of protein adsorption could be shown for the two proteins HSA and fibronectin. These exothermic adsorption processes are shifted towards the side of the free components, which at the same time proves that equilibrium is established to yield a reversible reaction. For protein-particle interactions where no enthalpy gain is involved, it is not possible to directly determine the temperature influence via ITC. It can only be assumed that those interactions become stronger at higher temperatures due to the entropy gain. Surprisingly, the number of proteins not showing any enthalpy related interaction with the particles was rather high. When generalized this means that protein adsorption overall is rather increased at higher temperatures than decreased as suggested for HSA and fibronectin. Also, this means that the composition of the protein corona changes depending on temperature. To be able to verify the adsorption of those proteins not developing heat changes, it would be necessary to perform further experiments in the future. Those could for example be SDS-PAGE experiments where the particles are incubated with the protein of interest, centrifuged and then detected again. Overall, ITC could provide a powerful tool to quantitate the temperature effect on protein-particle interactions and additionally help to distinguish between reversible and irreversible reactions.

5. Experimental

5.1 Materials

Unless otherwise stated, all chemicals were used as received without any further purification. The monomer styrene was freshly purified before the synthesis by filtration through aluminum oxide to remove the stabilizer 4-*tert*-butylcatechol. Blood was taken at the Transfusion Centre of the University Medical Centre of the Johannes Gutenberg-University Mainz from 10 healthy donors after obtaining informed consent. The study was approved by the local ethics committee.

5.1.1 Proteins

Bovine serum albumin (BSA) (> 99%, Sigma Aldrich), Human serum Albumin (HSA) (> 99%, Sigma Aldrich), Apolipoprotein A-I (ApoA-I) (> 95%, Biopur AG, Switzerland), Apolipoprotein E (ApoE) (> 96%, Biopur AG, Switzerland), Fibronectin (> 97%, Biopur AG, Switzerland), Plasminogen (> 10 U/mg, Biopur AG, Switzerland), Immunoglobulin G (Privigen®, 100 mg/mL, CSL Behring), Fibrinogen (CSL Behring), Transferrin (> 98%, Sigma Aldrich), FITC-BSA (> 99%, Life Technologies GmbH), AlexaFluor488®-BSA (> 99%, Life Technologies GmbH), Bodipy® FL-BSA (> 99%, Life Technologies GmbH).

5.1.2 Other reagents

Hydroxyethyl starch (HES, M_w = 200,000 g·mol^{-1}, Fresenius Kabi), toluene 2,4-diisocyanate (TDI, Sigma Aldrich), cyclohexane (> 99.9%, Sigma Aldrich), poly((ethylene-co-butylene)-*b*-(ethylene oxide)) (P(E/B-*b*-EO), consisting of a poly(ethylene-co-butylene) block (M_w = 3,700 g·mol^{-1}) and a poly(ethylene oxide) block (M_w = 3,600 g·mol^{-1}) was synthesized starting from ω-hydroxypoly(ethylene-co-butylene), which was dissolved in toluene after addition of ethylene oxide under anionic polymerization conditions[131]), sulforhodamine 101 (SR101, Sigma Aldrich), urea (> 99 %, Sigma Aldrich), thiourea (99%, Sigma Aldrich), CHAPS lysis buffer (Alfa Aesar GmbH), SeeBlue Plus2 Pre-Stained Standard (Thermo Fisher Scientific), Coomassie Brilliant Blue G-250 (SERVA Electrophoresis GmbH), ammonium sulfate (> 99%, Sigma Aldrich), phosphoric acid (85 wt% in H_2O, Sigma Aldrich), methanol (> 99%,

Sigma Aldrich), styrene (> 99%, Sigma Aldrich), hexadecane (> 99%, Sigma Aldrich), 2,2'-Azobis(2-methylbutyronitrile) (V59) (Wako Chemicals GmbH), Lutensol® AT50 (poly(ethylene glycol)-hexadecyl ether) (BASF AG), sodium dodecyl sulfate (SDS) (> 95 %, Merck KGaA), deuterium oxide (99 atom% D, Sigma Aldrich), Stains-All (95%, Sigma-Aldrich), isopropanol (> 99%, Sigma Aldrich), formamide (> 99%, Sigma Aldrich), hydroxylamine hydrochloride (99%, Sigma Aldrich), Gibco DPBS buffer (Ca/Mg free, Life Technologies GmbH), Bodipy® FL succinimidyl ester (> 95%, Life Technologies GmbH), dimethyl sulfoxide (> 99%, Sigma Aldrich), bromophenol blue (Alfa Aesar GmbH), dithiothreitol (98%, Acros Organics), SERVALYT™ carrier ampholyte (pH 3-10; SERVA Electrolysis GmbH), Immobiline DryStrip Cover Fluid (GE Healthcare), acetic acid (> 99%, Sigma Aldrich).

5.2 Methods and Instrumentation

5.2.1 Isothermal titration calorimetry (ITC)

The calorimetric measurements were performed using a NanoITC Low Volume (TA Instruments, Eschborn, Germany) equipped with a gold cell and an effective cell volume of 170 µL. For data analysis the software NanoAnalyze™ from TA Instruments was used. Since only aqueous systems were measured, the reference cell was filled with deionized water at all times.

5.2.2 Light scattering

All light scattering experiments were performed on a commercially available instrument from ALV GmbH (Langen, Germany) consisting of an electronically controlled goniometer and an ALV-5000 multiple tau full-digital correlators with 320 channels (resolution of 10^{-7} s $\leq t \leq 10^{3}$ s). A HeNe laser with a wavelength of 632.8 nm and an output power of 25 mW (JDS Uniphase, Milpitas, USA, Type 1145P) was utilized as the light source. The setup is displayed in Figure 5.2.1.

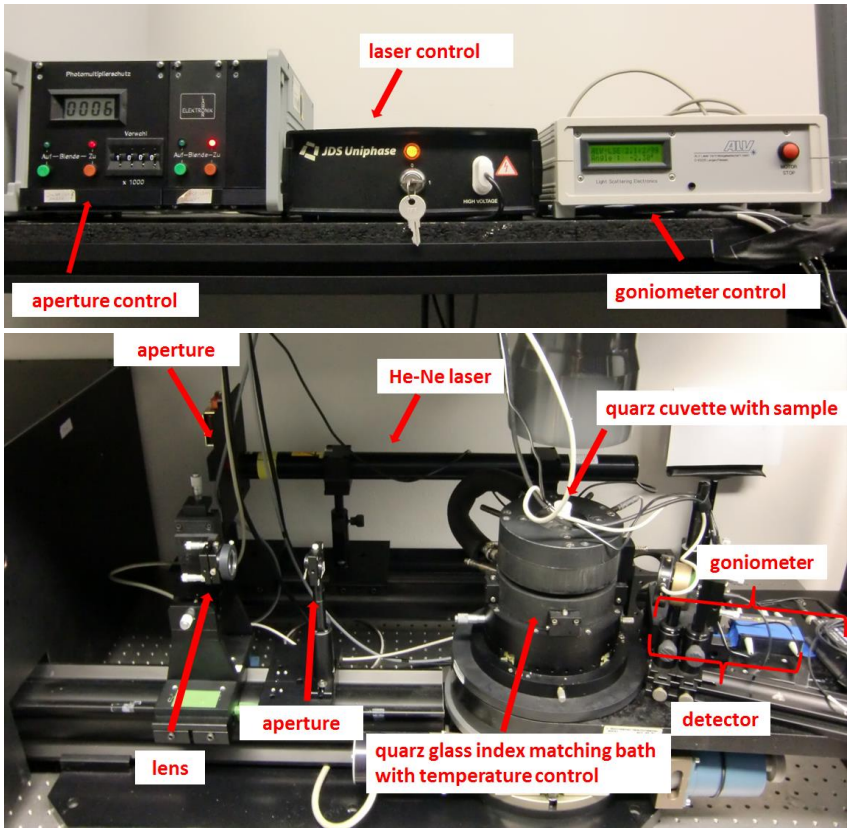

Figure 5.2.1 Setup used for light scattering measurements.

All samples prepared for light scattering measurements were filtered prior to the measurements to remove dust and other scattering impurities. Millex-SV filters with a pore size of 5 µm (Merck Millipore, Billerica, USA) were used for all samples to avoid filtering out aggregates formed after protein-particle interaction. The samples were filtered directly into quartz light scattering cuvettes (inner diameter 18 mm, Hellma, Müllheim), which were cleaned before in a Thurmont apparatus[132] with acetone.

5.2.3 Fluorescence correlation spectroscopy (FCS)

The FCS measurements were performed together with Dr. Kaloian Koynov at the Max Planck Institute for Polymer Research (MPIP, Mainz, Germany). The FCS measurements were performed on a commercial setup (Carl Zeiss, Germany) consisting of the modules LSM510, ConfoCor 2 and an inverted microscope model Axiovert 200 with a C-Apochromat 40×, NA 1.2 water immersion objective. Either argon laser (488 nm excitation wavelength) or HeNe laser (543 nm excitation wavelength) were used for excitation and the emission was collected after filtering respectively with a BP500-550 or BP560-615 long pass filters. 8-well, polystyrene chambered cover glasses (Laboratory-Tek, Nalge Nunc International) were used as sample cells. For each sample series of 15 measurements with a total duration 5 min were performed. As the radial dimension r_0 of the confocal probing volume is not known a priory it was determined by performing calibration experiments using a fluorophore with known diffusion coefficient in water, i.e. Alexa 488 or Rh6G.

5.2.4 Nuclear magnetic resonance (NMR) spectroscopy

NMR experiments were performed on a Bruker Avance III 850 MHz system equipped with a TXI 1H/13C/15N probehead with a z-gradient. All measurements were done with D_2O as a deuterated solvent.

5.2.5 Zeta-potential measurements

For zeta-potential measurements, 20 µL of each sample was diluted with 1 mL of 0.001 M KCl solution. The samples were then analyzed with a Zetasizer Nano Z (Malvern Instruments GmbH, Herrenberg, Germany).

5.2.6 High performance liquid chromatography (HPLC)

The HPLC measurements were performed on an Agilent Technologies Series 1200 setup equipped with a UV detector and an ELSD detector 385-LC (both Agilent Technologies, USA) by Beate Müller. The analysis of albumin was done using a MN Nucleosil® C4 column (Macherey-Nagel) and an eluent gradient from CH_3CN/water + 0.1% TFA 20/80 to 100/0.

5.2.7 Other instrumentation

Particle charge detection (PCD) was performed on a Mütek particle charge detector (BTG, Herrsching, Germany) in combination with a Titrino Automatic Titrator (Metrohm AG, Herisau, Switzerland) by Dr. Grit Baier. Scanning electron microscopy (SEM) images were recorded by using Zeiss 1530 Gemini (Oberkochen, Germany) microscope at 0.2 kV landing voltage by Gunnar Glaßer. Surface tension measurements were performed with a DCAT 21 tensiometer from DataPhysics Instruments GmbH (Filderstadt, Germany) by Elke Muth. Absorbance spectra were recorded on a Tecan Infinite® M1000 Plate Reader (Tecan Group, Männedorf, Germany).

5.3 Complementary analysis of the hard and soft protein corona

5.3.1 Plasma preparation

To prevent blood clotting Li-Heparin was added to the obtained plasma. The blood was centrifuged to pellet red and white blood cells and the plasma supernatant was pooled. Aliquots were stored at -80 °C. After thawing, the plasma was centrifuged at 20,000 g for 1 h at 4 °C to remove any residual protein precipitates. A protein concentration of 66 $g \cdot L^{-1}$ was determined for the plasma.

5.3.2 Hydroxyethyl starch nanocapsule (HES-NC) preparation and functionalization

The synthesis of HES-NC batches was performed by Dr. Grit Baier and Sarah Wald (MPIP). HES-NCs were synthesized by a polyaddition reaction performed at the miniemulsion droplet's interface similar to the previously published procedure.[133] Afterwards, the HES nanocapsules were functionalized to create positively and negatively charged HES-NCs. With the carboxymethylation procedure, the HES-NCs were covered with carboxylic groups.[133] For the NH_2-functionalization of HE-NCs, 2.0 g of HES-NC dispersion (in cyclohexane as continuous phase, solid content 3.0 wt%) were mixed with 20 mg Toluene 2,4-diisocyanate (TDI) and stirred for 24 h at 25 °C. The N`Cs were then transferred into the aqueous phase using the following procedure: 1 g of the NCs dispersion in cyclohexane (polymer solid content 3 wt%) was mixed with 5 g sodium dodecyl sulfate (SDS) aqueous solution (0.1 wt%) and kept under mechanical stirring conditions for 24 h at 25 °C. Next, the samples were redispersed for 15 min at 50 °C in a sonication bath (power 50%, 25 kHz). Finally, the NC dispersion was centrifuged (Sigma 3k-30, RCF 1467, 20 min). The supernatant was removed, the nanocapsules were redispersed in demineralized water and dialyzed for 24 h (MWCO: 12,000 $g \cdot mol^{-1}$) in order to remove residues of SDS.

5.3.3 Capsule characterization

The amount of surface charged groups was determined by titration experiments with a particle charge detector (PCD). The carboxylic groups were titrated against the positively charged polycation poly(diallyl dimethyl ammonium chloride) (P-DADMAC). The amine groups on the nanocapsules surface were titrated against the negatively charged polyelectrolyte poly(ethylene sulphonate) (PES-Na). The titrations were

performed on 10 mL of the nanocapsules dispersion with a solid content of 1 $g \cdot L^{-1}$. The amount of groups per gram of polymer was calculated from the consumed volume of the polyelectrolyte solution. Morphological studies were performed with scanning electron microscopy (SEM). The samples were prepared by diluting the nanocapsule dispersion to about 0.01% solid content and by placing a droplet onto silica wafers and drying under ambient conditions.

5.3.4 Preparation of samples for gel electrophoresis and protein quantitation

The preparation of the samples and subsequent protein quantitation and SDS-PAGE were performed by Dr. Susanne Schöttler (MPIP). The nanocapsule dispersions were diluted with ultrapure water to a constant particle surface concentration (0.1 m^2 in 150 µL) and incubated with 500 µL human blood plasma for 1 h at 37 °C under constant agitation. The particles were separated from the supernatant by centrifugation at 15,000 g for 1 h. The nanoparticles were washed with phosphate-buffered saline (PBS) in three centrifugation steps at 15,000 g for 1 h. To elute the adsorbed proteins, the particle pellet was resuspended in 7 M urea, 2 M thiourea and 4% CHAPS, and the nanoparticles were again pelleted. The supernatant was then used for protein quantitation and SDS-PAGE.

5.3.5 Sodium dodecyl sulfate polyacrylamide gel electrophoresis (SDS-PAGE)

16.25 µL of each protein sample was loaded onto a NuPAGE® Novex® 10% Bis-Tris Gel (Thermo Fisher Scientific) and subjected to SDS-PAGE according to standard procedures. As a molecular marker SeeBlue Plus2 Pre-Stained was run in parallel. Proteins were fixed in 10% acetic acid for 1 h and subsequently visualized by staining with 0.1% Coomassie brilliant blue G-250 in 10% ammonium sulfate, 2% phosphoric acid and 25% methanol for 24 h.

5.3.6 Protein quantitation assay

Protein concentrations were determined using a Pierce 660 nm protein Assay (Thermo Scientific, Rockford, USA) according to manufacturer's instructions with BSA as a standard. Each sample was measured in triplicate.

5.3.7 Isothermal Titration Calorimetry (ITC)

In an experiment 50 µL of an aqueous protein solution (human plasma 15 $g \cdot L^{-1}$, HSA 10 $g \cdot L^{-1}$ or ApoA-I 0.084 $g \cdot L^{-1}$) were titrated to 300 µL of a suspension of HES-NCs (0.1 $g \cdot L^{-1}$ in water for titration with human plasma and HSA; 4 $g \cdot L^{-1}$ for titration with ApoA-I). The experimental temperature was kept constant at 25 °C. Additionally, the same amount of each protein solution was titrated into pure water to determine the heat of dilution for reference. The number and injected volume of the titration steps were the same for all measurements (25 x 2 µL). The spacing between injections was set to 300 s. The integrated reference heats were then subtracted from the integrated heats of the adsorption experiments.

5.3.8 Dynamic light scattering DLS

For measurements of nanocapsules-protein mixtures the samples were prepared according to the ITC titration procedure. In every case, 300 µL of a capsule suspension was mixed with 50 µL of protein solution or water for the reference measurements (concentrations were the same as in ITC experiments). Plasma and individual proteins were prepared by adding the solutions into 300 µL of water to maintain the same dilutions. All plasma and HSA containing samples were then diluted with water up to 2 mL sample volume. ApoA-I containing samples were diluted up to 5 mL total volume. Capsule concentrations of 0.015 $g \cdot L^{-1}$ and 0.24 $g \cdot L^{-1}$ respectively were achieved.

5.4 Influence of surfactant type and concentration on protein adsorption

5.4.1 Synthesis of Polystyrene nanoparticles (PS-NPs)

PS-NPs were prepared by radical polymerization in miniemulsion as previously published in literature.[100, 101] Therefore, 74 mg of SDS or 200 mg of Lutensol AT50 were dissolved in 24 mL deionized water. Simultaneously, 98 mg of the initiator V59 and 323 µL of hexadecane were dissolved in 6.6 mL of purified styrene. After separate preparation of the two phases, they were combined and stirred for 1 h at room temperature for pre-emulsification. Afterwards the mixture was homogenized by ultrasonication for 120 s at 90% intensity with a Branson W 450 digital sonifier (1/2'' tip) whilst cooled with an ice-water bath. The polymerization was then carried out for 16 h at 72 °C. The purification was then carried out individually for each surfactant type. SDS-stabilized PS-NPs were dialyzed (MWCO 12,000 $g \cdot mol^{-1}$) against deionized water over night and two more times for 2 h each after exchanging the solvent. Afterwards, sufficient purification was verified by surface tension measurements. Lutensol-stabilized PS-NPs were centrifuged for 45 min at 9,000 rpm. After disposing of the supernatant the pellet was then resuspended in water. This procedure was repeated four more times until no further increase of the sample surface tension was detectable.

The synthesis of PS-NPs in D_2O was performed accordingly with both surfactants by Katja Klein (MPIP). D_2O was used instead of water as the continuous phase. After the reaction, the suspension was filtered through Kimtech wipes (Kimberly-Clark, USA) to remove large aggregates formed during synthesis. After that no further purification was applied.

5.4.2 PS-NP sample preparation with different surfactant content

To the purified samples different amounts of the respective surfactant solution in deionized water were added again. The amounts added correspond to a final concentration of 0.20 mM, 0.41 mM and 0.67 mM of SDS and 0.10 mM, 0.20 mM and 0.31 mM of Lutensol AT50 in the respective samples.

The size of the nanoparticles was measured by dynamic light scattering. Additionally, zeta potential and surface tension measurements were performed. The sample morphology was characterized by means of low voltage scanning electron microscopy (SEM).

5.4.3 Isothermal titration calorimetry (ITC)

For an experiment 50 µL of HSA solution (0.15 mM, 10 $g \cdot L^{-1}$ in water) were titrated into the different PS nanoparticle suspensions. The concentration of nanoparticles was $8.9 \cdot 10^{-6}$ mM (3.2 $g \cdot L^{-1}$) for all SDS-stabilized samples. For Lutensol stabilized nanoparticles the concentration was adjusted for each sample, so that concentrations of $4.2 \cdot 10^{-6}$ mM (14.3 $g \cdot L^{-1}$, unpurified), $4.7 \cdot 10^{-7}$ mM (1.6 $g \cdot L^{-1}$, purified and 0.10 mM Lut), $2.3 \cdot 10^{-7}$ mM (0.8 $g \cdot L^{-1}$, 0.20 mM Lut) and $1.2 \cdot 10^{-7}$ mM (0.4 $g \cdot L^{-1}$, 0.31 mM Lut) were obtained. For comparison also solutions of pure Lutensol (0.05 mM) and SDS (0.25 mM) in water were titrated with HSA (0.15 mM). The experimental temperature was kept constant at 25 °C. To determine the heat of dilution of HSA the same amount of HSA was titrated into pure water. The number and injected volume of the titration steps were the same for all measurements (25 x 2 µL). The spacing between injections was set to 300 s.

5.4.4 Dynamic light scattering (DLS) sample preparation

For measurements of nanoparticle-protein and surfactant-protein mixtures the samples were prepared according to the ITC titration procedure. In every case, 300 µL of the nanoparticle dispersion or surfactant solution was mixed with 50 µL of protein solution or water for the reference measurements of pure particles (concentrations were the same as in ITC experiments). Pure HSA was prepared by adding the ITC solution (10 $g \cdot L^{-1}$) into 300 µL of water to maintain the same dilution. All nanoparticle containing samples were then diluted 40 times with water while surfactant containing samples were diluted 6.5 times.

5.4.5 Sample preparation for nuclear magnetic resonance (NMR) experiments

For NMR experiments, the PS-NP suspensions in D_2O were used with a concentration of 3 wt%. Additionally, solutions of SDS in D_2O (3 $g \cdot L^{-1}$, 10.4 mM), Lut in D_2O (8.3 $g \cdot L^{-1}$, 3.4 mM) and HSA in D_2O (10 $g \cdot L^{-1}$, 0.15 mM) were prepared. For the preparation of the complexes, for each NMR sample 514 µL of PS-NP solution or pure surfactant solution were mixed with 86 µL of HSA solution to maintain the ratios as obtained from ITC. All NMR experiments were performed at 25 °C. For each sample a ^{1}H-NMR spectrum as well as DOSY spectrum were recorded.

5.5 SDS quantification in nanoparticle samples

To prepare the dye stock solution, 1 mg of Stains-All was dissolved in 500 µL of isopropanol and 500 µL water. This solution was stored in the dark at 4 °C. Then, the reactive dye solution was prepared by mixing the stock solution with formamide and water (1 : 1 : 18). For the setup of a calibration, aliquots of 200 µL reactive dye solution were each mixed with 1 or 2 µL of aqueous SDS solutions. The SDS standard solutions were prepared in concentrations of 0.1 mM, 0.25 mM, 0.5 mM, 0.75 mM, 1 mM, 2.5 mM, 5 mM and 10 mM. Also a sample without any SDS was prepared by just adding the same amount of water to the dye. Absorbance spectra were recorded for each sample in 96 well plates from 350 to 750 nm. Then at fixed wavelengths of 438 nm, 451 nm and 510 nm the absorbance was measured again separately. As a background the absorbance of the reactive dye solution without the dye (isopropanol, formamide, and water) was subtracted. Additionally, samples were prepared with aliquots where each 1 µL of nanoparticle solution was added. The Table (Table 4.3.1) containing all used nanoparticle samples can be found in the Results and Discussion section (Chapter 4.3). To compare SDS concentrations in samples with and without nanoparticles, two different PS-NP samples were centrifuged at 15,000 g for 5 h and another 2 h at 20,000 g and 4 °C. Then the supernatant of those samples was again used for quantitation by adding 1 µL to reactive dye solution aliquots.

5.6 Influence of protein fluorescence labels on the protein adsorption

5.6.1 Synthesis and purification of a Bodipy-HSA conjugate

The conjugation of Bodipy® FL with HSA was performed using the labeling protocol of Life Technologies GmbH. Therefore, 22 mg of HSA were dissolved in 2.2 mL DPBS buffer (10 $g \cdot L^{-1}$). Simultaneously, a stock solution of Bodipy® FL succinimidyl ester in dimethyl sulfoxide (DMSO) with a concentration of 5 $g \cdot L^{-1}$ was prepared. From the dye stock solution, 26 µL were added to the HSA solution. The reaction mixture was stirred at room temperature for 1 h. Then, 220 µL of Stop-Reagent (1.5 M hydroxylamine hydrochloride, pH 8.5) were added and the mixture stirred for another hour. For purification, the mixture was then dialyzed against DPBS buffer for 1 h using Slide-A-Lyzer™ MINI dialysis devices (Life Technologies GmbH, Darmstadt, Germany) with a MWCO = 10,000 $g \cdot mol^{-1}$. After exchange of the dialysate, the sample was dialyzed for another hour. For the removal of unreacted dye, the sample was then purified with size exclusion chromatography using Sephadex PD MiniTrap G-25 columns (GE Healthcare Life Sciences, Freiburg, Germany).

5.6.2 Isoelectric focusing (IEF) procedure

Isoelectric focusing of all proteins was performed by Dr. Susanne Schöttler (MPIP) using IPG strips (pH 3-10; ReadyStrip™ IPG strips 24 cm, Bio-Rad GmbH, München, Germany), which were rehydrated with a solution of ca. 100 µg of protein in 500 µL rehydration buffer (8 M urea, 4% (w/v) CHAPS, 0.001% (w/v) bromophenol blue, 3 $g \cdot L^{-1}$ dithiothreitol, 2% (v/v) SERVALYT™ carrier ampholyte (pH 3-10) over night at 20 °C. Rehydrated strips were focused using an IEF100 isoelectric focusing unit (Hoefer Inc., Holliston, USA) at 20 °C covered with Immobiline DryStrip Cover Fluid. For improved sample entry, initial voltage was limited using a gradient to 500 V for 3 h, then increased with a gradient up to 1,000 V for 3 h and up to 5,000 V for another 3 h. Afterwards a constant voltage of 8,000 V was applied using a total of 60,000 V / h, followed by a constant voltage of 500 V for 18 h. After IEF, the strip was incubated with 10% (v/v) acetic acid and 40% (v/v) ethanol for 2 h, before it was imaged under a UV lamp using a LAS-3000 Imager (Fujifilm, Düsseldorf, Germany). Then, strips with unlabeled proteins were incubated with staining solution (10% (w/v) ammonium sulfate, 2% (w/v) phosphoric acid, 0.1% (w/v) Coomassie Brilliant Blue G-250 in 100 mL water with 25

mL methanol) for 24 h, followed by washing with 1% (v/v) acetic acid (2 x 10 min) and imaged again.

5.6.3 Sample preparation for FCS measurements

For the FCS experiments, stock solutions of the fluorescent species were prepared. The solutions were prepared with concentrations of 0.001 $g \cdot L^{-1}$ AF488-BSA ($1.5 \cdot 10^{-5}$ mM), 0.01 $g \cdot L^{-1}$ BP-HSA ($1.5 \cdot 10^{-4}$ mM) and 0.5 $g \cdot L^{-1}$ HES-NCs ($9.6 \cdot 10^{-8}$ mM). Additionally, a stock solution of PS-NPs was prepared with a concentration of 0.16 $g \cdot L^{-1}$ ($4.4 \cdot 10^{-7}$ mM). The single components were measured with those concentrations, while the mixtures were prepared directly in the measurement chambers. Therefore, 18 µL of the AF488-BSA solution were mixed with 500 µL of the HES-NC solution (molar ratio 6 : 1). Additionally molar mixing ratios of 1 : 1 and 100.000 : 1 were prepared. Stock solutions of the same concentrations were prepared for FITC-BSA and BP-BSA. FITC-BSA was mixed with the HES-NCs at mixing ratios of 2.000 : 1 and 17.000 : 1, while BP-BSA was mixed with them at mixing ratios of 250 : 1 and 1.500 : 1. Also, 200 µL of BP-HSA solution were mixed with 200 µL of the PS-NP solution (molar ratio 340 : 1).

5.6.4 ITC measurements

In an experiment 50 µL of each albumin solution (0.15 mM in water for BSA and HSA, 0.075 mM in water for AF488-BSA, FITC-BSA and BP-BSA, 0.015 mM in water for BP-HSA) were titrated to 300 µL of a suspension of HES-NCs (1 $g \cdot L^{-1}$ in water for titration with AF488-BSA, FITC-BSA and BP-BSA; 0.1 $g \cdot L^{-1}$ for titration with BP-HSA) or PS-NPs (0.14 $g \cdot L^{-1}$ in water). The experimental temperature was kept constant at 25 °C. The titrations were performed as described previously (25 x 2 µL, 300 s spacing).

5.7 Evaluation of the temperature effect on protein adsorption characteristics

PS-NPs for the experiments were prepared by Katja Klein according to the above mentioned procedure (chapter 5.4.1). The particles were stabilized with Lutensol AT50 and purified thoroughly by repetitive centrifugation and resuspension in water. All protein solutions were prepared by adding a defined protein amount to deionized water. The following concentrations were used for ITC experiments: 10 $g \cdot L^{-1}$ ($2.22 \cdot 10^{-5}$ mM) for HSA, Fibronectin, Plasminogen, ApoA-I, ApoE, IgG and Transferrin titrations; 1 $g \cdot L^{-1}$

($2.22 \cdot 10^{-6}$ mM) for Fibrinogen titrations. In all experiments 50 µL of protein solution were titrated into 300 µL of PS-NP solution (10 $g \cdot L^{-1}$ (0.15 mM) HSA, 0.25 $g \cdot L^{-1}$ (0.0006 mM) Fibronectin, 10 $g \cdot L^{-1}$ (0.03 mM) Fibrinogen, 0.25 $g \cdot L^{-1}$ (0.003 mM) Plasminogen, 0.1 $g \cdot L^{-1}$ (0.0036 mM) ApoA-I, 0.1 $g \cdot L^{-1}$ (0.003 mM) ApoE, 10 $g \cdot L^{-1}$ (0.035 mM) IgG, 10 $g \cdot L^{-1}$ (0.013 mM) Transferrin). For DLS measurements all samples were used as received after ITC. For reference, the pure proteins and particles were prepared with the same concentrations. Then, all samples containing particles were diluted in pure water to a concentration of 0.05 $g \cdot L^{-1}$. The same dilution was then applied to the corresponding protein solution.

6. Summary and Outlook

The complementary analysis of the protein corona around HES-NCs allowed for characterizing the hard and soft corona at the same time. With SDS-PAGE the main proteins of the hard corona were identified and it was found that no HSA was present. Additionally, no differences between the adsorption patterns and protein amounts on the HES-NCs regardless of their different surface functionalizations (-COOH, -NH_2) could be detected. Afterwards, the adsorption of single proteins, HSA and ApoA-I, was examined with ITC and light scattering and compared to the adsorption of the full plasma protein mixture. Binding affinities of K_a = 0.4 - 0.8·10^5 L mol^{-1} and K_a = 188 - 333·10^5 L mol^{-1} for HSA and ApoA-I respectively were determined. Also, it was found that the adsorption of ApoA-I onto the amino-functionalized HES-NCs was endothermic, which is a hint for additional processes like protein denaturation or interactions with the surfactant. It was clearly demonstrated that shear force during the sample preparation (as required for the hard corona analysis) removes the proteins of the soft corona, which in this case was HSA.

In further experiments, the influence of shear force should be examined in detail. So far, it is not clear which shear force is actually applied to the protein corona in the blood stream and therefore which is the relevant corona form. To clarify this, the analysis of the protein corona in flow is planned to be performed using asymmetric field-field flow fractionation (AF-FFF) and light scattering measurements of the fractions. Also a setup with capillaries simulating blood vessels should be built to be able to directly analyze the protein corona with DLS in the flow.

In the next experiments, two different surfactants (SDS and Lutensol AT50) were used for the stabilization of PS-NPs. The concentration of the surfactants on the particle surface was found to influence the adsorption of HSA dramatically in terms of binding affinity and number of adsorbing proteins. While the binding affinity decreased about 3-4 times with higher SDS concentrations in the investigated range, the reverse phenomenon was observed for Lutensol (a 20fold increase). At certain surfactant concentrations on the particle surface, the binding parameters were the same as for the pure surfactants without particles. Using light scattering and NMR spectroscopy some evidence was obtained that SDS stays attached to the particle after HSA adsorption, while Lutensol is likely to detach and form soluble complexes with HSA, because some aggregates in addition to the

particles were found. Due to the fact, that the surfactant concentration has significant influence on the adsorption process, a method to quantify SDS in the presence of nanoparticles involving complexation with the dye Stains-All and absorbance measurement was adapted and modified from literature. Different particle systems were tested for their SDS content and the qualitative trends were verified for all systems except polystyrene particles due to the absorbance of polystyrene itself. First tests to clarify if also the SDS on the surface of the particles was detected were positive.

Here, the SDS quantification should be further developed, as e.g. the testing for complete detection and disturbing factors could not be finished yet. Also, an easy quantification method for Lutensol is not yet available but much needed for the application of the particles. Also, the question of the surfactant fate after adsorption of proteins could not fully be clarified. In the future, quantitative NMR experiments could be useful to obtain more information.

As a third influence factor for the protein adsorption process, the modification of albumin with fluorescent dyes was examined. While it was proven, that the nature of the dye molecule itself does not play an important role, FCS and ITC experiments revealed that the adsorption onto a hydrophilic material (HES-NCs) was completely suppressed by any label. In contrast, the adsorption on a more hydrophobic material (PS-NPs) was not affected even though the isoelectric point of the protein was decreased by the labels. This suggested that the influence of the label depends on the type and place of coupling to the protein and the type of interactions the protein is involved in.

Those results underline the importance of an adequate experiment design involving protein modification. Depending on the process investigated it should be carefully considered which label is being attached at which position and with which coupling technique. Any results should additionally be verified with another technique that does not require modification of the protein.

At last, the adsorption of several individual proteins onto PS-NPs was examined at two different temperatures (25 °C and 37 °C). For two proteins (HSA and Fibronectin) an exothermic reaction was observed that was shifted towards the side of the free proteins and particles with higher temperature. All other investigated proteins did not show any enthalpy driven adsorption processes. Using zeta potential measurements it was shown

that probably all proteins do adsorb to the particles, but on an entropy driven basis. For those proteins the adsorption would actually be enhanced at a higher temperature.

In further experiments, the adsorption of those proteins onto the particles should be verified using SDS-PAGE. The amount of protein adsorbed should also be investigated for both temperatures using a protein assay. By comparing the adsorption parameters of a protein at two temperatures it can be found out if the reaction is an equilibrium process (reversible) or not. However, to ensure that the application is correct, more proteins with heat involving adsorption processes have to be analyzed.

In general, several factors significantly influencing the protein adsorption process were found and investigated in detail and the results obtained are of relevance for further experiments regarding the subject. A complete understanding of all involved processes and driving forces to be able to predict the behavior of nanomaterials in biological environments however is not yet available.

List of Abbreviations

ACF	autocorrelation function
AF488	Alexa Fluor® 488
ApoA-I	apolipoprotein A-I
ApoE	apolipoprotein E
B	baseline
BG	background
BP	Bodipy FL®
BSA	bovine serum albumin
c	concentration
CHAPS	3-((3-Cholamidopropyl)dimethylammonio)-1-propanesulfonate
CMC	critical micelle concentration
COOH	carboxyl-
d	diameter
D	translational diffusion coefficient
D_Z	z-averaged diffusion coefficient
DAB	diaminobutane
DLS	dynamic light scattering
DLVO	Derjaguin-Landau-Verwey-Overbeek
DMSO	dimethylsulfoxide
DNA	desoxyribonucleic acid
DOSY	diffusion ordered spectroscopy
f	coherence factor, intensity fraction
FCS	fluorescence correlation spectroscopy
FID	free induction decay
FITC	fluorescein
ΔG	Gibbs free energy
$g_1(t)$	experimental field autocorrelation function
$g_2(t)$	intensity autocorrelation function
$G(t)$	FCS autocorrelation function
ΔH	reaction enthalpy
$H(\ln \tau)$	distribution of relaxation times
HDL	high density lipoprotein
HES	hydroxyethyl starch
HLB	hydrophilic – lipophilic balance
HSA	human serum albumin
I	scattering intensity
IDL	intermediate density lipoprotein
IgG	immunoglobulin G
ITC	isothermal titration calorimetry
k	Boltzmann constant
K_a	binding affinity
kDa	kilo Dalton
L	ligand
LCAT	lecithin-cholesterol acyltransferase
LDL	low density lipoprotein
Lp(a)	lipoprotein a

Lut	lutensol AT50
M	macromolecule
M_w	molecular weight
MRI	magnetic resonance imaging
MWCO	molecular weight cutoff
n_D	refractive index
N	stoichiometry / number of particles in a detection volume
NA	numerical aperture
NC	nanocapsule
NH_2	amino-
NMR	nuclear magnetic resonance
NP	nanoparticle
PBS	phosphate buffered saline
PCD	particle charge detection
P-DACMAC	poly(diallyl dimethyl ammonium chloride)
PDB	protein data base
PEG	polyethylene glycol
PES-Na	poly(ethylene sulphonate)
PET	positron emission tomography
PP	polyphosphate
PS	polystyrene
q	scattering vector
r	radius
r_0	radial dimension of confocal volume
R	universal gas constant, correlation coefficient
R_G	radius of gyration
R_h	hydrodynamic radius
RCT	reverse cholesterol transport
Rh6G	rhodamine 6G
RNA	ribonucleic acid
S	structure parameter in FCS
ΔS	reaction entropy
SDS	sodium dodecyl sulfate
SDS-PAGE	sodium dodecyl sulfate polyacrylamide gel electrophoresis
SEM	scanning electron microscopy
SPECT	single photon emission computed tomography
SR101	sulforhodamine 101
t	time
T	temperature
TDI	toluene 2,4-diisocyanate
TFA	trifluoracetic acid
THF	tetrahydrofurane
U	electrophoretic mobility
V	volume
VLDL	very low density lipoprotein
z_0	axial dimension of confocal volume

α	polarizability
ε	dielectric constant
η	viscosity
θ	scattering angle
λ	wavelength
ρ	structural parameter
τ	relaxation time
Γ	relaxation rate
ζ	zeta potential

Bibliography

1. Torchilin, V. P. Multifunctional, stimuli-sensitive nanoparticulate systems for drug delivery. *Nature Reviews Drug Discovery* 2014, 13, 813-827.

2. Duncan, R. Polymer conjugates as anticancer nanomedicines. *Nature Reviews Cancer* 2006, 6, 688-701.

3. Lynch, I.; Dawson, K. A. Protein-nanoparticle interactions. *Nano Today* 2008, 3, 40-47.

4. Aggarwal, P.; Hall, J. B.; McLeland, C. B.; Dobrovolskaia, M. A.; McNeil, S. E. Nanoparticle interaction with plasma proteins as it relates to particle biodistribution, biocompatibility and therapeutic efficacy. *Advanced Drug Delivery Reviews* 2009, 61, 428-437.

5. Walczyk, D.; Bombelli, F. B.; Monopoli, M. P.; Lynch, I.; Dawson, K. A. What the Cell "Sees" in Bionanoscience. *Journal of the American Chemical Society* 2010, 132, 5761-5768.

6. Cedervall, T.; Lynch, I.; Lindman, S.; Berggård, T.; Thulin, E.; Nilsson, H.; Dawson, K. A.; Linse, S. Understanding the nanoparticle–protein corona using methods to quantify exchange rates and affinities of proteins for nanoparticles. *Proceedings of the National Academy of Sciences* 2007, 104, 2050-2055.

7. Lindman, S.; Lynch, I.; Thulin, E.; Nilsson, H.; Dawson, K. A.; Linse, S. Systematic Investigation of the Thermodynamics of HSA Adsorption to N-iso-Propylacrylamide/N-tert-Butylacrylamide Copolymer Nanoparticles. Effects of Particle Size and Hydrophobicity. *Nano Letters* 2007, 7, 914-920.

8. Lück, M.; Paulke, B. R.; Schröder, W.; Blunk, T.; Müller, R. H. Analysis of plasma protein adsorption on polymeric nanoparticles with different surface characteristics. *Journal of Biomedical Materials Research* 1998, 39, 478-485.

9. Lundqvist, M.; Stigler, J.; Elia, G.; Lynch, I.; Cedervall, T.; Dawson, K. A. Nanoparticle size and surface properties determine the protein corona with possible implications for biological impacts. *Proceedings of the National Academy of Sciences* 2008, 105, 14265-14270.

10. Gessner, A.; Lieske, A.; Paulke, B.-R.; Müller, R. H. Functional groups on polystyrene model nanoparticles: Influence on protein adsorption. *Journal of Biomedical Materials Research Part A* 2003, 65A, 319-326.

11. Mohr, K.; Sommer, M.; Baier, G.; Schöttler, S.; Okwieka, P. Aggregation Behavior of Polystyrene-Nanoparticles in Human Blood Serum and its Impact on the in vivo Distribution in Mice. *Journal of Nanomedicine and Nanotechnology* 2014, 5, 2.

12. Roser, M.; Fischer, D.; Kissel, T. Surface-modified biodegradable albumin nano- and microspheres. II: effect of surface charges on in vitro phagocytosis and biodistribution in rats. *European Journal of Pharmaceutics and Biopharmaceutics* 1998, 46, 255-263.

13. Cedervall, T.; Lynch, I.; Foy, M.; Berggård, T.; Donnelly, S. C.; Cagney, G.; Linse, S.; Dawson, K. A. Detailed Identification of Plasma Proteins Adsorbed on Copolymer Nanoparticles. *Angewandte Chemie International Edition* 2007, 46, 5754-5756.

14. Tenzer, S.; Docter, D.; Rosfa, S.; Wlodarski, A.; Kuharev, J.; Rekik, A.; Knauer, S. K.; Bantz, C.; Nawroth, T.; Bier, C.; Sirirattanapan, J.; Mann, W.; Treuel, L.; Zellner, R.; Maskos, M.; Schild, H.; Stauber, R. H. Nanoparticle Size Is a Critical Physicochemical Determinant of the Human Blood Plasma Corona: A Comprehensive Quantitative Proteomic Analysis. *ACS Nano* 2011, 5, 7155-7167.

15. Dell'Orco, D.; Lundqvist, M.; Oslakovic, C.; Cedervall, T.; Linse, S. Modeling the Time Evolution of the Nanoparticle-Protein Corona in a Body Fluid. *PLoS ONE* 2010, 5, e10949.

16. Tenzer, S.; Docter, D.; Kuharev, J.; Musyanovych, A.; Fetz, V.; Hecht, R.; Schlenk, F.; Fischer, D.; Kiouptsi, K.; Reinhardt, C.; Landfester, K.; Schild, H.; Maskos, M.; Knauer, S. K.; Stauber, R. H. Rapid formation of plasma protein corona critically affects nanoparticle pathophysiology. *Nature Nanotechnology* 2013, 8, 772-781.

17. Lundqvist, M.; Sethson, I.; Jonsson, B.-H. Protein Adsorption onto Silica Nanoparticles: Conformational Changes Depend on the Particles' Curvature and the Protein Stability. *Langmuir* 2004, 20, 10639-10647.

18. Salvati, A.; Pitek, A. S.; Monopoli, M. P.; Prapainop, K.; Bombelli, F. B.; Hristov, D. R.; Kelly, P. M.; Aberg, C.; Mahon, E.; Dawson, K. A. Transferrin-functionalized nanoparticles lose their targeting capabilities when a biomolecule corona adsorbs on the surface. *Nature Nanotechnology* 2013, 8, 137-143.

19. Ritz, S.; Schöttler, S.; Kotman, N.; Baier, G.; Musyanovych, A.; Kuharev, J.; Landfester, K.; Schild, H.; Jahn, O.; Tenzer, S.; Mailänder, V. Protein Corona of Nanoparticles: Distinct Proteins Regulate the Cellular Uptake. *Biomacromolecules* 2015, 16, 1311-1321.

20. Howard, M. D.; Jay, M.; Dziubla, T. D.; Lu, X. PEGylation of Nanocarrier Drug Delivery Systems: State of the Art. *Journal of Biomedical Nanotechnology* 2008, 4, 133-148.

21. Kang, B.; Okwieka, P.; Schöttler, S.; Winzen, S.; Langhanki, J.; Mohr, K.; Opatz, T.; Mailänder, V.; Landfester, K.; Wurm, F. R. Carbohydrate-Based Nanocarriers Exhibiting Specific Cell Targeting with Minimum Influence from the Protein Corona. *Angewandte Chemie International Edition* 2015, 7436-7440.

22. Perry, J. L.; Reuter, K. G.; Kai, M. P.; Herlihy, K. P.; Jones, S. W.; Luft, J. C.; Napier, M.; Bear, J. E.; DeSimone, J. M. PEGylated PRINT nanoparticles: the impact of PEG density on protein binding, macrophage association, biodistribution, and pharmacokinetics. *Nano Letters* 2012, 12, 5304-5310.

23. Dai, Q.; Walkey, C.; Chan, W. C. Polyethylene glycol backfilling mitigates the negative impact of the protein corona on nanoparticle cell targeting. *Angewandte Chemie International Edition* 2014, 53, 5093-5096.

24. Berg, J. M.; Tymoczko, J. L.; Stryer, L.; Häcker, B. *Biochemie*. Elsevier Spektrum Akademischer Verlag: 2007.

25. Everett, D. H. *Basic principles of colloid science*. Royal Society of Chemistry: 1988.

26. https://www.blutspendedienst.com/blutspende/blutbestandteile/page/ (accessed 30.05.2015).

27. Martin, E. A. *Concise medical dictionary*. Oxford University Press: 2010.

28. http://www.medical-labs.net/difference-between-plasma-and-serum-1531/ (accessed 30.05.2015).

29. Fibrinogen Studies, C. Plasma fibrinogen level and the risk of major cardiovascular diseases and nonvascular mortality: An individual participant meta-analysis. *JAMA* 2005, 294, 1799-1809.

30. Le, T.; Bhushan, V.; Rao, D. A. *First Aid for the USMLE Step 1: 2008: 2008*. McGraw Hill Professional: 2007.

31. Gonzalez-Quintela, A.; Alende, R.; Gude, F.; Campos, J.; Rey, J.; Meijide, L.; Fernandez-Merino, C.; Vidal, C. Serum levels of immunoglobulins (IgG, IgA, IgM) in a general adult population and their relationship with alcohol consumption, smoking and common metabolic abnormalities. *Clinical & Experimental Immunology* 2008, 151, 42-50.

32. Helander, A. Absolute or relative measurement of carbohydrate-deficient transferrin in serum? Experiences with three immunological assays. *Clinical Chemistry* 1999, 45, 131-135.

33. Sigma Aldrich, http://www.sigmaaldrich.com/life-science/proteomics/mass-spectrometry/protein-aqua/absolute-quantification-of-serum-proteome.html (accessed 12.06.2015).

34. Wikimedia Commons, https://commons.wikimedia.org/wiki/File:Aufbau_eines_Lipoproteins.png#/media/File:Aufbau_eines_Lipoproteins.png (accessed 29.05.2015).

35. Wikimedia Commons, https://commons.wikimedia.org/wiki/File:The_Modular_Structure_of_Fibronectin

_and_its_Binding_Domains.png#/media/File:The_Modular_Structure_of_Fibronectin_and_its_Binding_Domains.png (accessed 09.06.2015).

36. Ringsdorf, H. In *Structure and properties of pharmacologically active polymers*, Journal of Polymer Science: Polymer Symposia, Wiley Online Library: 1975; pp 135-153.

37. Matsumura, Y.; Kataoka, K. Preclinical and clinical studies of anticancer agent-incorporating polymer micelles. *Cancer Science* 2009, 100, 572-579.

38. Maeda, H.; Wu, J.; Sawa, T.; Matsumura, Y.; Hori, K. Tumor vascular permeability and the EPR effect in macromolecular therapeutics: a review. *Journal of Controlled Release* 2000, 65, 271-284.

39. Azzazy, H. M. E.; Mansour, M. M. H. In vitro diagnostic prospects of nanoparticles. *Clinica Chimica Acta* 2009, 403, 1-8.

40. Zhang, M.; Kataoka, K. Nano-structured composites based on calcium phosphate for cellular delivery of therapeutic and diagnostic agents. *Nano Today* 2009, 4, 508-517.

41. Xie, J.; Lee, S.; Chen, X. Nanoparticle-based theranostic agents. *Advanced Drug Delivery Reviews* 2010, 62, 1064-1079.

42. Janib, S. M.; Moses, A. S.; MacKay, J. A. Imaging and drug delivery using theranostic nanoparticles. *Advanced Drug Delivery Reviews* 2010, 62, 1052-1063.

43. Monopoli, M. P.; Aberg, C.; Salvati, A.; Dawson, K. A. Biomolecular coronas provide the biological identity of nanosized materials. *Nature Nanotechnology* 2012, 7, 779-786.

44. Lynch, I.; Salvati, A.; Dawson, K. A. Protein-nanoparticle interactions: What does the cell see? *Nature Nanotechnology* 2009, 4, 546-7.

45. Deng, Z. J.; Liang, M.; Monteiro, M.; Toth, I.; Minchin, R. F. Nanoparticle-induced unfolding of fibrinogen promotes Mac-1 receptor activation and inflammation. *Nature Nanotechnology* 2011, 6, 39-44.

46. Vroman, L.; Adams, A. L. Findings with the recording ellipsometer suggesting rapid exchange of specific plasma proteins at liquid/solid interfaces. *Surface Science* 1969, 16, 438-446.

47. Vilaseca, P.; Dawson, K. A.; Franzese, G. Understanding surface-adsorption of proteins: the Vroman effect. *arXiv preprint arXiv:1202.3796* 2012.

48. Verwey, E. J. W.; Overbeek, J. T. G.; Overbeek, J. T. G. *Theory of the stability of lyophobic colloids*. Courier Dover Publications: 1999.

49. Chudakov, D. M.; Lukyanov, S.; Lukyanov, K. A. Fluorescent proteins as a toolkit for in vivo imaging. *Trends in Biotechnology* 2005, 23, 605-613.

50. Lewis, E.; Murphy, K. Isothermal Titration Calorimetry. In *Protein-Ligand Interactions*, Ulrich Nienhaus, G., Ed. Humana Press: 2005; Vol. 305, pp 1-15.

51. Freire, E.; Mayorga, O. L.; Straume, M. Isothermal titration calorimetry. *Analytical Chemistry* 1990, 62, 950A-959A.

52. Einstein, A. Theorie der Opaleszenz von homogenen Flüssigkeiten und Flüssigkeitsgemischen in der Nähe des kritischen Zustandes. *Annalen der Physik* 1910, 338, 1105.

53. Arndt, K.-F.; Müller, G. *Polymercharakterisierung*. Hanser: München, 1996; p XVII, 328 S.

54. Smoluchowski, M. Molekular-kinetische Theorie der Opaleszenz von Gasen im kritischen Zustande, sowie einiger verwandter Erscheinungen. *Annalen der Physik* 1908, 330, 205.

55. Kratochvil, P. *Classical light scattering from polymer solutions*. Elsevier: Amsterdam, 1987; p XI, 334 S.

56. Schärtl, W. *Light scattering from polymer solutions and nanoparticle dispersions: with 16 tables*. Springer: Berlin, 2007; p XIV, 191 S.

57. Siegert, A. J. F. *MIT Radiation Laboratory Report No. 465* 1943.

58. Provencher, S. W. Inverse Problems in Polymer Characterization - Direct Analysis of Polydispersity with Photon Correlation Spectroscopy. *Makromolecular Chemistry* 1979, 180, 201-209.

59. Provencher, S. W. A Constrained Regularization Method for Inverting Data Represented by Linear Algebraic or Integral-Equations. *Computer Physics Communications* 1982, 27, 213-227.

60. Provencher, S. W. Contin - a General-Purpose Constrained Regularization Program for Inverting Noisy Linear Algebraic and Integral-Equations. *Computer Physics Communications* 1982, 27, 229-242.

61. Wikimedia Commons, https://commons.wikimedia.org/wiki/File:Diagram_of_zeta_potential_and_slipping_planeV2.svg#/media/File:Diagram_of_zeta_potential_and_slipping_planeV2.svg (accessed 03.06.2015).

62. Hunter, R. J. *Zeta potential in colloid science: principles and applications*. Academic press: 2013; Vol. 2.

63. Schwille, P.; Haustein, E. Fluorescence correlation spectroscopy An introduction to its concepts and applications. *Spectroscopy* 2009, 94, 1-33.

64. Rigler, R. a. E. S. E. Fluorescence correlation spectroscopy. *Springer* 2001.

65. Milani, S.; Baldelli Bombelli, F.; Pitek, A. S.; Dawson, K. A.; Rädler, J. Reversible versus Irreversible Binding of Transferrin to Polystyrene Nanoparticles: Soft and Hard Corona. *ACS Nano* 2012, 6, 2532-2541.

66. Dobrovolskaia, M. A.; Patri, A. K.; Zheng, J.; Clogston, J. D.; Ayub, N.; Aggarwal, P.; Neun, B. W.; Hall, J. B.; McNeil, S. E. Interaction of colloidal gold nanoparticles with human blood: effects on particle size and analysis of plasma protein binding profiles. *Nanomedicine: Nanotechnology, Biology and Medicine* 2009, 5, 106-117.

67. Lundqvist, M.; Stigler, J.; Cedervall, T.; Berggård, T.; Flanagan, M. B.; Lynch, I.; Elia, G.; Dawson, K. The Evolution of the Protein Corona around Nanoparticles: A Test Study. *ACS Nano* 2011, 5, 7503-7509.

68. Liu, W.; Rose, J.; Plantevin, S.; Auffan, M.; Bottero, J.-Y.; Vidaud, C. Protein corona formation for nanomaterials and proteins of a similar size: hard or soft corona? *Nanoscale* 2013, 5, 1658-1668.

69. Wang, F.; Yu, L.; Monopoli, M. P.; Sandin, P.; Mahon, E.; Salvati, A.; Dawson, K. A. The biomolecular corona is retained during nanoparticle uptake and protects the cells from the damage induced by cationic nanoparticles until degraded in the lysosomes. *Nanomedicine: Nanotechnology, Biology and Medicine* 2013, 9, 1159-1168.

70. Dobrovolskaia, M. A.; Aggarwal, P.; Hall, J. B.; McNeil, S. E. Preclinical studies to understand nanoparticle interaction with the immune system and its potential effects on nanoparticle biodistribution. *Molecular Pharmaceutics* 2008, 5, 487-95.

71. Mortensen, N. P.; Hurst, G. B.; Wang, W.; Foster, C. M.; Nallathamby, P. D.; Retterer, S. T. Dynamic development of the protein corona on silica nanoparticles: composition and role in toxicity. *Nanoscale* 2013, 5, 6372-6380.

72. Lundqvist, M. Nanoparticles: Tracking protein corona over time. *Nature Nanotechnology* 2013, 8, 701-702.

73. Rausch, K.; Reuter, A.; Fischer, K.; Schmidt, M. Evaluation of Nanoparticle Aggregation in Human Blood Serum. *Biomacromolecules* 2010, 11, 2836-2839.

74. Nuhn, L.; Gietzen, S.; Mohr, K.; Fischer, K.; Toh, K.; Miyata, K.; Matsumoto, Y.; Kataoka, K.; Schmidt, M.; Zentel, R. Aggregation Behavior of Cationic Nanohydrogel Particles in Human Blood Serum. *Biomacromolecules* 2014, 15, 1526-1533.

75. Bouchemal, K. New challenges for pharmaceutical formulations and drug delivery systems characterization using isothermal titration calorimetry. *Drug Discovery Today* 2008, 13, 960-972.

76. Rocker, C.; Potzl, M.; Zhang, F.; Parak, W. J.; Nienhaus, G. U. A quantitative fluorescence study of protein monolayer formation on colloidal nanoparticles. *Nature Nanotechnology* 2009, 4, 577-580.

77. Maffre, P.; Nienhaus, K.; Amin, F.; Parak, W. J.; Nienhaus, G. U. Characterization of protein adsorption onto FePt nanoparticles using dual-focus fluorescence correlation spectroscopy. *Beilstein Journal of Nanotechnology* 2011, 2, 374.

78. Pino, P. d.; Pelaz, B.; Zhang, Q.; Maffre, P.; Nienhaus, G. U.; Parak, W. J. Protein corona formation around nanoparticles - from the past to the future. *Materials Horizons* 2014.

79. Torchilin, V. PEGylated Pharmaceutical Nanocarriers. In *Long Acting Injections and Implants*, Wright, J. C.; Burgess, D. J., Eds. Springer US: 2012; pp 263-293.

80. Pozzi, D.; Colapicchioni, V.; Caracciolo, G.; Piovesana, S.; Capriotti, A. L.; Palchetti, S.; De Grossi, S.; Riccioli, A.; Amenitsch, H.; Lagana, A. Effect of polyethyleneglycol (PEG) chain length on the bio-nano-interactions between PEGylated lipid nanoparticles and biological fluids: from nanostructure to uptake in cancer cells. *Nanoscale* 2014, 6, 2782-2792.

81. Marchant, R. E.; Yuan, S.; Szakalas-Gratzl, G. Interactions of plasma proteins with a novel polysaccharide surfactant physisorbed to polyethylene. *Journal of Biomaterials Science, Polymer Edition* 1995, 6, 549-564.

82. Österberg, E.; Bergström, K.; Holmberg, K.; Schuman, T. P.; Riggs, J. A.; Burns, N. L.; Van Alstine, J. M.; Harris, J. M. Protein-rejecting ability of surface-bound dextran in end-on and side-on configurations: Comparison to PEG. *Journal of Biomedical Materials Research* 1995, 29, 741-747.

83. Orlando, M. Modification of proteins and low molecular weight substances with hydroxyethyl starch (HES). Universitätsbibliothek Giessen, 2003.

84. Besheer, A.; Vogel, J.; Glanz, D.; Kressler, J.; Groth, T.; Mäder, K. Characterization of PLGA Nanospheres Stabilized with Amphiphilic Polymers: Hydrophobically Modified Hydroxyethyl Starch vs Pluronics. *Molecular Pharmaceutics* 2009, 6, 407-415.

85. Lemarchand, C.; Gref, R.; Couvreur, P. Polysaccharide-decorated nanoparticles. *European Journal of Pharmaceutics and Biopharmaceutics* 2004, 58, 327-341.

86. Winzen, S.; Schoettler, S.; Baier, G.; Rosenauer, C.; Mailaender, V.; Landfester, K.; Mohr, K. Complementary analysis of the hard and soft protein corona: sample preparation critically effects corona composition. *Nanoscale* 2015, 7, 2992-3001.

87. Baier, G.; Costa, C.; Zeller, A.; Baumann, D.; Sayer, C.; Araujo, P. H. H.; Mailänder, V.; Musyanovych, A.; Landfester, K. BSA adsorption on differently charged polystyrene nanoparticles using isothermal titration calorimetry and the influence on cellular uptake. *Macromolecular Bioscience* 2011, 11, 628-638.

88. Cifuentes-Rius, A.; de Puig, H.; Kah, J. C. Y.; Borros, S.; Hamad-Schifferli, K. Optimizing the Properties of the Protein Corona Surrounding Nanoparticles for Tuning Payload Release. *ACS Nano* 2013, 7, 10066-10074.

89. Michnik, A.; Michalik, K.; Kluczewska, A.; Drzazga, Z. Comparative DSC study of human and bovine serum albumin. *Journal of Thermal Analysis and Calorimetry* 2006, 84, 113-117.

90. Pikal, M. J.; Rigsbee, D.; Roy, M. L. Solid state stability of proteins III: Calorimetric (DSC) and spectroscopic (FTIR) characterization of thermal denaturation in freeze dried human growth hormone (hGH). *Journal of Pharmaceutical Sciences* 2008, 97, 5122-5131.

91. Hemmelmann, M.; Mohr, K.; Fischer, K.; Zentel, R.; Schmidt, M. Interaction of pHPMA-pLMA copolymers with human blood serum and its components. *Molecular Pharmaceutics* 2013, 10, 3769-75.

92. Štěpánek, P. Static and dynamic properties of multiple light scattering. *The Journal of Chemical Physics* 1993, 99, 6384-6393.

93. Bantle, S.; Schmidt, M.; Burchard, W. Simultaneous static and dynamic light scattering. *Macromolecules* 1982, 15, 1604-1609.

94. Annathur, G. V.; Kawas, S.; Das, T. K.; Ho, S. V. Ultrafiltration of a highly self-associating protein. *Journal of Membrane Science* 2010, 353, 41-50.

95. Vogler, E. A. Protein adsorption in three dimensions. *Biomaterials* 2012, 33, 1201-1237.

96. Laemmli, U. K. Cleavage of Structural Proteins during the Assembly of the Head of Bacteriophage T4. *Nature* 1970, 227, 680-685.

97. Maiolo, D.; Bergese, P.; Mahon, E.; Dawson, K. A.; Monopoli, M. P. Surfactant Titration of Nanoparticle–Protein Corona. *Analytical Chemistry* 2014.

98. Podila, R.; Chen, R.; Ke, P. C.; Brown, J. M.; Rao, A. M. Effects of surface functional groups on the formation of nanoparticle-protein corona. *Applied Physics Letters* 2012, 101, 263701.

99. Jedlovszky-Hajdú, A.; Bombelli, F. B.; Monopoli, M. P.; Tombácz, E.; Dawson, K. A. Surface Coatings Shape the Protein Corona of SPIONs with Relevance to Their Application in Vivo. *Langmuir* 2012, 28, 14983-14991.

100. Landfester, K.; Bechthold, N.; Tiarks, F.; Antonietti, M. Miniemulsion Polymerization with Cationic and Nonionic Surfactants: A Very Efficient Use of Surfactants for Heterophase Polymerization. *Macromolecules* 1999, 32, 2679-2683.

101. Landfester, K.; Bechthold, N.; Tiarks, F.; Antonietti, M. Formulation and Stability Mechanisms of Polymerizable Miniemulsions. *Macromolecules* 1999, 32, 5222-5228.

102. Davies, J. In *A quantitative kinetic theory of emulsion type, I. Physical chemistry of the emulsifying agent*, Gas/Liquid and Liquid/Liquid Interface. Proceedings of the International Congress of Surface Activity, 1957; pp 426-438.

103. Griffin, W. C. Calculation of HLB values of non-ionic surfactants. *The American Perfumer and Essential Oil Review* 1955, 65, 26-29.

104. Vargaftik, N. B.; Volkov, B. N.; Voljak, L. D. International Tables of the Surface Tension of Water. *Journal of Physical and Chemical Reference Data* 1983, 12, 817-820.

105. Myers, D. *Surfaces, interfaces and colloids*. Wiley-Vch New York etc.: 1990.

106. Markus, G.; Karush, F. Structural Effects of the Interaction of Human Serum Albumin with Sodium Decyl Sulfate1. *Journal of the American Chemical Society* 1957, 79, 3264-3269.

107. Nielsen, A. D.; Borch, K.; Westh, P. Thermochemistry of the specific binding of C12 surfactants to bovine serum albumin. *Biochimica et Biophysica Acta (BBA) - Protein Structure and Molecular Enzymology* 2000, 1479, 321-331.

108. Hecht, L. L.; Schoth, A.; Muñoz-Espí, R.; Javadi, A.; Köhler, K.; Miller, R.; Landfester, K.; Schuchmann, H. P. Determination of the Ideal Surfactant Concentration in Miniemulsion Polymerization. *Macromolecular Chemistry and Physics* 2013, 214, 812-823.

109. Valstar, A.; Almgren, M.; Brown, W.; Vasilescu, M. The Interaction of Bovine Serum Albumin with Surfactants Studied by Light Scattering. *Langmuir* 1999, 16, 922-927.

110. Ragi, C.; Sedaghat-Herati, M. R.; Ouameur, A. A.; Tajmir-Riahi, H. A. The effects of poly(ethylene glycol) on the solution structure of human serum albumin. *Biopolymers* 2005, 78, 231-236.

111. Raj, T.; Flygare, W. H. Diffusion studies of bovine serum albumin by quasielastic light scattering. *Biochemistry-Us* 1974, 13, 3336-3340.

112. Rusconi, F.; Valton, É.; Nguyen, R.; Dufourc, E. Quantification of Sodium Dodecyl Sulfate in Microliter-Volume Biochemical Samples by Visible Light Spectroscopy. *Analytical Biochemistry* 2001, 295, 31-37.

113. Campbell, K. P.; MacLennan, D. H.; Jorgensen, A. O. Staining of the Ca2+-binding proteins, calsequestrin, calmodulin, troponin C, and S-100, with the cationic carbocyanine dye "Stains-all". *Journal of Biological Chemistry* 1983, 258, 11267-73.

114. Bean, R. C.; Shepherd, W. C.; Kay, R. E.; Walwick, E. R. Spectral Changes in a Cationic Dye Due to Interaction with Macromolecules. III. Stoichiometry and Mechanism of the Complexing Reaction1. *The Journal of Physical Chemistry* 1965, 69, 4368-4379.

115. Jerabek-Willemsen, M.; Wienken, C. J.; Braun, D.; Baaske, P.; Duhr, S. Molecular Interaction Studies Using Microscale Thermophoresis. *ASSAY and Drug Development Technologies* 2011, 9, 342-353.

116. Oleg, K.; Grégoire, B. Fluorescence correlation spectroscopy: the technique and its applications. *Reports on Progress in Physics* 2002, 65, 251.

117. Jiang, X.; Weise, S.; Hafner, M.; Röcker, C.; Zhang, F.; Parak, W. J.; Nienhaus, G. U. Quantitative analysis of the protein corona on FePt nanoparticles formed by transferrin binding. *Journal of The Royal Society Interface* 2010, 7, S5-S13.

118. Maffre, P.; Brandholt, S.; Nienhaus, K.; Shang, L.; Parak, W. J.; Nienhaus, G. U. Effects of surface functionalization on the adsorption of human serum albumin onto nanoparticles – a fluorescence correlation spectroscopy study. *Beilstein Journal of Nanotechnology* 2014, 5, 2036-2047.

119. Luo, N.; Zhang, C.; Hirt, D. E.; Husson, S. M. Adsorption of fluorescently labeled protein residues on poly(ethylene-co-acrylic acid) films modified with affinity functionalities. *Colloids and Surfaces B: Biointerfaces* 2006, 50, 89-96.

120. Czeslik, C.; Jansen, R.; Ballauff, M.; Wittemann, A.; Royer, C. A.; Gratton, E.; Hazlett, T. Mechanism of protein binding to spherical polyelectrolyte brushes studied *in situ* using two-photon excitation fluorescence fluctuation spectroscopy. *Physical Review E* 2004, 69, 021401.

121. Landry, J. P.; Zhu, X.; Gregg, J. P.; Guo, X. In *Detection of biomolecular microarrays without fluorescent labeling agents*, 2004; pp 121-128.

122. Boylan, N. J.; Zhou, W.; Proos, R. J.; Tolbert, T. J.; Wolfe, J. L.; Laurence, J. S. Conjugation Site Heterogeneity Causes Variable Electrostatic Properties in Fc Conjugates. *Bioconjugate Chemistry* 2013, 24, 1008-1016.

123. Teske, C. A.; Lieres, E. v.; Schröder, M.; Ladiwala, A.; Cramer, S. M.; Hubbuch, J. J. Competitive adsorption of labeled and native protein in confocal laser scanning microscopy. *Biotechnology and Bioengineering* 2006, 95, 58-66.

124. Yin, L.; Wang, W.; Wang, S.; Zhang, F.; Zhang, S.; Tao, N. How does fluorescent labeling affect the binding kinetics of proteins with intact cells? *Biosensors and Bioelectronics* 2015, 66, 412-416.

125. Guan, A.; Li, Z.; Phillips, K. S. The Effect of Fluorescent Labels on Protein Sorption in Polymer Hydrogels. *Journal of Fluorescence* 2014, 24, 1639-1650.

126. Koynov, K.; Butt, H.-J. Fluorescence correlation spectroscopy in colloid and interface science. *Current Opinion in Colloid & Interface Science* 2012, 17, 377-387.

127. Righetti, P. G.; Caravaggio, T. Isoelectric points and molecular weights of proteins : A table. *Journal of Chromatography A* 1976, 127, 1-28.

128. Life Technologies, https://products.invitrogen.com/ivgn/product/A20006?ICID==%3Dsearch-a20006 (accessed 27. August 2012).

129. Mahmoudi, M.; Abdelmonem, A. M.; Behzadi, S.; Clement, J. H.; Dutz, S.; Ejtehadi, M. R.; Hartmann, R.; Kantner, K.; Linne, U.; Maffre, P.; Metzler, S.; Moghadam, M. K.; Pfeiffer, C.; Rezaei, M.; Ruiz-Lozano, P.; Serpooshan, V.; Shokrgozar, M. A.; Nienhaus, G. U.; Parak, W. J. Temperature: The "Ignored" Factor at the NanoBio Interface. *ACS Nano* 2013, 7, 6555-6562.

130. Prin, C.; Bene, M. C.; Gobert, B.; Montagne, P.; Faure, G. C. Isoelectric restriction of human immunoglobulin isotypes. *Biochimica et Biophysica Acta (BBA) - General Subjects* 1995, 1243, 287-289.

131. Schlaad, H.; Kukula, H.; Rudloff, J.; Below, I. Synthesis of α, ω-heterobifunctional poly(ethylene glycol)s by metal-free anionic ring-opening polymerization. *Macromolecules* 2001, 34, 4302-4304.

132. Thurmont, D. *Journal of Polymer Science* 1952, 8, 607.

133. Baier, G.; Baumann, D.; Siebert, J. M.; Musyanovych, A.; Mailänder, V.; Landfester, K. Suppressing Unspecific Cell Uptake for Targeted Delivery Using Hydroxyethyl Starch Nanocapsules. *Biomacromolecules* 2012, 13, 2704-2715.